Development of an Electromyography Detection System for the Control of Functional Electrical Stimulation in Neurological Rehabilitation

vorgelegt von

M.Sc.

Raafat El-Sayed Shalaby

Von der Fakultät IV - Elektrotechnik und Informatik

der Technischen Universität Berlin

zur Erlangung des akademischen Grades

Doktor der Ingenieurwissenschaften

– Dr.-Ing. –

genehmigte Dissertation

Promotionsausschuss:

Vorsitzender:	Prof. Dr.-Ing. Reinhold Orglmeister
Berichter:	Prof. Dr.-Ing. Jörg Raisch
Berichter:	Prof. Dr. Fabio Previdi

Tag der wissenschaftlichen Aussprache: 19. July 2011

Berlin: 2011

D83

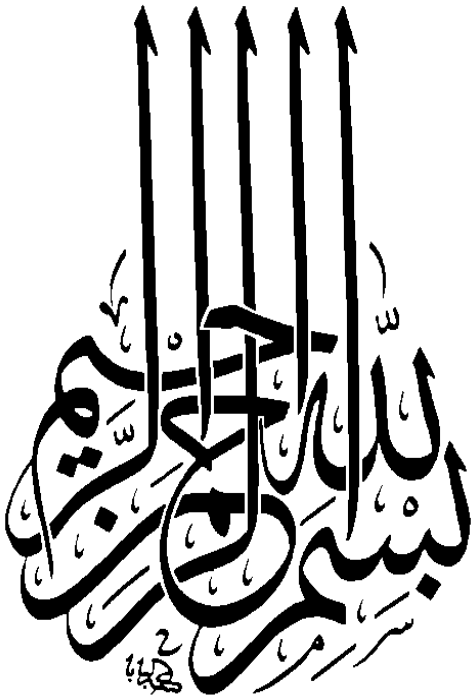

In the name of Allah the most Gracious the most Merciful

Dedication and Acknowledgements

Dedication: This thesis is firstly dedicated to the Egyptian young people who have been steadfast in the field and to the souls of the martyrs of our revolution who were killed and their blood paid the price for freedom and the salvation of the regime.

Secondly it is dedicated to my family. All through my life my parents have always been there, supporting and trusting me during those difficult times. I would like to dedicate this research and everything I do to both of them. It is dedicated to the soul of my aunt – Nabaweya Shalaby – who taught me that I can accomplish even the largest task if I do it one step at a time. I wish to thank my wife – Manar Khalifa – for her supporting, endless patience and encouragement when it was most required.

Acknowledgements: I wish to acknowledge and thank Prof. Jörg Raisch, who gives me the opportunity to be here in Germany and to study my Ph.D. in his research group at the TU-Berlin.

I would like to express my deep thanks and appreciations to the coordinator of this work – Dr. Thomas Schauer –, who introduced me to the interesting field of electromyography and functional electrical stimulation and has shown a consistent interest in my project during the times, and whose ideas, and advices made this work possible.

I am grateful to the whole biomedical research staff in the control systems group at the TU-Berlin who shared their times memories and experiences, especially Holger Nahrstaedt and Christian Klauer.

I like also to acknowledge the EN11 secretary – Ulrike Locherer – for her endless support and help in many accommodation issues since my first day in Berlin. I wish also to thank the technical staff people Astrid Bergmann and Ralph Stephan.

Abstract

Paralysis can be caused by a stroke or by an injury of the spinal cord; usually stroke is the most common reason of neurological impairment. Approximately two-third of people having stroke survive and can be rehabilitated. Fortunately, the brain can re-learn because of its “plasticity”. New parts of the brain can learn to substitute the functions that have been lost due to stroke; this process is known as neurological rehabilitation. The re-learning process of the brain is a repetition-based task. The brain needs the task to be repeated for large number of times (could be ten thousands) to regain the lost movement skills and to become able to redo it voluntarily. Standard neurological rehabilitation is performed manually. Here, the physiotherapists have initially to move the patients’ paralyzed limbs in a repetitive way during a rehabilitation program. Such a rehabilitation program may take weeks or even months.

In stroke patients and those having incomplete Spinal Cord Injury (iSCI), weak residual motor functions can be observed by means of Electromyography (EMG), which records the small electrical activity associated with muscle contractions. As the paretic muscles remain innervated they can be artificially activated by applying small electrical current pulses in a process known as Functional Electrical Stimulation (FES). FES can produce strong enough muscle contractions and has been used to support physiotherapists performing the repetition-based rehabilitation tasks.

Different EMG signal components can be observed during the application of FES. These components are either related to muscle contractions induced by FES or related to muscle activity that is independent of FES. The second class of EMG signals consists of the volitional Electromyogram (vEMG) which is generated by intended movements and a non-volitional part which results from eventual muscle spasticity and/or increased muscle tone.

The detection of non FES-induced EMG during active FES is a big challenge. Normally, EMG detection devices utilize high-gain amplifiers, which are supposed to saturate due to the interaction between measuring electrodes and stimulation pulses (stimulation artifacts). The resulting saturation period could be too long, not allowing any EMG detection between stimulation pulses. The high-voltage stimulation pulses could even damage the amplifier input circuitry. Additionally, electric polarization of the electrode/skin interface could happen and lead to a reduction of the recorded EMG signals. This phenomenon is known as EMG suppression due to FES. These problems will be even more prominent if EMG is to be measured from the stimulation electrodes during active stimulation periods.

Due to these difficulties faced by the recording of EMG during electrical stimulation, existing clinical FES systems do not offer a control of stimulation dependent on the patient’s residual motor

function. Furthermore, as they are not allowing any EMG recording during the active period of stimulation, the patient's response to stimulation cannot be observed. Unwanted spastic reactions often remain undetected.

In most existing devices, the timing of FES is manually controlled by the patient or physiotherapist or by force resistive sensors (switches) e.g. in FES-assisted gait training. After the activation of stimulation, a pre-programmed stimulation profile is applied. Some innovative systems are offering EMG-triggered stimulation patterns; the stimulation starts when vEMG exceeds a certain threshold level. However, the recording of EMG stops due to the difficulties mentioned above after the stimulation started. The stimulation stays active for a pre-defined time interval and then automatically stops. Neither the manually/switch controlled FES nor the EMG-triggered FES are taking into account the patient's intention during the period of active FES.

At the level of research, there are a few devices developed which measure EMG during FES, mostly using two electrodes for electrical stimulation and two different electrodes for EMG detection. This thesis is presenting a new 4-channel EMG detection system. The system is named "StiMyo" for its ability to measure myo-electric signals during stimulation. In presence of the above mentioned difficulties, StiMyo is able to measure vEMG during active stimulation between stimulation pulses directly from the stimulation electrodes. Using StiMyo it will be easier to observe muscle reactions (e.g. muscle spasticity and some FES-related reflexes) and to actively involve the patient's intention during the rehabilitation process. The ability of StiMyo to measure the non FES-related activity of electrically stimulated muscles makes it usable in the neurological rehabilitation after stroke or iSCI.

A switching circuit driven by a microcontroller has been developed to protect the amplifier input from any damage by the stimulation pulses. The circuit also introduces a fast discharging path to repeatedly remove the accumulated charge under the FES/EMG electrodes. This fast discharging is needed to minimize the saturation period of the pre-amplifier due to the residual DC voltage under the FES/EMG electrodes and also to reduce the effects of electrode polarization. An optional permanent electrode/skin discharging resistor has been added to prevent any severe effects of electrode polarization, which could appear due to unbalanced stimulation charge produced by possible unsymmetrical stimulation pulses. The current flow associated with electrode discharging can trigger a second action potential that causes another muscle contraction following the first direct muscle activation caused by the stimulation pulse. The timing of the discharge related action potential wave (firstly as an experimental observation in this work and named as D-wave) in the EMG can be influenced by the timing of the switches and the use of the permanent discharging resistor. An occurrence of the D-wave during the measurement interval for non FES-induced EMG activity should be avoided to allow a clear assessment of vEMG etc.

The design process showed that the non FES-induced EMG can be extracted from the recorded signal by using mixed time and frequency domain filter approaches. Big portions of the EMG

response related to the direct muscular response on the stimuli, the so-called M-wave, as well as stimulation and switching artifacts are blanked in time domain by means of a mute filter. The required muting period is with up to 35 ms relatively long compared to a stimulation period of 50ms at a stimulation frequency of 20 Hz yielding an EMG measurement period of at least 15 ms between stimuli. For this measurement period, the separation of the non FES-induced EMG from the remaining low-frequent artifacts (tails of discharging curve and M-wave) is achieved in frequency domain by means of a High-Pass Filter (HPF). The corner frequencies of the HPF, the timing of the electrode/skin discharger and the artifact mute switches have been experimentally optimized in a study including 5 healthy subjects. An assessment of the FES induced muscular contraction is not possible when measuring EMG from the stimulation electrodes due to the too long muting period hiding the main part of the M-wave. This is the main limitation of the developed EMG amplifier.

Two FES applications of the StiMyo device have been experimentally investigated with neurologically intact subjects.

In the first application, StiMyo had been employed for EMG-controlled FES of the wrist and fingers extensors. Thanks to the StiMyo amplifier, EMG can also be evaluated between stimulation pulses. This fact clears the way for sophisticated control approaches which modulate the stimulation intensity (e.g. pulse charge) continuously according to the measured volitional EMG if spasticity is not present or mild. Two control methods have been investigated. Experimental validation of the proposed methods was carried out in a pilot study with 5 healthy subjects. The first control method aims at exploiting as much as possible the residual motor control of the patient by quasi linear amplification of the detected volitional motor activity. Therefore, a stimulation intensity which is proportional to the detected volitional EMG is applied. Using this EMG-proportional stimulation, subjects could perform tracking tasks for the wrist-joint angle with less voluntary effort compared to pure volitional movements. However, tracking performance/accuracy suffered from using EMG-proportional control. When subjects/patients are not able to generate smooth volitional EMG profiles, EMG-proportional FES will not be applicable due to risk of oscillating movements. To mitigate this problem, a second control approach was proposed. This approach can be seen as a compromise between EMG-triggered and EMG-proportional stimulation. The stimulation is initiated as soon vEMG goes above a defined EMG threshold and stays active until vEMG drops below a second lower EMG threshold. To avoid spastic reactions by the stimulation, a rate limitation is implemented for switching on and off the stimulation. This control approach is called EMG-carried stimulation as the patients must constantly contract a muscle to maintain a supportive, but constant, stimulation. The results related to both control approaches showed the feasibility of using vEMG to obtain an intention-related FES assistance.

The second application considered in this work is FES-cycling on an ergo meter with an auxiliary electrical motor. The cycling movement is supported by timed electrical stimulation of the

quadriceps and hamstrings muscle groups. In a pilot study with one healthy subject the feasibility to monitor non FES-related volitional muscle activity even when electrical stimulation is active was demonstrated. Volitional EMG activity could be measured when applying electrical pulses with high intensity (current amplitude of 50 mA and pulse width of 500 µs) as they were used in stroke rehabilitation at a maximum.

The stimulation intensity controlled in this thesis was always the charge of the electrical pulses which is determined by the product of current amplitude and pulse width. This is in contrast to the common practice where either current amplitude or pulse width is modulated while keeping the other variable constant. The selection of the right values is usually time-consuming so that direct control of charge was investigated in order to simplify the process. However, this was opening the question on how to realize a given charge by automatically choosing current amplitude and pulse with. Different distributions/relations of pulse widths and current amplitudes have been experimentally compared with respect to the minimum charge required for maintaining a desired muscular action and with respect to muscular fatigue. The outcome of this study with healthy subjects was that pulses with high current amplitudes and short pulse widths are preferred. The implemented automatic mapping from a given charge to a pulse width and current amplitude is named charge control in this thesis.

Zusammenfassung in deutscher Sprache

Lähmungen können durch einen Schlaganfall oder eine Verletzung des Rückenmarks verursacht werden. Der Schlaganfall stellt dabei die häufigste Ursache für neurologische Beeinträchtigungen dar. Ungefähr zwei Drittel derjenigen, die einen Schlaganfall erleiden, überleben und können rehabilitiert werden. Glücklicherweise kann das Gehirn aufgrund seiner „Plastizität“ neu lernen. Funktionen, die durch den Schlaganfall beeinträchtigt sind, können durch noch gesunde Teile des Gehirns im Rahmen eines Lernprozesses wiederhergestellt werden. Dieser Lernprozess basiert auf einer häufigen Wiederholung (bis zu zehntausende Male) der zu lernenden Aufgabe. Die neurologische Rehabilitation wird derzeit überwiegend mittels manueller Physiotherapie durchgeführt. Während dieses Rehabilitationsprogramms, das Wochen bis Monate in Anspruch nehmen kann, müssen anfänglich Physiotherapeuten die gelähmten Gliedmaßen der Patienten von Hand wiederholt bewegen.

Bei Schlaganfallpatienten und Patienten mit inkompletter Rückenmarksverletzung können noch verbliebende schwache Muskelaktivitäten mittels der Elektromyographie (EMG) erfasst werde. Die Elektromyographie misst kleine elektrische Aktivitäten, welche mit den Muskelkontraktionen in Verbindung gebracht werden können. Da der teilweise gelähmte (paretische) Muskel immer noch vollständig innerviert ist, kann dieser durch Applikation kleiner elektrischer Impulse künstlich aktiviert werden, um funktionelle Bewegungen zu erzeugen. Dieser Vorgang ist bekannt als Funktionelle Elektrostimulation (FES). Mittels FES können genügend starke Muskelkontraktionen hervorgerufen werden, um wiederholte Bewegungen in der motorischen Rehabilitation zu erzeugen. Durch die Verwendung der FES können Therapeuten entlastet und die Rehabilitation verbessert werden.

Während der Anwendung der FES können verschiedene EMG Bestandteile betrachtet werden. Diese sind entweder durch die FES hervorgerufen oder stehen in Bezug zu einer muskulären Aktivität, welche unabhängig von der FES ist. Die letztere Klasse von EMG-Signalen beinhaltet das willkürliche Elektromyogramm (volitional Electromyogram - vEMG), das durch beabsichtigte Bewegungen generiert wird, und nichtwillkürliche Bestandteile, die von einer eventuellen Muskelspastik oder einem erhöhten muskulären Tonus herrühren.

Die Erfassung von nicht durch FES erzeugten EMG-Anteilen zwischen den Stimulationsimpulsen stellt eine große Herausforderung dar. Üblicherweise verwenden EMG-Messsysteme Verstärker mit sehr hoher Verstärkung. Diese Systeme können aufgrund der Interaktion zwischen den Messelektroden und den Stimulationsimpulsen in die Beschränkung gehen. Die Zeit, in der die Systeme in der Beschränkung verbleiben, kann mitunter so lang sein, dass keine Erfassung von EMG zwischen den Stimulationsimpulsen möglich ist. Im schlimmsten Fall kann der Verstärker

durch die Stimulationsimpulse sogar dauerhaft beschädigt werden. Zusätzlich können die Stimulationsimpulse zu einer Polarisation der Elektroden-Haut-Verbindung führen, welche sich durch eine deutliche Abschwächung der gemessenen EMG-Signale bemerkbar macht. Dieses Phänomen, welches auch als EMG-Unterdrückung durch FES bekannt ist, tritt im Fall einer EMG-Messung über die Stimulationselektroden wesentlich häufiger auf als bei Verwendung separater Elektroden für die EMG-Messung.

Aufgrund der zuvor genannten Probleme, ermöglichen die existierenden klinischen FES Systeme keine EMG-Messung während der Stimulation und bieten auch keine Möglichkeit, die Stimulation an die noch vorhandenen motorischen Fähigkeiten der Patienten anzupassen. Die Reaktion der Patienten auf die Stimulation kann nicht erfasst werden. Unerwünschte spastische Reaktionen bleiben somit oft unerkannt.

Bei den meisten existierenden FES-Systemen erfolgt die Aktivierung der FES manuell durch den Physiotherapeuten oder mittels Kraftsensoren (Schalter), z.B. beim FES-unterstützten Gangtraining. Nach der Aktivierung der Stimulation, wird in der Regel ein vordefiniertes Stimulationsprofil angewandt. Einige innovative Systeme bieten EMG-getriggerte Stimulationsmuster: Die Stimulation startet, wenn vEMG eine gegebene Schaltschwelle überschreitet. Mit dem Beginn der Stimulation endet jedoch die EMG-Messung aufgrund der oben genannten Probleme. Bei keinem dieser FES-Ansätze wird die Intention des Patienten während der Stimulationsphase berücksichtigt.

Im Bereich der Forschung sind einige wenige Geräte entwickelt wurden, die eine EMG Messung während der FES erlauben. Die Mehrheit dieser Systeme benötigt zwei Elektroden für die Elektrostimulation und zwei andere Elektroden für die EMG-Detektierung. In dieser Arbeit wird ein neu entwickeltes 4-kanaliges EMG-System vorgestellt, welches den Namen “StiMyo” trägt. Trotz der zuvor genannten Schwierigkeiten, ist das Gerät in der Lage, nicht durch FES generiertes EMG während einer aktiven Stimulation zwischen den Stimulationsimpulsen zu messen. Die EMG-Messung erfolgt dabei direkt über die Stimulationselektroden. Mittels StiMyo wird es einfacher sein, muskuläre Reaktionen (z.B. Spastiken) während der FES zu beobachten und die Intentionen des Patienten aktiv in den Rehabilitationsprozess einzubinden.

Ein spezieller Schaltkreis mit Photo-MOS-Schaltern wurde entwickelt, um die Verstärkereingänge vor Schäden durch die Stimulationsimpulse zu schützen. Die Ansteuerung der Schalter erfolgt dabei über einen Mikrocontroller. Mittels der Schalter wird ferner eine schnelle Entladung der FES/EMG realisiert, welche wiederholt nach jedem Stimulationsimpuls aktiviert wird. Durch die wiederholte Entladung der Elektroden soll verhindert werden, dass sich Ladung unter den Stimulationselektroden akkumuliert. Sollte diese Maßnahme nicht ausreichend sein um einer Elektrodenpolarisation vorzubeugen (z.B. bei nicht ausreichend ausgeglichenen bipolaren Stimulationsimpulsen), so kann optional eine permanente Entladung über einen weiteren Entladungswiderstand durchgeführt werden. Der mit der Entladung verbundene Stromfluss kann ein

zweites Aktionspotential auslösen, das zu einer zweiten Muskelkontraktion nach der ersten, durch den eigentlichen Stimulationsimpuls verursachten Muskelkontraktion, führt. Der zeitliche Versatz zwischen dem Stimulus und dem durch Entladung verursachten Aktionspotential kann durch die zeitliche Steuerung der Schalter und die Verwendung des permanenten Ladungswiderstandes gezielt beeinflusst werden. Es ist folglich möglich, das Aktionspotential so zu verschieben, dass es die Messung der Willküraktivität und Spastik nicht stört.

Der Entwurfsprozess zeigte, dass die nicht mit FES in Bezug stehenden EMG-Anteile vom EMG durch gemischte Filteransätze im Zeit- und Frequenzbereich extrahiert werden können. Der Anteil des gemessenen EMG, welcher neben Stimulations- und Schaltartefakten den Hauptanteil der Stimulationsantwort im EMG, die sogenannte M-Welle, enthält, wird durch einen Mute-Schalter zu Null gesetzt. Die notwendige Ausblendperiode ist mit bis zu 35 ms relativ lang im Vergleich zur Stimulationsperiode von 50 ms (entspricht einer Stimulationsfrequenz von 20 Hz), so dass sich eine EMG-Messperiode von 15 ms ergibt. Für dieses Messintervall erfolgt die Trennung von nicht durch FES generierten EMG-Anteilen und noch vorhandenen niederfrequenten Artefakten (Abklingkurven der Entladung und M-Welle) im Frequenzbereich mittels eines Hochpassfilters. Die Knickfrequenzen des Hochpassfilters und die zeitliche Steuerung der Schalter wurden in einer Studie mit 5 gesunden Probanden experimentell optimiert.

Eine Beurteilung der durch FES verursachten Kontraktionen ist mit dem entwickelten EMG-Verstärker nicht möglich. Aufgrund der relativ langen Signalausblendung kann die die M-Welle nicht erfasst werden. Dies ist eine wesentliche Einschränkung, die mit einer EMG-Messung über die Stimulationselektroden verbunden ist.

Im Rahmen dieser Arbeit wurden zwei FES-Anwendungen für die Verwendung des StiMyo-Gerätes mit gesunden Probanden experimentell untersucht.

In der ersten Anwendung wurde StiMyo eingesetzt für eine EMG-geregelte Stimulation der Handgelenk- und Fingerstrecker. Willkürliche Muskelkontraktionen können nun auch zwischen den Stimulationsimpulsen erfasst werden. Dies erlaubt die Realisierung fortgeschrittener Regelungsansätze, bei denen die Stimulationsintensität (z.B. Ladung des Stimulationsimpulses) kontinuierlich an die gemessene willkürliche EMG-Aktivität angepasst wird. Dieses Vorgehen setzt jedoch voraus, dass Spastik nur moderat oder gar nicht vorhanden ist. Zwei Regelungsverfahren wurden analysiert und experimentell in einer Studie mit 5 gesunden Probanden validiert. Das erste Verfahren zielt darauf, die noch vorhandenen motorischen Fähigkeiten durch quasi-lineare Verstärkung der detektierten willkürlichen Muskelaktivitäten möglichst stark zu nutzen. Hierfür wurde eine Stimulationsintensität appliziert, die proportional zum gemessenen Willkür-EMG ist. Durch Verwendung dieser EMG-proportionalen Stimulation konnten die Probanden geforderte Sollbewegungen mit weniger willentlicher Anstrengung absolvieren als normal. Die Güte der

erzeugten Bewegungen im Sinne von Glattheit und Abweichungen von Sollwerten verschlechterte sich jedoch mit EMG-proportionaler Stimulation im Vergleich zu rein willkürlichen Bewegungen.

Für Probanden und Patienten, die nicht genügend glatte EMG-Profile generieren, eignet sich die EMG-proportionale Stimulation nicht, da ihre Anwendung zu Schwingungen in der resultierenden Bewegung führen kann. Ein zweites Regelungsverfahren wurde speziell für diese Gruppe von potentiellen Nutzern vorgeschlagen, welches einen Kompromiss zwischen EMG-getriggerter Stimulation und EMG-proportionaler Stimulation darstellt. Die Stimulation wird aktiviert, sobald das Willkür-EMG über eine vordefinierte Schwelle steigt und bleibt aktiv bis das Willkür-EMG unter eine zweite, niedrigere, Schwelle fällt. Um spastische Reaktionen und Sehnenreflexe zu vermeiden, wurde eine Ratenbeschränkung für das Ein- und Ausschalten der Stimulation implementiert. Dieses neue FES-Regelverfahren wurde in dier vorliegenden Arbeit als EMG-getragene Stimulation bezeichnet, da der Proband/Patient den Muskel fortlaufend aktiviert halten muss, um eine unterstützende, aber konstante Stimulation zu erhalten. Die Ergebnisse für beide Regelungsverfahren belegen die Machbarkeit einer Intentions-bezogenen FES-Unterstützung durch Verwendung von EMG-Messungen am stimulierten Muskel.

Die zweite Anwendung, die in dieser Arbeit betrachtet wurde, ist das FES-Fahrradfahren an einem Ergometer mit Hilfsmotor. Die Trittbewegung wird hier durch elektrische Stimulation der Kniebeuger und -strecker unterstützt. In einer Pilotstudie mit einem gesunden Probanden demonstriert, dass eine Erfassung der willkürlichen Muskelaktivitäten beim FES-Fahrradfahren über die Stimulationselektroden möglich ist. Untersucht wurden auch hohe Stimulationsintensitäten (Stromstärke bis 50 mA und Pulsbreite bis 500 µs), wie sie in der Behandlung von Schlaganfallpatienten maximal verwendet werden.

Die Stimulationsintensität wurde in dieser Arbeit stets über die Ladung der elektrischen Pulse eingestellt. Die Ladung bezieht sich dabei auf eine Phase des bipolaren Stimulus und ist durch Produkt von Stromstärke und Pulsbreite definiert. Daraus ergibt sich die Frage, wie eine geforderte Ladung durch Stromstärke und Pulsbreite konkret realisiert werden soll. In der Arbeit wurden verschiedene Verteilungen/Beziehungen zwischen Stromstärke und Pulsbreite experimentell mit dem Ziel verglichen, die Relation der Größen zu finden, welche für eine gewünschte Muskelkontraktion die kleinste Ladung erfordert und möglichst wenig Ermüdung verursacht. Das Ergebnis einer Studie mit gesunden Probanden war, dass Impulse mit hoher Stromstärke und kleiner Pulsbreiten vorzuziehen sind.

Table of Contents

ABSTRACT ..... **VIII**

ZUSAMMENFASSUNG IN DEUTSCHER SPRACHE ..... **XII**

TABLE OF CONTENTS ..... **XVI**

LIST OF FIGURES ..... **XX**

LIST OF TABLES ..... **XXIV**

ACRONYMS ..... **XXVI**

1. INTRODUCTION **1**

1.1. Motivation **1**

1.2. Neurological Diseases **2**
1.2.1. Stroke 3
1.2.2. Spinal cord injury 3

1.3. Skeletal Muscles **4**
1.3.1. Motor Unit (MU) 6
1.3.2. Recruitment of Motor Units 6

1.4. Functional Electrical Stimulation **8**
1.4.1. Limitations of FES 9
1.4.2. Benefits of FES in Neurological Rehabilitation 10

1.5. Electromyography **11**
1.5.1. Non FES-related Electromyogram 12
1.5.2. FES-related Electromyogram 12
1.5.3. Clinical Uses of Surface EMG 14

1.6. Contributions of the Thesis **14**

1.7. Thesis Outline **15**

1.8. Publications List **15**

2. EMG-CONTROLLED FES – A REVIEW **17**

2.1. Introduction **17**

2.2. Classification of EMG-Controlled Electrical Stimulation **17**
2.2.1. Biomimetic FES Patterns 18
2.2.2. EMG-triggered FES 18
2.2.3. EMG-driven FES 18

2.3. EMG Recording Combined with FES 19

2.4. Clinical Applications of EMG-Controlled FES 21
2.4.1. Rehabilitation of upper limb 21
2.4.2. Rehabilitation of lower limb 25

2.5. Summary and Outlook 29

3. STIMULATION DEVICE AND CHARGE CONTROL 31

3.1. Introduction 31

3.2. Stimulation Device 31
3.2.1. Pulse-Generation Modes 33

3.3. Charge-Control Modes 36
3.3.1. Mode-0 “Equally distributed normalized- pulse width and normalized current” 38
3.3.2. Mode-I “The Dominating Current Mode” 38
3.3.3. Mode-II “The Dominating Pulse width Mode” 39

3.4. Experimental Evaluations 40
3.4.1. Experimental procedure 40
3.4.2. Results 42

3.5. Conclusions and Discussion 43

4. EMG-AMPLIFIER DESIGN AND ELECTRODE DISCHARGING 45

4.1. Introduction 45

4.2. Basic Requirements of EMG-Amplifiers 45
4.2.1. Common Mode Rejection Ratio 46
4.2.2. Input Impedance 46
4.2.3. Signal to Noise Ratio 47
4.2.4. DC Signal Suppression 47

4.3. Typical EMG Pre-Amplifier 47

4.4. Design of the EMG-Amplifier “StiMyo” 50
4.4.1. EMG Pre-amplifier 51
4.4.2. Amplifier Protection and Electrode/Skin Discharging 54
4.4.3. Signal Processing 56
4.4.4. Active shielding and Reference Generator 57

4.5. Experimental Evaluation of the StiMyo Amplifier 58
4.5.1. Common Mode Rejection Ratio 58
4.5.2. Input Resistance of the Amplifier (R_{in}) 59
4.5.3. Signal to Noise Ratio (SNR) 62

4.6. Observations on Electrode Polarization and Fast Discharging 66
4.6.1. Electrode-Skin Model 67
4.6.2. Permanent Electrode/Skin Discharging 68
4.6.3. Discharging-Related Action Potential (D-wave) 71

4.6.4. Experimental Setup 74
4.6.5. Results on EMG Suppression 75
4.6.6. Observations on the Latency of D-wave 78

4.7. Discussion and Conclusions 80

5. APPLICATION OF EMG IN FES-CYCLING 83

5.1. Introduction 83

5.2. FES Cycling in Stroke Rehabilitation 84

5.3. Experimental Setup 87

5.4. Experimental Procedure and Data Analysis 91

5.5. Results 92

5.6. Discussion and Conclusions 95

6. EMG-DRIVEN FES OF WRIST–JOINT AND FINGER EXTENSORS 99

6.1. Introduction 99

6.2. Experimental Setup 100

6.3. Tuning of Timing-chart and High-Pass Filter Frequency 103
6.3.1. Experimental Procedure and Data Analysis 104
6.3.2. Results and Discussion 105

6.4. EMG-Proportional FES 109
6.4.1 Experimental Procedure and Data Analysis 110
6.4.2 Results and Discussion 113

6.5. EMG-Carried FES 117
6.5.1. Experimental Procedure and Data Analysis 119
6.5.2. Results and Discussion 120

6.6. Conclusions and Outlook 121

7. CONCLUSIONS AND OUTLOOK 123

BIBLIOGRAPHY 127

List of Figures

FIGURE 1. 1: THE CENTRAL NERVOUS SYSTEM (CNS) 4
FIGURE 1. 2: THE SPINAL CORD AND SPINAL NERVES..... 5
FIGURE 1. 3: THE CONTRACTILE CHARACTERISTICS OF FAST-TWITCH AND SLOW-TWITCH MUSCLE FIBERS 5
FIGURE 1. 4: THE MOTOR UNIT CONSISTS 6
FIGURE 1. 5: A TYPICAL TWITCH CONTRACTION IN RESPONSE TO A SINGLE STIMULUS. 7
FIGURE 1. 6: THE FORCE OF SKELETAL MUSCLE CONTRACTION CAN BE CONTROLLED VIA STIMULATION FREQUENCY 7
FIGURE 1. 7: HENNEMAN'S SIZE PRINCIPLE. 8
FIGURE 1. 8: NATURAL MUSCLE ACTIVATION VERSUS FES ARTIFICIAL MUSCLE ACTIVATION..... 10
FIGURE 1. 9: SAMPLE EMG SIGNALS..... 12
FIGURE 1. 10: ACTION POTENTIALS INDUCED BY ELECTRICAL STIMULATION. 13
FIGURE 1. 11: ELECTRICALLY ELICITED MUSCLE RESPONSE (M-WAVE). 13

FIGURE 2. 1: BLOCK DIAGRAM SHOWING THE PRINCIPLE OF EMG-DRIVEN FUNCTIONAL ELECTRICAL STIMULATION. 18
FIGURE 2. 2: BLOCK DIAGRAM FOR THE CREATION OF BIOMIMETIC STIMULATION PATTERNS. 21
FIGURE 2. 3: EMG-PROPORTIONAL CONTROL 23
FIGURE 2. 4: BLOCK DIAGRAM SHOWING A RECIPROCAL FES CONTROLLER 23
FIGURE 2. 5: THE SYSTEM DIAGRAM OF EMG-CONTROLLED FES FOR PATHOLOGICAL TREMOR SUPPRESSION. . 24
FIGURE 2. 6: RELATION BETWEEN THE RECORDED VEMG OF ONE MUSCLE DURING FES CYCLING AND THE APPLIED STIMULATION..... 25
FIGURE 2. 7: SCHEMATIC OF ABOVE-LESION EMG CONTROL OF FES..... 26
FIGURE 2. 8: BLOCK DIAGRAM SHOWING THE MEASUREMENT OF EMG AND THE APPLICATION OF FES TO THE TIBIALIS ANTERIOR TO CORRECT DROP-FOOT..... 28

FIGURE 3. 1: PORTABLE 8 CHANNEL REHASTIM PRO^{TM} STIMULATOR..... 32
FIGURE 3. 2: THE DEFINITION OF PULSE WIDTH AND CURRENT AMPLITUDE FOR A BIPHASIC PULSE. 32
FIGURE 3. 3: EXAMPLE SHOWING THE CONTINUOUS CHANNEL LIST MODE OF THE STIMULATOR. 35
FIGURE 3. 4: CHARGE CONTROL, THREE CHARGE-CONTROL MODES ARE ILLUSTRATED..... 36
FIGURE 3. 5: CHARGE CONTROL, THREE DIMENSIONAL ILLUSTRATION..... 37
FIGURE 3. 6: EXPERIMENTAL SETUP FOR EVALUATING DIFFERENT CHARGE-CONTROL MODES.. 41
FIGURE 3. 7: PI CONTROLLED WRIST-JOINT ANGLE..... 42
FIGURE 3. 8: THE PERCENTILE FATIGUE INDEX 43

FIGURE 4. 1: CIRCUIT DIAGRAM OF THE TYPICAL EMG PRE-AMPLIFIER. 48
FIGURE 4. 2: BLOCK DIAGRAM SHOWING ONE CHANNEL OF THE EMG STIMYO AMPLIFIER. 50
FIGURE 4. 3: THE RESISTOR DIODE CIRCUIT IS CLAMPING THE INPUT SIGNALS FROM ELECTRODES TO THE ± 5V SUPPLY. 51
FIGURE 4. 4: ANALYSIS OF THE AC-COUPLED INSTRUMENTATION AMPLIFIER. 52
FIGURE 4. 5: AC-COUPLED PRE-AMPLIFIER 53
FIGURE 4. 6: TIMING CHART SHOWING THE OPERATION OF THE DIFFERENT PHOTO-MOS SWITCHES..... 55
FIGURE 4. 7: ACTIVE SHIELDING..... 58
FIGURE 4. 8: MEASURED *CMRR* OF THE PRE-AMPLIFIER VERSUS INPUT FREQUENCY. 59
FIGURE 4. 9: CIRCUIT DIAGRAM SHOWING THE EXPERIMENTAL SETUP FOR THE EVALUATION OF STIMYO INPUT RESISTANCE. 60
FIGURE 4. 10: THE OUTPUT SIGNAL V_O VERSUS THE VALUE OF THE SERIES RESISTOR R_S..... 61
FIGURE 4. 11: BLOCK DIAGRAM SHOWING THE SIGNAL FLOW 62

FIGURE 4. 12: INTERACTION BETWEEN THE MEASURING WINDOW T_R AND THE PERIOD OF THE MEASURED SIGNAL T_{V_3} 64
FIGURE 4. 13: SAMPLE SIGNALS SHOWING THE DESIRED AND THE NOISE RELATED OUTPUT OF THE STIMYO DEVICE 66
FIGURE 4. 14: LINEAR ELECTRICAL MODEL WHICH REPRESENTS THE INTERFACE BETWEEN ELECTRODES/SKIN AND DEEP TISSUES 68
FIGURE 4. 15: DIAGRAM SHOWING THE CONNECTION OF THE PERMANENT DISCHARGING RESISTOR R_D 68
FIGURE 4. 16: DIAGRAM SHOWING THE INSTANTANEOUS VALUE OF Z_D. 70
FIGURE 4. 17: OPERATION OF S_2 (PERIODIC ELECTRODE/SKIN DISCHARGER) 71
FIGURE 4. 18: ELECTRODE/SKIN DISCHARGING PHASE, ($T_{D1} < T_{D2}$) 73
FIGURE 4. 19: ELECTRODE/SKIN DISCHARGING PHASE, ($Q_1 < Q_2$) 73
FIGURE 4. 20: THE EXPERIMENTAL SETUP FOR THE INVESTIGATION OF THE EFFECTS OF THE PERMANENT ELECTRODE DISCHARGER R_D ON EMG SUPPRESSION 75
FIGURE 4. 21: THE LEFT SIDE SHOWS EMG SUPPRESSION DUE TO ELECTRODE POLARIZATION 77
FIGURE 4. 22: THE EFFECT OF THE RESISTOR R_D UNDER NORMAL EMG RECORDING CONDITIONS 77
FIGURE 4. 23: SUPERPOSED INTERNAL AMPLIFIER SIGNALS DUE TO ($Q_1 < Q_2 < Q_3$) 78
FIGURE 4. 24: SUPERPOSED INTERNAL AMPLIFIER SIGNALS DUE TO SUDDEN CHANGE IN THE T_D PERIOD FROM 6 MS TO 7 MS 79
FIGURE 4. 25: SUPERPOSED INTERNAL AMPLIFIER SIGNALS DUE TO SUDDEN CHANGE IN THE T_D PERIOD FROM 8 MS TO 7 MS 79

FIGURE 5. 1: ANATOMY OF THE RIGHT LEG 86
FIGURE 5. 2: COMPUTER-CONTROLLED FES CYCLING ERGOMETER SYSTEM WITH INTEGRATED EMG MEASUREMENT FROM STIMULATION ELECTRODES. 88
FIGURE 5. 3: ONE STIMULATION PERIOD SHOWING STIMULATION PULSES FOR THE STIMULATED MUSCLE GROUPS AND THE TIMING CHARTS OF THE DIFFERENT PHOTO-MOS SWITCHES 88
FIGURE 5. 4: STATIC STIMULATION PATTERN 90
FIGURE 5. 5: TRAPEZOIDAL STIMULATION PATTERNS WITH UP AND DOWN RAMPS OVER 50 DEGREE CRANK ANGLE 91
FIGURE 5. 6: THE INTERNAL EMG AMPLIFIER SIGNALS (AFTER RECTIFICATION). 93
FIGURE 5. 7: EMG PROFILES OF THE HAMSTRING (H) AND QUADRICEPS (Q) OF THE LEFT LEG FOR ALL 94
FIGURE 5. 8: TANGENTIAL FORCES RECORDED AT THE LEFT CRANK ARM. 95

FIGURE 6. 1: THE EXPERIMENTAL SETUP SHOWING THE INTEGRATION OF STIMYO EMG-AMPLIFIER INTO A COMPUTER-CONTROLLED FES SYSTEM. 101
FIGURE 6. 2: ANATOMY OF THE POSTERIOR FOREARM MUSCLES 102
FIGURE 6. 3: PROTOCOL FOR A SINGLE EXPERIMENTAL SESSION DURING THE TUNING PROCESS OF THE STIMYO DEVICE 105
FIGURE 6. 4: PERFORMANCE INDEX PI_{AMP} FOR DIFFERENT SETTINGS OF THE STIMYO AMPLIFIER 107
FIGURE 6. 5: INTERNAL AMPLIFIER SIGNALS DURING MAXIMAL STIMULATION WITHOUT VOLITIONAL MUSCLE ACTIVITY 108
FIGURE 6. 6: BLOCK DIAGRAM OF EMG-PROPORTIONAL FES 109
FIGURE 6. 7: EXPERIMENTAL PROTOCOL TO DETERMINE Q_{MIN}, Q_{MAX}, $vEMG_{MIN}$ AND $vEMG_{MAX}$ 111
FIGURE 6. 8: EXPERIMENTAL PROTOCOL FOR EVALUATION OF THE EMG-CONTROLLED FES 112
FIGURE 6. 9: CONTRACTION GAINS AT THE DIFFERENT WRIST-JOINT EXTENSION WITH AND WITHOUT FES SUPPORT 115
FIGURE 6. 10: RESULTS OF A TRACKING EXPERIMENT FOR SUBJECT 1 116
FIGURE 6. 11: RESULTS OF A TRACKING EXPERIMENT FOR SUBJECT 2 117
FIGURE 6. 12: THE BLOCK DIAGRAM OF THE EMG-CARRIED FES SYSTEM. 118
FIGURE 6. 13: BLOCK DIAGRAM OF EMG-CARRIED FES CONTROLLER 119

FIGURE 6. 14: THE OPERATION OF EMG-CARRIED STIMULATION. 119
FIGURE 6. 15: EXPERIMENTAL PROTOCOL FOR INVESTIGATING THE EMG-CARRIED FES CONTROLLER. 120
FIGURE 6. 16: RESULT OF THE EXPERIMENTAL EVALUATION OF EMG-CARRIED FES FOR ONE SUBJECT. 121

List of Tables

TABLE 1. 1: IMPORTANT PROPERTIES OF DIFFERENT MUSCLE FIBERS. 4

TABLE 3. 1: TECHNICAL DETAILS OF THE STIMULATION DEVICE 32
TABLE 3. 2: THE AVERAGE STIMULATION CHARGE Q_o^{AV} AND THE FATIGUE INDEX $F\%_{AV}$ FOR ALL SUBJECTS USING CHARGE-CONTROL MODE-I AND MODE-II. 43

TABLE 4. 1: *CMRR* OF THE PRE-AMPLIFIER CALCULATED AT DIFFERENT FREQUENCIES. 59
TABLE 4. 2: MEASUREMENT OF INPUT RESISTANCE, V_{OUT} VS. R_S 62
TABLE 4. 3: SIGNAL TO NOISE RATIO IN DECIBEL AT DIFFERENT HPF FREQUENCIES. 66
TABLE 4. 4: THE TOTAL DISCHARGING IMPEDANCE Z_D FOR ALL POSSIBLE STATES OF THE SWITCHES S_1, S_2 AND S_D. 69
TABLE 4. 5: PERFORMANCE INDEX *PI* REPRESENTING THE RATIO BETWEEN $vEMG_{AV}$ AND THE AVERAGE WRIST-JOINT ANGLE Θ_{AV}. 78

TABLE 5. 1: DIFFERENT SUB-TESTES WHICH ARE CARRIED OUT DURING FES CYCLING EXPERIMENTS. 92
TABLE 5. 2: STIMULATION PATTERN DEFINED BY ANGULAR RANGES OF THE CRANK FOR A CADENCE OF 30 RPM. 92
TABLE 5. 3: AVERAGE EMG VALUES FOR THE LEFT QUADRICEPS (EMG_{LQ}) AND LEFT HAMSTRING (EMG_{LH}) AS WELL AS AVERAGE TANGENTIAL FORCES AT THE LEFT CRANK DURING KNEE EXTENSION (F_{EXT}) AND FLEXION PHASE (F_{FLEX}). ALL VARIABLES ARE NORMALIZED WITH REGARD TO THE AVERAGE VALUES OF SUB-TEST A (VOLITIONAL CYCLING WITHOUT STIMULATION). 94

TABLE 6. 1: EXPERIMENTAL SESSIONS TOGETHER WITH THE APPLIED TIME PERIODS T_D AND T_R. 104
TABLE 6. 2: STIMYO PERFORMANCE INDEX FOR DIFFERENT HPF FILTER FREQUENCIES COMBINED WITH DIFFERENT TIMINGS OF THE ELECTRODE/SKIN DISCHARGING TIME T_D AND EMG RECORDING TIME T_R. 106
TABLE 6. 3: PARAMETERS OF THE EMG-PROPORTIONAL CONTROLLER AND TRACKING TEST RESULTS FOR THE 5 SUBJECTS (S). 114

Acronyms

A/D	Analog to Digital converter
AON	All-Or-None
AP	Action Potential
ASS	Artificial Support System
ATP	Adenosine Tri-phosphate
BFB	Biofeedback
CD	Common Drive
CMRR	Common Mode Rejection Ratio
CNS	Central Nervous System
DSP	Digital Signal Processing
ECR	Extensor Carpi Radialis
EMG	Electromyography
ES	Electrical Stimulation
FCR	Flexor Carpi Radialis
FES	Functional Electrical Stimulation
FES-LCE	FES Leg Cycle Ergometry
FF	Fast Fatigue
FNS	Functional Neuromuscular Stimulation
FR	Fatigue Resistance
iSCI	incomplete Spinal Cord Injury
LED	Light Emitting Diode
MAP	Membrane Action Potential
MOS	Metal-Oxide Semiconductor
MTU	Motion Tracking Unit
MU	Motor Unit
MVC	Maximum Voluntary contraction
OSNR	Operative Signal to Noise Ratio
PSD	Power Spectral Density
PRT	Physiotherapy Rehabilitation Technique
RC	Reciprocal Control
RF	Radio Frequency
RMS	Root Mean Square
sEMG	Surface Electromyography
SCI	Spinal Cord Injury
TA	Tibialis Anterior

µC	Microcontroller
vEMG	Volitional Electromyography

Chapter 1

1. Introduction

1.1. Motivation

Stroke or “brain attack” is a major cause for disability and death in Western countries. The World Health Organization (WHO) reported that an estimated 17.1 million people died from Cardiovascular Diseases (CVD) in the whole world in 2004, representing 29% of all global mortality. Of these deaths, an estimated 7.2 million were due to coronary heart disease and 5.7 million were due to stroke. 82% of CVD deaths take place in low and middle income countries and occur almost equally in men and women. By 2030, almost 23.6 million people will die from CVD, mainly from heart disease and stroke. These are projected to remain the single leading causes of death. The largest percentage increase will occur in the Eastern Mediterranean Region[1]. In the EU, about one million first ischemic strokes occur each year [1]. In Germany about 250 thousand people suffer a stroke each year [2], and 110 thousand in the UK[2].

Approximately two-third of the stroke patients survives and requires neurological rehabilitation. The neurological rehabilitation is to help the patient to re-learn the movement skills that are lost when a part of the brain was damaged. The brain has the ability to re-learn the functions lost due to stroke and this is known as “brain plasticity”. The re-learning process of the brain is a repetition-based task. The brain needs the motor function to be repeated for large number of times to regain the lost skills and to become able to redo it voluntarily. During the neurological rehabilitation programs, usually the physiotherapist has to move the patient’s paralyzed hand or leg in a repetitive way. Such a rehabilitation program may take weeks or months.

Fortunately, the paretic muscles in stroke patients and those having incomplete Spinal Cord Injury (iSCI) remain innervated and can be activated by applying Functional Electrical Stimulation (FES) which can produce strong enough muscle contractions. FES has been used to support physiotherapists in performing the repetition-based rehabilitation tasks. Residual motor functions can be observed from paretic muscles in stroke patients and those having iSCI. In neurological

[1] *http://www.who.int/mediacentre/factsheets/fs317/en/index.html*
[2] *http://www.dh.gov.uk/en/Healthcare/Stroke/index.htm*

rehabilitation it is of high interest to investigate the residual motor function by means of Electromyography (EMG) when applying FES. EMG could be used to control the functional electrical stimulation according to the patient's residual motor functions or to monitor any muscle activity not directly related to FES. This would allow the online detection of volitional muscle coordination or unwanted spastic reactions. However, most existing FES systems are not able to measure EMG during an active stimulation between the stimulation pulses. Reasons for this are many: the possible damage of the EMG amplifiers caused by the high voltage electrical pulses, measurement artifacts caused by the stimulation and the suppression of EMG signals due to electrode polarization. These difficulties are even more pronounced when EMG has to be directly acquired from stimulation electrodes. No satisfactory solution is available for this case at the moment.

This chapter is organized as follows: Two main neurological diseases causing motor impairment are presented in the next section. Section 1.3 will introduce the basic terminologies of the skeletal muscles and physiological recruitment of motor units. The definition of FES is given in Section 1.4, and that of EMG is presented in Section 1.5. Section 1.6 is summarizing the contributions of this thesis and gives a short outlook. Section 1.7 is showing the outline of the thesis. In Section 1.8, the publications that have been originated from this work are listed.

1.2. Neurological Diseases

As shown in Figure 1.1 the brain and the spinal cord form the Central Nervous System (CNS). The branching nerves that supply the body parts are called the peripheral nervous system. The nerve bundles branching out from the spinal cord are known as spinal nerve roots. When we decide to make a movement, motor signals emerge from the brain and travel to the limbs through the spinal cord. Other signals known as sensory signals start at a limb, the trunk, or the head and carry electrical messages about muscle tension and length, touch, pressure or pain back to the brain. To achieve a certain action a variety of mechanisms which regulate the skeletal muscle activity are needed. The sum of these mechanisms is known as **motor control** and lies in both the brain and the spinal cord. The spinal cord initiates reflexes, and contains sub-routines for coordinated muscle movements such as walking. The brain controls voluntary movement, and commands the actions of the spinal cord which controls execution of the sub-routines. For example, to walk, the brain must initiate the command to walk, but the spinal cord handles many of the low level logistics such as balance and the sequence of motions [3], [4].

Any damage in the CNS components could lead to neurological diseases and motor impairment. Stroke is leading to a brain damage while SCI leads to the damage of spinal cord.

1.2.1. Stroke

The most accepted definition of stroke is a clinical syndrome characterized by rapidly developing clinical symptoms and/or signs of focal and at times global loss of cerebral function, with symptoms lasting longer than 24 hours or leading to death, with no apparent cause other than vascular [5]. Symptoms can be a weakness or paralysis of a limb, or the sudden inability to speak. The carrier of the brain's nutrition and oxygen is the blood flow; any interruption to the brain's blood flow could result in sudden neurological deficits. For example, unconsciousness could happen due to only 10 seconds of cerebral blood flow interruption. Neurological deficits are reversible if sufficient blood flow is restored immediately, otherwise it may be permanent.

There are two categories of stroke: those caused by a blockage of a blood vessel in the brain or neck (**ischemic**) and those caused by bleeding (**hemorrhagic**). Ischemic stroke is the most frequent type of stroke. Stroke may cause a lot of disabilities. The type and degree of disabilities depend upon which area of the brain was damaged. Problems in controlling movements (motor control) are the most common disabilities resulting from stroke. The paralysis that is caused by stroke is usually on the side of the body opposite to the side of the brain damage. Stroke may affect the face, an arm, a leg, or the entire side of the body. **Hemiparesis** is one of disabilities following stroke and is defined as a weakness of one side of the body or partial paralysis. Stroke may also lead to more severe symptoms such as the complete paralysis of one body side also known as **Hemiplegia**. Muscle immobility after stroke leads to muscle **Spasticity**. Spasticity is a condition in which muscles are continuously contracted[3], a form of muscle hypertonic. There is a resistance to passive stretch of a spastic muscle which starts with a minimal initial resistance at the beginning of the stretching followed by an incremental increase in muscle tone. The tone increases proportionally to the velocity of stretch. Spasticity can be clinical assessed by the Ashworth scale. Spasticity related muscle contractions cause stiffness or tightness of the muscles and may cause difficulties in performing movements. The degree of spasticity varies from mild muscle stiffness to severe, painful, and uncontrollable muscle spasms. Spasticity often interferes with rehabilitation in patients with upper neuron diseases like stroke or SCI, and often interferes with daily activities.

1.2.2. Spinal cord injury

Spinal cord injury refers to an injury to the spinal cord which is shown in Figure 1.2. In [6] Bromley has summarized the causes of SCI and the neurological disabilities following it. It is mainly resulting from traumatic cases such as road traffic accidents, work accidents, sport-related injuries

[3] http://www.ninds.nih.gov/disorders/spasticity/spasticity.htm

and accidents at home. The non-traumatic cases are transverse myelitis, tumours and vascular accidents. Those reasons can cause damage to nerve roots or myelinated fiber tracts that carry signals to and from the brain. Based on the SCI lesion level the patient may suffer either quadriplegia or paraplegia, and the lesion may be complete or incomplete. **Quadriplegia** is also known as Tetraplegia and refers to the impairment or loss of motor and/or sensory function in the cervical segments of the spinal cord due to damage of neural elements within the spinal canal. Quadriplegia results in an impairment of function in the arms as well as in the trunk, legs and pelvic organs. The term **Paraplegia** refers to the impairment or loss of motor and/or sensory function in the thoracic, lumbar or sacral segments of the spinal cord. With paraplegia, arm function is spared, but depending on the level of injury, the trunk, legs and pelvic organs may be involved.

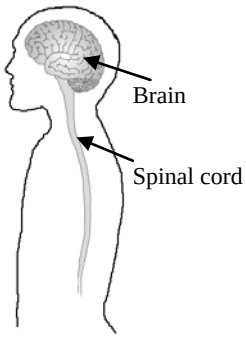

Figure 1. 1: The central nervous system (CNS) is formed by the brain and the spinal cord.

1.3. Skeletal Muscles

Skeletal muscles are named for their connection to skeletal bones. Skeletal muscles are mainly composed of three fiber types [7-9]. Type I is a slow twitch fiber that is found in high proportions in the postural muscles of the back, where slow sustained contractions are necessary. Type II is a fast twitch fiber and may be subdivided into two subtypes: Fatigue-Resistance (FR) fibers (type II-A), and Fatigable Fibers (FF) (type II-B). Main properties of different muscle fibers are listed in Table 1.1, and Figure 1.3 is showing the relative size and the contractile properties of different muscle fiber types.

Table 1. 1: Important properties of different muscle fibers.

Fiber type / specifications	Type I	Type II-A	Type II-B
Firing stimuli threshold level	High	High	Low
Associated nerve axon size	Small	Small	Large
Twitch speed	Slow	Fast	Fast
Fatigability	FR	FR	FF

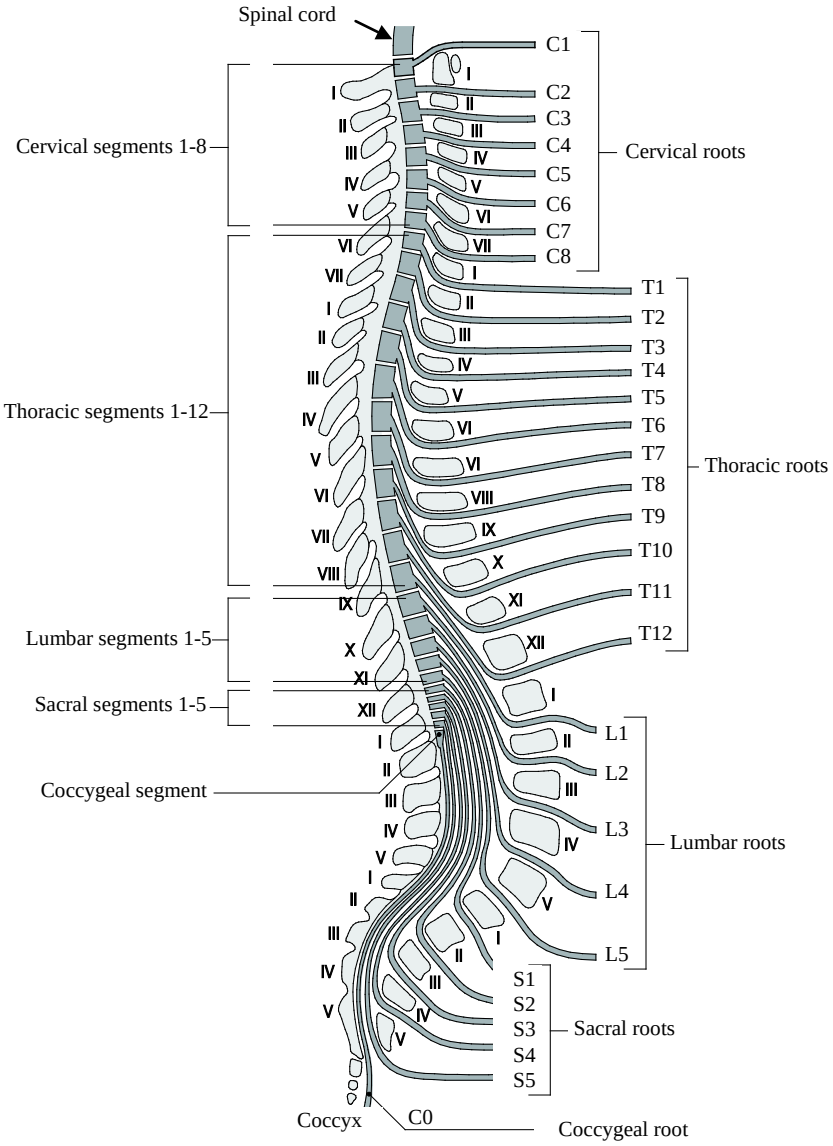

Figure 1. 2: The spinal cord and spinal nerves.

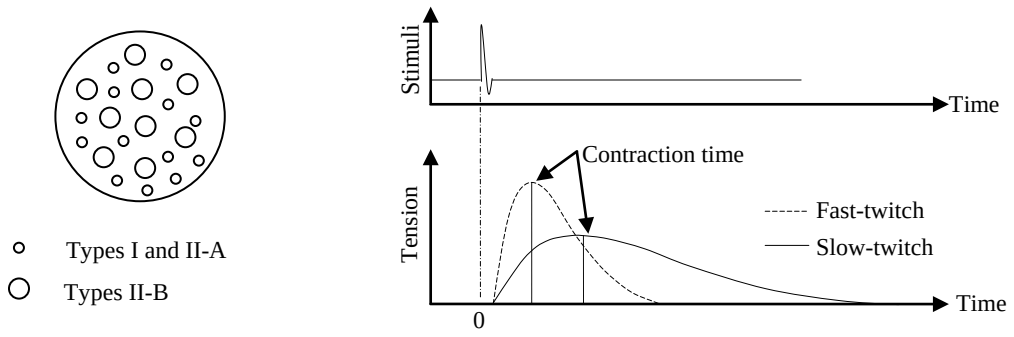

Figure 1. 3: Left side is showing the relative size muscle fibers, on the other side, the contractile characteristics of fast-twitch and slow-twitch muscle fibers are shown. The contraction time is the time from onset of the stimulus to the instant of peak force.

1.3.1. Motor Unit (MU)

The Motor Unit (MU) is the smallest unit for force generation. Each fiber of a muscle can contribute to the force generation when it is recruited by the brain. One motoneuron can branch into tens, hundreds, or even a thousand branches, each branch terminating at a different muscle fiber of the same type. The more precise definition is that a motor unit consists of an alpha-motoneuron cell body within the spinal cord, the motor axon, and all branches plus all muscle fibers it innervates. A simplified schematic diagram showing a motor unit is given in Figure 1.4.

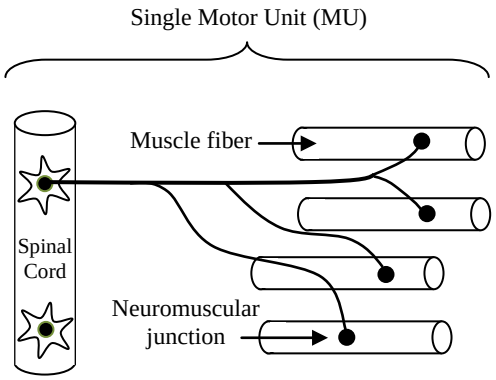

Figure 1. 4: The motor unit consists of a single alpha-motoneuron and all the muscle fibers it innervates (adapted from [10]).

For MU fibers to be contracted, an electrical signal from the CNS must first reach the alpha-motoneuron which is responsible for initiating the muscle contraction. As the contraction signal spreads from the alpha-motoneuron across the muscle fiber, a series of electrophysiological and electrochemical processes take place. This produces an electrically measurable de-polarization and re-polarization event known as the Action Potential (AP) [10]. The AP is important as it carry information within the body by means of diffusion. The intensity of muscle contraction is controlled by how often the nerve impulses arrive and innervate muscle fibers, i.e. as the AP arrives more often the muscle contracts harder.

1.3.2. Recruitment of Motor Units

The terminal branches of α-motoneuron axons are normally in a ‘one-to-one’ relationship with their muscle fibers: a muscle fiber receives only one terminal branch, and any terminal branch innervates only one muscle fiber. When an α-motoneuron is excited, an AP propagates along the axon and its

terminal branches to all related muscle fibers. The passage of a single action potential through a motor unit elicits a twitch contraction that lasts 25-75 ms [7]. Figure 1.5 is showing a typical twitch contraction in response to a single stimulus.

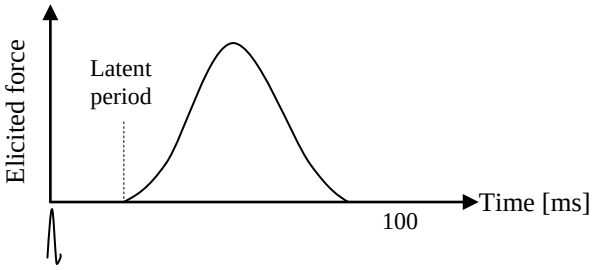

Figure 1. 5: A typical twitch contraction in response to a single stimulus.

According to the All-Or-None (AON) principle, the strength by which a muscle fiber is responding to the stimulus is independent of the stimulus amplitude [11]. However, the motoneuron can deliver a second stimulus before the muscle fiber relaxes. This induces the muscle fiber to contract again, building the tension to a higher level. Because of this mechanical summation, a sequence of impulses can evoke a larger force than a single impulse. This means that, the higher the stimulation frequency the more produced muscle force, as shown in Figure 1.6. The rates of sustained firing of motor units are commonly from 8 Hz to 35 Hz. The CNS controls the force of muscle contraction by changing the number of recruited motor units and/or by controlling the firing rate of the already recruited motor units [12].

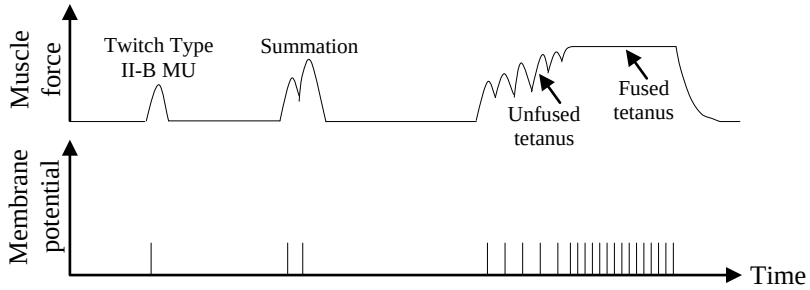

Figure 1. 6: The force of skeletal muscle contraction can be controlled via stimulation frequency. A sequence of action potentials may lead to sustained contraction (tetanus). At high frequent action potentials, individual contractions may fuse, creating a smooth tetanus.

Between 1964 and 1965 Henneman was formulating a principle known as "**size principle**" [13-15]. The size principle states that the recruitment of motor units within a muscle proceeds from slow twitch motor units to fast ones. That is, if a person contracts a muscle at a low force, nearly all the force will be produced by the slowest motor units (Type I). If the contraction force is to be increased the larger motoneurons starts to fire. This is recruiting the larger motor units. The recruitment curves explaining the Henneman size principle are shown in Figure 1.7.

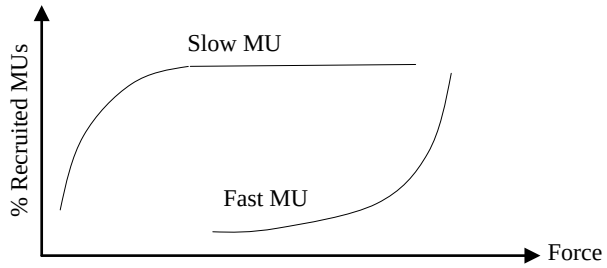

Figure 1. 7: Henneman's size principle. Small motor units are recruited first at low muscle forces. An increase in muscle force leads to recruitment of larger, faster, motor units [16].

1.4. Functional Electrical Stimulation

FES is a technique used to produce contractions in paralyzed muscles by the application of small electrical pulses to the nerve innervating the paralyzed muscle. The main components of clinical FES systems are the electrodes, the stimulator, and sensors or switches. The sensors or switches control the starting and stopping of the stimulation pulses supplied by the stimulator.

The application of FES does not reverse paralysis itself. However, it assists the weak bio-signals in stroke patients and substitutes the absent signals in SCI. In both cases FES induced afferent-efferent stimulation together with cutaneous and proprioceptive inputs could be important in "reminding" subjects how to perform the movement properly. Indeed, this complete afference of the task could enhance the synaptic controls and modify the excitability of specific motor neurons, thus, facilitating the re-organization of the motor schemes and accelerating the process of functional recovery. Such effects of FES have already been described in literature concerning the stimulation of the upper extremity and FES for drop foot treatment in stroke survivors [17].

Functional electrical stimulation is effective only if the target muscles are undamaged and innervated. For this reason FES can be used in Stroke patients, T12 and above SCI[4], Multiple Sclerosis (MS), Parkinson's disease, Cerebral Palsy (CP), familial or hereditary spastic paraparesis, and head injury [18]. In these conditions paralysis is due to lesion in the upper motor neuron, while the lower motor neurons innervating muscles are intact. FES can also be used when muscle weakness is present due to immobilization after surgeries. In case of muscle denervation, FES pulses will not cause muscle contraction because the nerve-muscle connection is broken. Much higher stimulation intensities are then required to directly stimulate muscle fibers. However this is not the case in stroke patients.

In recent years, medical scientists and engineers have invented several methods and devices to assist the paralysed individuals via FES. A survey of FES application in neurological rehabilitation may found in [19]. FES has been used to assist patients having stroke and SCI to restore or improve the motor control for example during standing and/or walking [20-31], and for cycling [32-39].

1.4.1. Limitations of FES

Although FES can elicit strong and effective muscle contractions, significant limitations exist. With FES, the action potentials of different motor units are triggered simultaneously. This is different from the recruitment of MUs by the CNS which activates motor units asynchronously. Figure 1.8 illustrates the differences in recruitment between the electrically stimulated muscle and the muscle activated by the CNS.

According to the size principle, the physiological recruitment of motor units within a muscle proceeds from slow-twitch motor units which are FR, to the fast-twitch ones FF. Thus, the FR motoneurons are mostly responsible for the production of low muscle contraction. The fatigable motoneurons start to fire if the contraction force is required to be increased.

In FES recruitment, low muscle contraction is achievable by using low FES intensity. Referring to Table 1.1, low FES levels activate the lower firing stimuli threshold MUs which are close to the stimulation electrodes. Unfortunately those are mainly the fatigable MUs (type II-B). As the intensity of FES increases the fatigue resistance MUs type I and type II-A (with higher firing thresholds) start to fire, as well as the deep type II-B motor units. In addition to this, a constant FES for the same electrode position activates the same motor units all the time. This results in an early fatigue of the electrically stimulated muscles. Thus, the recruitment with FES starting with fatigable MUs is thought to be inverted [40]. Residual sensation of stroke patients may limit the tolerated stimulation intensity and therefore the amount of force that can be produced by FES in stroke

[4] http://www.odstockmedical.com/patientssite/whocanbenefit.html

patients. Figure 1.8 illustrates the differences in motor unit recruitment for muscle contractions under FES and voluntary control.

1.4.2. Benefits of FES in Neurological Rehabilitation

Generally, the artificial activation of the paralyzed or paretic muscles by FES may slow or prevent the effects of muscle atrophy by keeping the weakened muscles active [41-44]. The application of FES may prevent or reduce pressure sores which represent a common problem for patients who are bound to wheelchairs, beds and other equipment that results in constant pressure being applied to certain areas of the body [45], [46]. FES applications can be also used as a cardiovascular training [47-49]. A comprehensive overview of the clinical use of FES for functional and therapeutic applications in subjects with stroke and SCI can be found in [17]. In stroke patients, FES can be used to retrain the motor functions in order to compensate, totally or partially, the lost motor functions. In this case the benefits are often remaining even after the stopping of FES application. FES can also take place in SCI subjects where the communication between the brain and the lower motor neurons is broken. In SCI the FES should permanently replace the natural motor control. The application areas contain for example the stimulation of hand functions, arm control, walking/standing movements and recumbent cycling.

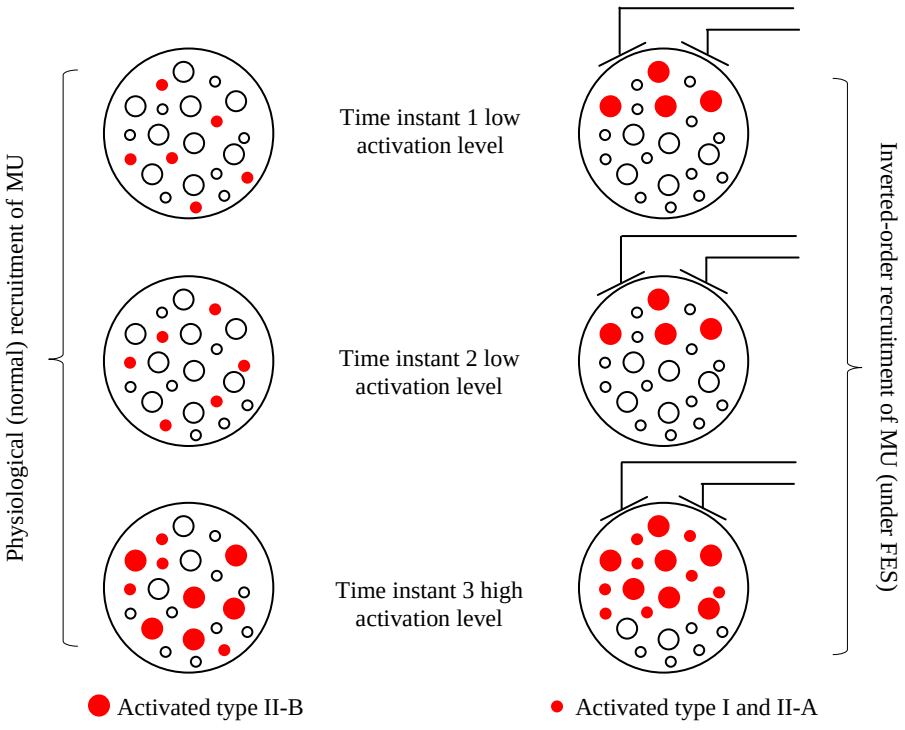

Figure 1. 8: Natural muscle activation versus FES artificial muscle activation [50].

1.5. Electromyography

The Electromyogram (EMG) recorded during Electromyography (EMG) is based on the linear propagation of the APs along muscle fibers. EMG literally means recording the electrical activity of the muscle cell membrane [51]. EMG is useful in the fields of both medicine and engineering and can be measured by surface electrodes attached to the skin surface over the target muscle (interferential), or invasively using thin needle electrodes (with a diameter of less than 1mm) inserted into the muscle tissues (intramuscular). Needle electrodes detect the action potentials from a few fibers, whereas surface EMG (sEMG) electrodes measure the summation of all action potentials in the muscle fibers within their recording area. The electrode function is to pick up the APs generated during muscle contraction due to the firing of motor units.

sEMG detection is based on the relative difference in surface voltages as the AP moves. Interferential EMG is more frequently used in the studies of neurological rehabilitation, since it is non-invasive and can be conducted by staff other than the medical doctors with minimal risk to the subject. Two electrodes are taped on the skin over the muscle belly to sum up the activity of the motor units which is lying under the electrodes. The difference of potential between the two electrodes is fed to a bio-signal amplifier to rescale it. Using large electrodes the activity of many muscles will be summed up. In many studies researchers want to focus on a single muscle and to avoid recording the muscle activity from its neighborhood. Each muscle is composed of different types of muscle fibers (fast and slow twitch fibers). This makes the Power Spectral Density (PSD) and the amplitude of EMG highly variable. The position of electrodes is usually affecting amplitude and PSD of the EMG signals. Thus placement of electrodes is a very important issue. If the electrodes are too close together a very low or no action potential will be recorded as the voltage under both electrodes will change simultaneously. However, greater distance between the electrodes also causes more filtering to occur. If a series of action potentials has a wavelength equal to the distance between electrodes no differential will be recorded. By using surface electrodes the action potentials from different muscle fibers are collected together, all on top of each other (named cross-talk). The EMG signal appears as a small electrical current generated by muscle fibers prior to the production of muscle force.

Different types of electromyograms can be observed on an electrically stimulated muscle which can be caused by FES-related contractions and non FES-related contractions. The second part can be divided into a volitional electromyogram (vEMG) which is related to the intended movement of the patient and a non-volitional component which appears due to muscle abnormality such as spasticity.

1.5.1. Non FES-related Electromyogram

The sEMG signals related to volitional muscle activity and spasticity have amplitudes ranging from µV to some mV [8]. These EMG signals can be treated as random signals, while the main power spectrum energy is located between 30 and 300 Hz, with the dominant energy being at 120 Hz [52]. The amplitude (intensity of the random signal) is directly related to the strength of non-FES muscle contraction.

An example for sEMG signals measured at the Tibialis Anterior (TA) muscle during several contractions is presented in Figure 1.9.

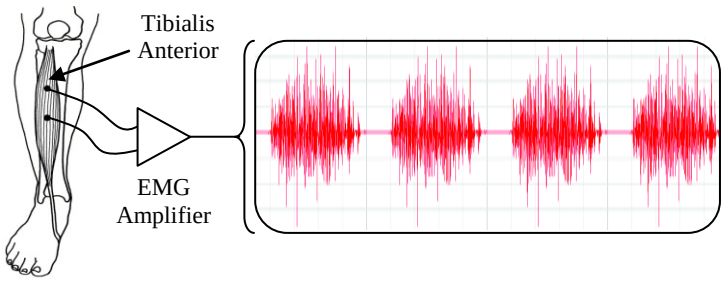

Figure 1. 9: Sample EMG signals detected from the tibialis anterior (TA) muscle.

1.5.2. FES-related Electromyogram

The FES-related Electromyogram is linked to all muscle contractions directly caused by FES. During the application of FES, the action potentials induced by the stimuli in the efferent nerves (motor nerves) travels in two directions (cf. Figure 1.10); the first AP called Orthodromic proceeds directly to the motor point of the muscle and generates the compound motor unit action potential, known as **M-wave**. This EMG signal is corresponding to the main response of the muscle to the stimuli. As several motor units will fire synchronously the AP of the MU will superpose. The amplitude of the M-wave can reach for this reason up to 100 mV. All FES-related EMG are more deterministic signals compared to the non FES-related EMG signals. As shown in Figure 1.11 the M-wave is an early muscle response that occurs a couple of milliseconds after the onset of stimulus. As the stimulus increases, the amplitude of M-wave increases as well.

The second FES-elicited AP in the efferent nerve is called antidromic. This part travels towards the cell body in the spinal cord and might be reflected to the motor nerve causing an AP which is known

as **F-wave**. Because of the increased traveling time, the F-wave appears after the M-wave in the EMG. F-wave cannot be volitionally repressed by the subject intention [53].

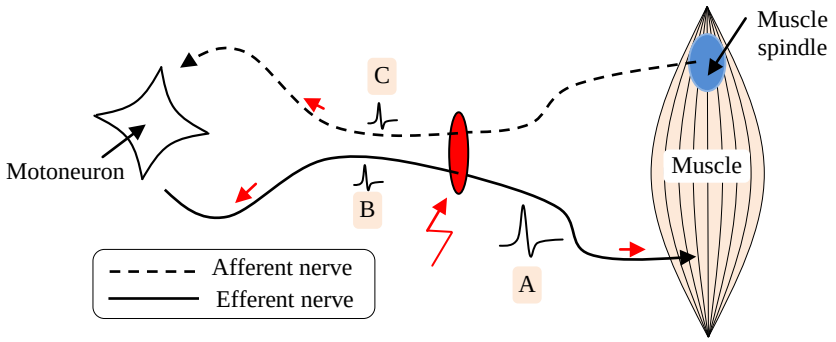

Figure 1. 10: Action potentials induced by electrical stimulation: “A” is an orthodromic AP causing M-wave; “B” is an antidromic AP causing F-wave and “C” is the AP induced in the sensory nerve causing H-reflex.

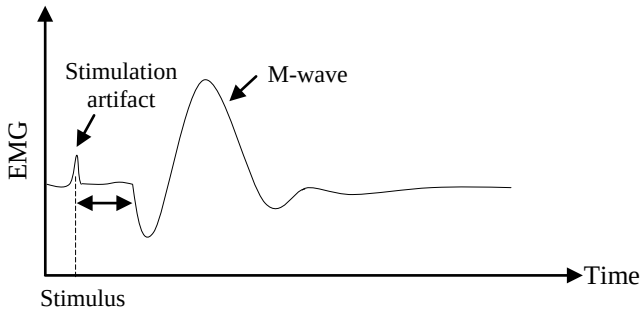

Figure 1. 11: Electrically elicited muscle response (M-wave).

The Hoffmann or **H-reflex** is a reflectory muscle reaction following the stimulation of its afferent nerves (sensory nerves). When applying stimuli with low intensity a clear wave, the so-called H-reflex, appears. The H-reflex will have a larger latency than the M-wave. Successive stimuli will inhibit the H-reflex in healthy people. This is usually not the case if the muscle suffers spasticity [54]. In contradiction to M-wave, the amplitude of H-reflex decreases for higher stimulation intensities. There is a point of minimal stimulation intensity where the M-wave is absent and the H-reflex is maximal while at supra-maximal stimulation the H-reflex disappears and M-wave reaches its maximum.

Under some circumstances, a Tendon (T) - reflex can be triggered when a muscle stretch is caused by a sudden stop of stimulation [10].

1.5.3. Clinical Uses of Surface EMG

The volitional EMG and FES-induced EMG responses such as M-wave can be used to study muscle fatigue. Muscle fatigue is usually accompanied with longer latency and amplitude reduction of M-wave [55] and changes in the PSD of EMG [8]. The amplitude of vEMG signal may be used as a biofeedback signal during rehabilitation or to assess motor coordination [56], [57].

1.6. Contributions of the Thesis

This thesis introduces a 4-channel EMG detecting device which is able to monitor the residual muscle activity from stroke and iSCI patients. The developed device is named StiMyo for its ability to measure myo-electric signals between stimulation pulses during FES. StiMyo is using mixed time and frequency domain filter approaches to extract the non FES-induced EMG from the recorded signal. The non FES-induced EMG during active FES is detected from the stimulation electrodes and used to control the stimulation intensity. To overcome the challenges facing EMG detection from FES electrodes, a switching circuit synchronized with the stimuli has been developed to prevent any amplifier damage due to stimulation pulses. After the delivery of each stimulation pulse, a fast discharging path is enabled to reduce the remaining charge under electrodes. This minimizes the saturation period of the pre-amplifier and reduces the effects of electrode polarization. An optional electrode/skin discharging resistor has been added to furthermore reduce the effects of electrode polarization in case of unbalanced pulses.

Two FES application of StiMyo device have been experimentally investigated. Experimental validation of the proposed methods was carried out in a pilot study with 5 neurologically intact subjects.

The first application was EMG-controlled FES of the wrist and fingers extensors. Thanks to the ability of StiMyo amplifier, volitional EMG could be measured between stimulation pulses and directly applied to control the charge of stimulation pulses continuously according to the measured vEMG. Two control approaches have been investigated. The first approach aims at exploiting as much as possible the residual motor control of the patient by quasi linear amplification of the detected vEMG. Therefore, a stimulation intensity which is proportional to the detected vEMG is applied. The results showed good ability for wrist-joint tracking tasks with less voluntary effort compared to pure volitional movements. In the second approach, the stimulation is initiated as soon vEMG goes above a defined EMG threshold and stays active until vEMG drops below a second

lower EMG threshold. To avoid spastic reactions by the stimulation, an adjustable ramping up and down of stimulation is implemented. In this control approach the patients must constantly contract a muscle to maintain a supportive, but constant, stimulation. The results related to both control approaches showed the feasibility of using vEMG to obtain an intention-related FES assistance.

The second application is FES-cycling on an ergo meter with an auxiliary electrical motor. The cycling movement is supported by timed electrical stimulation of the quadriceps and hamstrings muscle groups. In a pilot study with one healthy subject the feasibility to monitor non FES-related volitional muscle activity was demonstrated for typically used stimulation intensity in stroke patients.

Commonly one stimulation parameter (current amplitude or pulse width) is modulated as stimulation intensity while keeping the other variable constant. The selection of the right values is usually time-consuming so that an automatic mapping from a given charge to a pulse width and current amplitude has been used in this thesis. This technique is named charge control. Different distributions of pulse widths and current amplitudes have been experimentally compared with respect to the minimum charge required for maintaining a desired muscular action and with respect to muscular fatigue.

1.7. Thesis Outline

Chapter 2 is giving a review of the use of EMG in FES systems in clinical rehabilitation. Chapter 3 is introducing the concept of charge control and the stimulation device that was used during this work. The detailed design steps of the StiMyo amplifier, its experimental evaluation as well as some observations on electrode polarization are discussed in detail in Chapter 4. Chapter 5 shows the integration of StiMyo device in the FES-Cycling system, and presents the experimental results which prove the feasibility to monitor vEMG during FES-Cycling. EMG-Controlled FES of fingers is analyzed in Chapter 6. Conclusions and outlook for future work are given in Chapter 7.

1.8. Publications List

The results presented in this thesis have previously been published in the following articles:

[1] R. Shalaby, T. Schauer, W. Liedecke, and J. Raisch, “Amplifier design for EMG recording from stimulation electrodes during functional electrical stimulation leg cycling ergometry,” Biomedizinische Technik/Biomedical Engineering, vol. 56, no. 1, pp. 23-33, 2011.

[2] R. Shalaby, H. Nahrstaedt, T. Schauer, W. Liedecke, and J. Raisch, “Voluntary Muscle Activity Detection using a Single Pair of Electrodes for EMG-Controlled FES,” Proc. of the 14th Annual

Conference of the International Functional Electrical Stimulation Society (IFESS), Seoul, Korea: 2009, pp. 69–71.

[3] R. Shalaby, T. Schauer, and H. Nahrstaedt, “Gain-Scheduled EMG-Controlled Electrical Stimulation,” Proc. of the 13th Annual Conference of the International Functional Electrical Stimulation Society (IFESS 2008), Freiburg, Germany: 2008.

[4] H. Nahrstaedt, T. Schauer, R. Shalaby, S. Hesse, and J. Raisch, “Automatic Control of a Drop-Foot Stimulator based on Angle Measurement using Bioimpedance,” Artificial Organs, vol. 32, 2008, pp. 649-654.

Chapter 2

2. EMG-Controlled FES – A Review

2.1. Introduction

FES is the process of delivering sequences of small electrical pulses to stimulate paretic or paralyzed muscles in order to functionally contract. Most FES systems make use of pre-programmed stimulation profiles that are triggered manually or sensor-based. Often these types of FES systems necessitate the continuous attention of the patient and/or the physiotherapist for finger/hand manipulation [58]. A good example for a sensor-based triggering is the use of force resistive foot switches in FES-assisted gait. More sophisticated systems trigger the stimulation by detection of EMG related to intended movements of the patient. However, a major disadvantage of all existing clinical FES systems is that residual voluntary activity of the stimulated muscles is not continuously taking into account when controlling the stimulation intensity.

This chapter is reviewing methods in which electromyography has been exploited to control FES. The review will focus on approaches where the volitional EMG has been measured on the same limb where also the stimulation is applied.

This chapter is organized as follows: Different classes of EMG-based control are presented in Section 2.2. In Section 2.3, the difficulties related to EMG recording during stimulation will be discussed in detail. An overview of current research on EMG-controlled FES in stroke and SCI rehabilitation is given in Section 2.4. Section 2.5 contains a short summary of this chapter.

2.2. Classification of EMG-Controlled Electrical Stimulation

Related to FES control there are two questions: Which stimulation pattern has to be used and when should it be applied? Electromyography can be applied to answer both questions. In this subsection different approaches of EMG-based FES control will be classified under the assumption that the EMG is measured from muscles of the stimulated limb.

2.2.1. Biomimetic FES Patterns

Biomimetic FES patterns are derived from EMG signals which were recorded from healthy subjects performing certain movements. The created stimulation patterns can be applied to the patient's impaired muscles to elicit similar movements as in healthy people.

2.2.2. EMG-triggered FES

EMG-triggered FES involves the patient movement intention in the rehabilitation process. During EMG-triggered FES, movement intentions are measured in form of residual vEMG on the patient, while stimulation is not active. As soon as the patient's activity exceeds a pre-defined level of vEMG, a pre-programmed stimulation profile starts. However, the recording of EMG stops due to the difficulties related to the measurement of vEMG during electrical stimulation. The stimulation usually stays active for a pre-defined time interval and then stops automatically.

2.2.3. EMG-driven FES

In the EMG-driven FES, the volitional EMG of the patient is continuously monitored also during electrical stimulation and used to drive the FES. This method is representing the major scope of this thesis. Figure 2.1 depicts the basics of EMG-controlled FES in which the residual muscle activity is to be detected, processed and fed to the stimulator in the form of a control command. An adjustment of the stimulation intensity proportional to the vEMG is the most common form of EMG-driven FES. The weak movements of the patient are amplified by FES in a natural way. The EMG-driven FES is sometimes named power-assisted FES or locally driven FES.

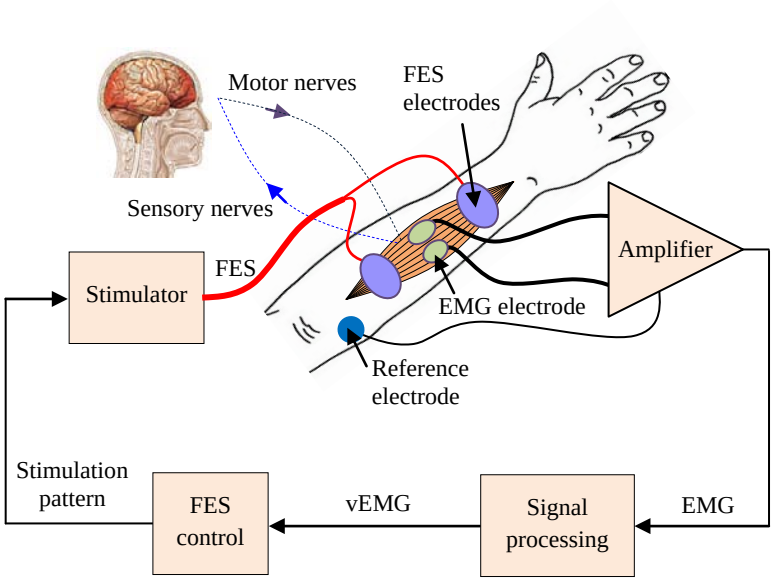

Figure 2. 1: Block diagram showing the principle of EMG-driven functional electrical stimulation.

2.3. EMG Recording Combined with FES

The detection of non-FES induced EMG activity (related to volitional movements or spasticity) during electrical stimulation (between the stimulation pulses) is problematic as large measurement artifacts occur [59]. The electrical stimulation pulses cause stimulation artifacts which may drive the EMG amplifier into saturation or even damage the amplifier; especially during FES cycling (cf. Chapter 5) where the stimulation intensity is relatively high. Parameters of electrical stimulation pulses used in FES cycling with stroke patients are as follows: current controlled bipolar pulses, pulse widths up to 500μs (one phase), stimulation frequency of 20 Hz, and current amplitudes up to 50 mA. To deal with the problem of stimulation artifacts, the EMG amplifier can either be disconnected from measurement electrodes (muted) when applying stimulation pulses [60-66] or must give a very fast recovery from input overloads [67]. After delivery of an electrical stimulation pulse, an asymmetrical charge might stay under the measurement electrodes. The related discharging process causes another measurement artifact. This artifact will be larger if EMG is directly measured from stimulation electrodes also due to their larger size. For this reason most existing systems are using separate electrodes for stimulation and EMG measurement.

Another problem in detecting volitional muscle activity and/or spasticity reactions represents the so-called M-wave resulting from a synchronous contraction of several motor units induced by the electrical stimulation pulses. The amplitude of this EMG signal part is generally in the range of several mV whereas the intensity of the volitional/spastic EMG components is usually in the range of μV. The M-wave starts a couple of milliseconds after the stimulus and has its mean activity within 20 ms after the stimulus. This artifact superposes the non-FES induced EMG which is of interest.

About 20 to 30 ms after a stimulation pulse, usually only lower frequency parts of stimulation artifacts remain (tails of discharging curve and M-wave) in the measured signal. These artifacts can be eliminated by applying a high-pass filter with a cutoff frequency reported in the range of 100 to 330 Hz [60], [64], [68]. It should be noted that the main frequency content of the spectral energy of the EMG is located from 30 to 300 Hz with a peak around 120 Hz [52]. By applying such a high-pass filter only higher frequency parts of the volitional/reflex EMG are taken into account. In the resulting signal, the period with filter transients and remaining stimulation artifacts is usually blanked (signal set to zero) before carrying out the standard EMG processing (rectification followed by a low-pass filter). The blanking period is usually from the onset of the stimulation pulse to about 20 to 30 ms after delivery of the stimulation pulse. Having a stimulation period of 50 ms for example, about 20 to 30 ms of non-FES induced EMG signal can be obtained.

When no other artifacts hide M-wave and non-FES induced EMG then the M-wave can be predicted from EMG recordings of old stimulation periods under the assumption that M-wave and non-FES induced EMG are not correlated [69-73]. Hence, the non-FES induced EMG may be determined by subtracting the estimated M-wave from the amplifier output. This represents an often used alternative to the high-pass filter approach outlined before. However, this requires complex digital signal processing. A simple, but not very precise, solution for direct estimation and extraction of the M-wave within one step is to use a comb filter which subtracts from the actual measurement during a stimulation period the identical sample of the previous stimulation period [69].

Several clinical studies have been published investigating the detection and use of non-FES induced EMG activity during FES (cf. Section 2.4). The aim of many studies was to amplify a weak movement intention of the patient by an electrical stimulation proportional to the measured volitional EMG. In most cases single channel EMG detection and stimulation systems were employed using five electrodes: two separate pairs of electrodes, one for stimulation and one for EMG detection, plus a single reference electrode. Extending this approach to multiple target muscles is not practical because of the large number of electrodes involved. Also attaching four surface electrodes for EMG and ES over small target muscles might be challenging.

Only a very limited number of articles describing EMG-recording systems from stimulation electrodes using switching circuits have been reported [61], [62], [64]. Kamono et al. [61], [62] developed a device for gait assistance that applies electrical stimulation via the EMG electrodes. The stimulation pulses were repeated at a rate of 15 Hz, and a micro-controller was used to switch electrodes between stimulation circuit and EMG amplifier. The authors did not provide detailed information about the timing sequence and/or measurement artifacts. However, from the low stimulation frequency it can be speculated that stimulation artifacts last so long that the standard stimulation frequency of 20 Hz could not be used. The large interval between stimulation pulses of 66.7 ms was probably selected to obtain sufficiently long artifact free EMG recording intervals. This solution is not acceptable in FES cycling since stimulation frequencies of 20 Hz and above are used.

Muraoka [64] developed a similar device that detects a volitional EMG interval of up to 25 ms for a stimulation period of 50 ms, but for a rather narrow frequency band (330 Hz ~ 460 Hz). During stimulation the stimulator is directly connected to the pre-amplifier terminals with the amplifier gain being set to zero. During measurement, the voltage controlled stimulator is disconnected from the stimulation electrodes. One possible reason for this action may be the low output resistance of the stimulator stage which may attenuate the EMG measurement.

The mentioned FES systems with EMG recording from the stimulation electrodes have only been applied for stimulation of dorsiflexor and upper limb muscles which require low stimulation intensity. It is therefore questionable, if the previously described EMG amplifiers work adequately for higher stimulation intensities, applied for example during FES cycling in stroke patients. For both devices, a quantitative assessment of signal quality was not performed. In [61], [62], [64] the presented volitional EMG activities were not linked to measured biomechanical values like forces or angles. Therefore it is hard to predict which level of residual volitional activity can be detected and which residual motor skills the patients must have to use the systems.

2.4. Clinical Applications of EMG-Controlled FES

2.4.1. Rehabilitation of upper limb

Matsushita et al. applied a biomimetic control strategy to generate stimulation patterns for hand grasping in C4 and C5 quadriplegics [74]. The authors presented a controller to restore hand- and wrist-joint functions. The aim was to control the joint angles in their functional ranges for grasping. To obtain wrist-joint fixation and grasping movement similar to that of healthy hands, volitional EMG from the left forearm of 15 healthy subjects was recorded and analyzed to construct standard FES patterns (cf. Figure 2.2).

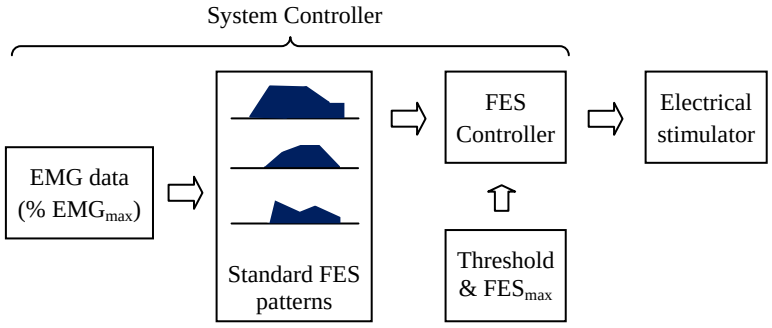

Figure 2. 2: Block diagram for the creation of biomimetic stimulation patterns. The standard FES patterns are based on the EMG from healthy subjects. Stimulation thresholds and maximum stimulation intensities are exclusive for each patient.

In clinical practice, EMG-triggered stimulation of the wrist and finger extensors is often used to improve brain relearning after stroke by reinstating proprioceptive feedback time-locked to each attempted movement [75], [76]. The movement intention is detected from EMG recordings using the stimulation electrodes while stimulation is not active. As soon as a patient exceeds a predefined level of EMG activity the electrodes are switched from the EMG amplifier input to the stimulator

output. Afterwards, a predefined stimulation pattern (pulse train) will be applied for a fixed time period to the patient. During this time interval there is no EMG recording possible. Several commercial devices for EMG-triggered stimulation are on the market.

In [68], a study investigating the continuous control of FES by means of vEMG detected from the stimulated paretic muscle or from another muscle was presented by Thorsen et al. The aim was to evaluate the functional improvement when using this method in terms of produced force and joint movement. The study involved six tetraplegic patients with a spinal cord lesion and one stroke hemiplegic patient. The residual volitional EMG signals from the paretic wrist extensor were used to control stimulation of either the same muscle or thumb flexion. EMG was always recorded using separate electrodes. Biphasic stimulation pulses were delivered with a fixed stimulation period of 60 ms. A digital comb FIR-filter was applied to suppress stimulation artifacts and M-wave. After each stimulation pulse the signal was muted for 20 ms which leaves 40 ms of EMG signals detectable in each stimulation interval. A subsequent bandpass filter emphasizes frequencies of 100–300 Hz. Finally, a moving average filter over 1.2 s was applied and an offset (base level of EMG) was subtracted to obtain the control signal. This control signal was multiplied by a gain factor to obtain the stimulation amplitude. The stimulation output was limited to between zero and an upper limit to protect the subject from excessive stimulation. A tracking test based on a visual feedback of the produced force or movement compared to a reference target trajectory was used to quantify the control accuracy. Results showed that the wrist extension was improved in three out of five C5 SCI patients and the thumb flexion was largely increased in one incomplete C3 SCI patient. The hemiplegic patient showed limited thumb control with the MeCFES but indicated the possibility of a carryover effect. It was found that a low residual natural force resulted in a less accurate movement but also with a large increase (up to ten times) of the muscle output. On the other hand, persons with a medium residual force obtained a smaller amplification of muscle force with a higher tracking accuracy. The general performance of the FES system was quite limited because the time delay introduced by the various filtering steps could also lead to system instability. Therefore only very slow movements will be supported by the controller.

The group lead by Rune Thorsten presented also a method for tenodesis grip enhancement in C6/C7 level SCI [77]. The used system contains again an amplifier, a signal processor, and a single-channel stimulator, similar to the setup described before. The EMG measured from wrist extensors was used to proportionally control the electrical stimulation of the extrinsic finger and thumb flexors. Control of FES was similar to the work outlined before. As shown in Figure 2.3, the signal level corresponding to the relaxed wrist extensors was set as ($EMG_{\min}$). The gain was chosen to produce $I_{\max}$ at the subject's full volitional wrist extension ($EMG_{\max}$). $I_{\max}$ corresponds to the maximum stimulation intensity which gives a desired force/movement.

In [78], an EMG-triggered grasping system for tetraplegics was presented by Saxena et al. The threshold of the processed volitional EMG of the wrist extensor muscle was used to switch the FES of forearm finger and thumb flexors on and off.

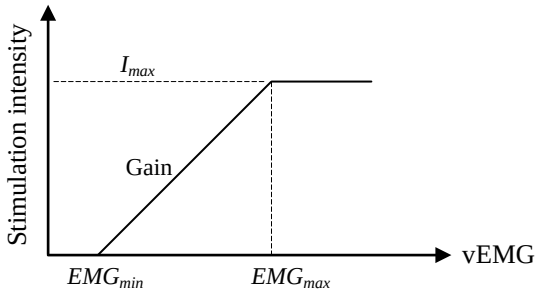

Figure 2. 3: EMG-proportional control used in SCI [77]. A piecewise linear function that defines the relation between vEMG level and stimulation intensity was used. The function is defined by the base vEMG level (EMG_{min}), maximum vEMG level (EMG_{max}), controller gain, and maximal stimulation level (I_{max}).

In [79], [80], the clinical use of EMG-proportional FES was investigated in the upper limb rehabilitation of chronic stroke patients. Motor function, spasticity and functional scores significantly improved after the interventions. Hara et al. [79] performed a controlled study on home rehabilitation over 5 months using a two-channel system with EMG measurement from the stimulation electrodes. The amplifier was based on the work by Muraoka, published in [64] and discussed in Section 2.3. In [79], [80] only the rehabilitation outcome was reported which represents the carry-over effect by the use of EMG-proportional FES therapy. Technical details on the tuning of the controller and its evaluation during the interventions are missing.

Giuffrida et al. [81] have investigated a reciprocal control (RC) scheme which employs biceps EMG to modulate triceps stimulation. In reciprocal control, increasing biceps vEMG proportionally reduces the electrical stimulation of triceps (cf. Figure 2.4). This reciprocal control is an effective method for restoring elbow extension in C5-C6 spinal cord injury patients as shown in [81].

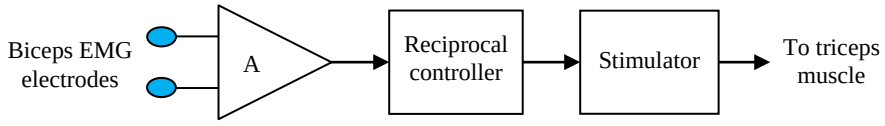

Figure 2. 4: Block diagram showing a reciprocal FES controller helping individuals with SCI to modulate stimulation intensity of triceps via vEMG detected at the biceps muscle.

In [82], Zhang et al. presented the idea of using EMG-controlled stimulation of biceps and triceps muscles to reciprocally compensate the effect of pathological tremor caused by the Parkinson disease. The purpose was to attenuate the tremor with minimum effects on the voluntary movement. A system with separated electrodes has been used to record electromyograms from biceps and triceps muscles and to reciprocally use the processed vEMG as feedback information to regulate FES of both muscles. The experiment was performed with neurologically intact subjects. The objective was to reduce limb vibration due to the tremulous motion while preserving the voluntary motion. The key problem involved with the tremor suppression is to distinguish the tremulous component from the voluntary motion in the EMG. The healthy subject was instructed to perform two types of movements. A voluntary forearm flexion and extension had to be performed over the range (0 – 90^o) with slow rhythm (less than 1 Hz). A tremor-like movement has been achieved by shaking of forearm as fast as possible in a range of (± 5^o) while the elbow joint was held at the 90^o angle (cf. Figure 2.5). To handle the detection problem, a two stage filter was proposed to process the raw EMG signals. The first stage was an FES artifact removing filter and the second was separating the high frequency tremulous-related EMG from the low frequency vEMG components.

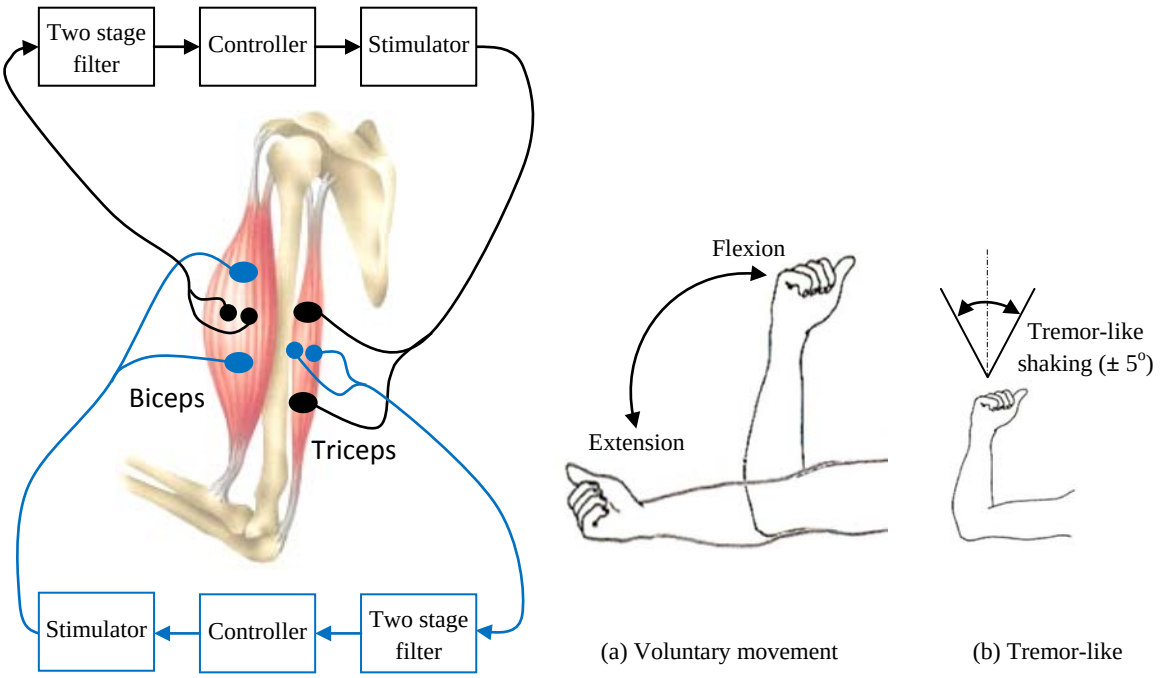

Figure 2. 5: The right side shows system diagram of EMG-controlled FES for pathological tremor suppression. In order to attenuate the tremulous motion, the extracted tremor-related EMGs which are recorded from biceps and triceps are used to reciprocally control the stimulation of biceps and triceps.

The extracted tremor-related EMG signals (from biceps and triceps) have been used as control inputs to stimulate the two muscles reciprocally. The results published in [82] showed a good FES artifact suppression for both volitional movements and tremor-like forearm shaking. But there was no information given about the separation of tremor EMG from that related to volitional movements. Also there is no information about the overlapping between the PSD of both signals, and how the system will respond under fast voluntary movements.

2.4.2. Rehabilitation of lower limb

Recently, Chen et al. [83] have used the intensity of the residual EMG to modulate the intensity of stimulation during FES-assisted cycling on an ergo meter in stroke patients. The recorded EMG signal of each muscle was divided into four suitable ranges as shown in Figure 2.6. According to the range of EMG the stimulation patterns determine when to stimulate and which muscle should be stimulated. The EMG was mapped to distinct levels of stimulation intensity as illustrated in Figure 2.6. The proposed method simply distinguishes between correct and incorrect muscle activation by comparing the activities of both legs to avoid activation of electrical stimulation due to incorrect muscle activation. For the EMG measurement, recording electrodes different from the stimulation electrodes were used.

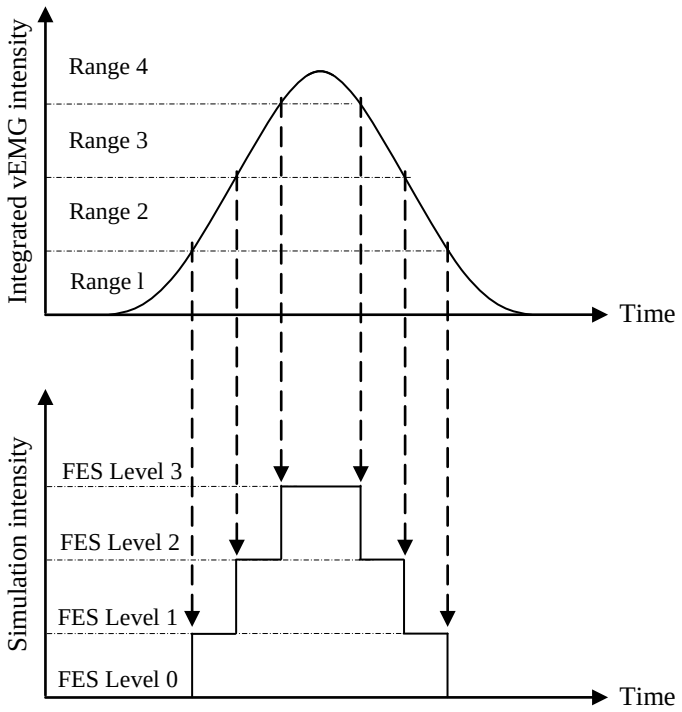

Figure 2. 6: Relation between the recorded vEMG of one muscle during FES cycling and the applied stimulation intensity to the same muscle.

In [84], Graupe has discussed a patient-responsive EMG control for FES. The EMG was measured from the trunk muscles above the level of lesion in paraplegics. As shown in Figure 2.7, the EMG signals measured from different upper trunk muscles were analyzed by an EMG signature discriminator to recognize the different intended walking functions such as right step, left step, standing-up, or sitting-down. The below-lesion FES-induced EMG from the stimulated muscles was used to regulate stimulation intensity to counteract the muscle fatigue.

In [85], Graupe et al. were using the surface EMG signals measured at the patient's erector spinae muscles above lesion level (a muscle group of the back known as extensor spinae) to provide control commands to the neuromuscular stimulator attached to the paralyzed lower limb muscles.

The potential of using sEMG as a natural trigger signal during FES-assisted gait was investigated by Dutta et al. [86]. The retaining motor activity below the level of injury in two volunteers with iSCI was detected, integrated, and then used to trigger the FES-assisted stepping. The quality of FES-assisted gait initiation using EMG-triggered control was compared with the auto-triggered FES (in which stimulation was triggered automatically at a fixed rate) and with hand-switch-triggered control. Four neurologically intact volunteers provided normative data for comparison. The gait initiation using EMG-triggered FES was found to be more coordinated and dynamically more stable than auto-triggered and hand-switch-triggered techniques.

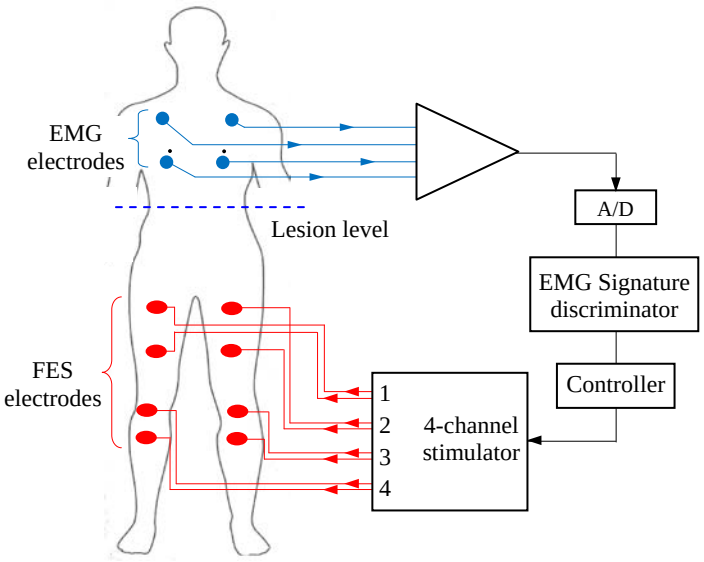

Figure 2. 7: Schematic of above-lesion EMG control of FES used in paraplegics, (adapted from [84]).

In [87], Yamaguchi et al. presented a sEMG-triggered stimulation system to help hemiplegics in standing-up tasks by means of FES. By exploiting the synchronization of both lower limbs, the EMG detected at the intact quadriceps, hamstrings, rectus abdominis and Erector spine during standing-up was used to predict the action that the patient intends to do and to trigger the stimulation of the impaired side. The experiment was performed using one hemiplegic subject having a paretic left leg. The EMG signal processing is containing signal detection and rectification. First, the sampled raw EMG is rectified, and then filtered by using a moving average filter. For each muscle, the integrated EMG is compared to a threshold. If the integrated vEMG from all muscles are simultaneously above the corresponding threshold levels, then the stimulation is switched on.

Peasgood et al. introduced in [88] a single channel closed-loop system for EMG-controlled FES in drop foot patients. Ineffective dorsiflexion during swing phase (drop foot) is present in 20 percent of the stroke population with partial recovery [89]. Figure 2.8 shows the system used to electrically stimulate the dorsiflexor (tibialis anterior) peroneal nerve which is responsible for lifting the foot during gait swing-phase and to increase the overall mobility. Residual EMG activity of tibialis anterior was detected and processed to control the stimulation intensity of the same muscle. This gives the patient the ability to control the stimulation level. To apply EMG-proportional control the authors had to low-pass filter the volitional EMG signal to obtain a smooth control action. However, the system slowly responded to the patient intention because of the time delay introduced by this filtering. A delay of 700 ms was reported. In walking tests, it was shown, that the time delay forced patients with drop foot to walk more slowly to obtain the support at the right time. In [90], Yeom et al. presented a similar system to continuously control the lower extremity paretic muscles by means of EMG-controlled FES. Separate stimulation and EMG recording electrodes have been used. Compared to the work by Peasgood et al. [88], an adaptive Gram-Schmidt filtering algorithm has been applied in real-time to cancel the stimulation artifacts from the recorded electromyograms. The feasibility of using vEMG to continuously control the FES-assist dorsiflexion was tested using one healthy subject. The results showed the feasibility of using EMG-controlled FES with adaptive stimulation-artifact removing filter.

In [91], Futami et al. proposed a locally EMG-controlled FES system for the knee extension of partially paralyzed patients. The intensity of the applied FES was controlled in proportion to the voluntary EMG detected from the paretic knee extensor muscle. The authors reported that this EMG-driven FES is applicable to daily activities such as transfer from bed to wheelchair, and standing-up, without any control-mode selection for each consecutive activity to aid, since EMG reflects the neural commands from the brain. A switching circuit was used to protect the input stage of EMG amplifier from any damage by stimulation pulses, and to reduce the transient artifacts.

Electrodes for EMG measurement were different from the stimulation electrodes and placed between them.

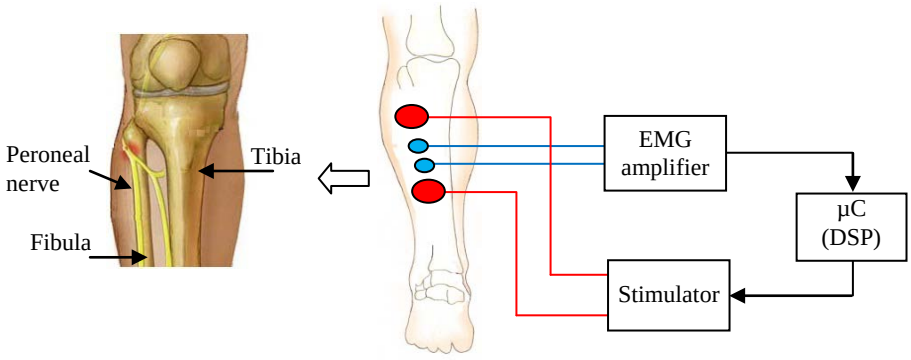

Figure 2. 8: Block diagram showing the measurement of EMG and the application of FES to the tibialis anterior to correct drop-foot.

Kamono et al. investigated an EMG-driven FES system with EMG recording from the stimulation electrodes for correction of drop foot. Electrodes were placed on the belly of tibialis anterior. The stimulation took place at a low frequency of 15 Hz and intensity of the stimulation was set again proportionally to the recorded volitional EMG at the same muscle [61]. From the low stimulation frequency it can be concluded that stimulation artifacts last longer. The device has been experimentally evaluated by a 24 years old intact subject.

In 2002, Muraoka investigated a 2-channel EMG amplifier to control FES-assisted gait in hemiplegic patients [66]. The same electrodes were used for stimulation and EMG recording. Described in the article is a EMG-proportional stimulation of the dorsiflexor to correct drop foot. The system was modulating the stimulation pulse width proportionally to the maximum amplitude of vEMG. The indented use of the second stimulation channel is not described. The repetition of stimulation pulses was limited to a period of 60 ms. Only during the last 20 ms of each stimulation period EMG could be assessed. The system was evaluated experimentally with one intact male subject. In [80] Fujiwara et al. were using the EMG detection system developed by Muraoka, the authors had to place the FES/EMG electrodes very closed to each other to minimize observed large EMG fluctuations during FES. They speculated that the strong disturbance in the EMG level is resulting from the activity of adjacent muscles. They had also to use the maximum volitional muscle activity within the 20 ms measurement interval instead of using the integrated vEMG to control the stimulation intensity.

2.5. Summary and Outlook

The literature review showed that only a limited number of systems can measure vEMG from the stimulation electrodes during the active stimulation periods. None of these systems was intensively evaluated. The quality of the detected volitional EMG signals was not quantitatively assessed and compared to the level of muscle contraction. No forces or movement ranges have been reported together with the detected vEMG. Signal to noise ratio (SNR) was not specified at all. SNR is an important parameter which gives an indication on the smallest detectable level of volitional EMG. And this determines which stroke and/or iSCI patients can use such a device and gain rehabilitation benefits. SNR should be as high as possible as only low residual motor functions are expected to be retained in the impaired muscles.

Because of the highly fluctuating nature of the volitional electromyogram, a low-pass filtering must be applied to smooth the vEMG before using it as control input to the FES. The time delay introduced by this filtering may cause instability of the formed closed-loop system with the brain as central element.

The majority of the published articles are not discussing the tuning of controller parameters in detail, regardless if EMG was measured from stimulation electrodes or not. In [79], [80], no information is given at all. In all published articles it was assumed that the amplitude of vEMG is not affected by the application of FES. This is usually not true. Once the stimulation pulses are delivered to the muscles, both FES and EMG electrodes start to polarize unless special measures are taken. The electrode polarization dramatically reduces the level of detectable vEMG. EMG suppression due to electrode polarization may explain the problems reported by Thorsen et al. [77] in finding the right controller parameter. Several iterations were needed to obtain suitable settings so that the patient was able to control the system smoothly. The problem of EMG suppression is more serious in case of recording vEMG from stimulation electrodes.

Outlook:

The strength of electrode polarization strongly depends on the amount of charge remaining under the electrodes. Using stimulation pulses with lower charge will therefore reduce the risk of electrode polarization. In Chapter 3, the optimal settings for pulse width and current amplitude of the stimulation pulses will be investigated with respect to the minimal charge required for maintaining a specified level of muscle contraction and with respect to fatigue. The technique for selecting pulse width and current amplitude for a given charge is named charge control in this work. Charge will be used as input signal in FES control.

In Chapter 4, a new EMG detection device will be presented which allows EMG measurement from stimulation electrodes for four stimulation channels. The developed system utilizes fast electrode/skin discharging techniques to furthermore reduce the polarization effects.

Before applying the new EMG detecting systems with FES to stroke and iSCI patients, a proper evaluation was carried out with healthy subjects. The intensive evaluation of the StiMyo amplifier during FES-cycling is presented in Chapter 5. The use of the device for EMG-proportional FES control is investigated in Chapter 6.

Chapter 3

3. Stimulation Device and Charge Control

3.1. Introduction

This chapter explains the principle of charge control which should liberate the physicians from selecting the current amplitudes and pulse widths of the electrical stimulation individually. It explains also the stimulation device that has been used during this work.

This chapter is organized as follows: The operation modes of the RehaStim stimulator (which was previously introduced in [50], [92]) are presented in detail in Section 3.2. Section 3.3 introduces the principle of charge control and the mathematical description of different charge-control modes. The experimental evaluation of different charge-control modes is presented in Section 3.4. Section 3.5 gives general conclusions about the realized charge-control modes and an outlook for future work related to this issue.

3.2. Stimulation Device

The RehaStim pro™ portable stimulation device employed in this work was produced by the German company HASOMED GmbH. The current-controlled 8 channel stimulator is a certified medical product and possesses two independent current sources which are multiplexed to 4 outputs each. The main processor of the stimulator is an ultra-low-power 16-bit RISC mixed-signal processor from Texas Instruments (MSP430F169). There are two independent stimulation modules hosting each one of the current sources. Each stimulation module includes another microprocessor (MSP430F149), which is responsible for the pulse generation timing. The stimulation module A feeds the stimulation channels 1 to 4; stimulation module B feeds the stimulation channels 5 to 8. Since both modules function independently simultaneous pulse generation on module A and B is possible.

Figure 3.1 is showing the RehaStim pro™ stimulator device. The device is operated by a touch panel with illumination. The technical specifications are listed in Table 3.1. Notice that the RS232

and USB interfaces share the same UART interface of the MSP430 so that multiplexing must be applied when using both interfaces at the same time. In the PC-controlled configuration the USB interface is employed for communication with the PC and the RS232 is free. The stimulator possesses additional inputs and outputs which are not used here. Galvanic isolation between high voltage generation/electrodes and the rest of the stimulator electronics has been realized for safety reasons.

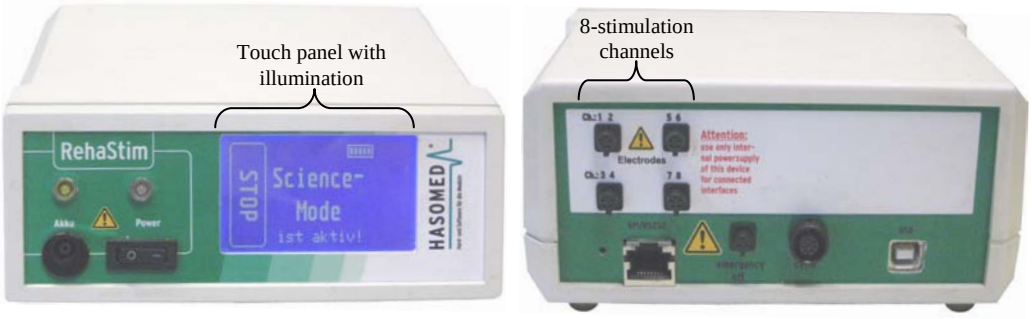

Figure 3. 1: Portable 8 channel RehaStim pro™ stimulator.

Table 3. 1: Technical details of the stimulation device

Current	0 . . . 126 mA in 2 mA steps
Pulse width	0, 20 . . . 500 µs in 1 µs steps
Frequency	See Section 3.2.1
Pulse form	Biphasic
Channels	8 (2 times 4 on two modules)
Serial ports	RS232 and USB with galvanic isolation
Digital and analogue I/O	8 pins which can be assigned individually as 12-bit analogue inputs (8 available), 12-bit analogue outputs (2 available) or digital inputs /outputs (8 available)
Sensor supply	5V / 100 mA

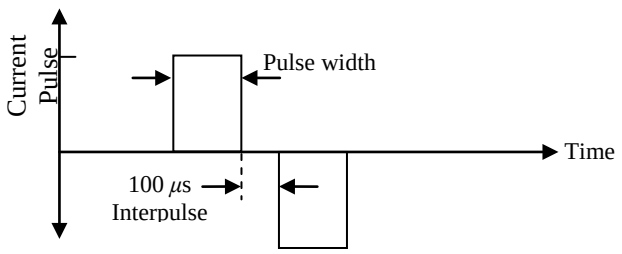

Figure 3. 2: The definition of pulse width and current amplitude for a biphasic pulse.

A sample biphasic stimulation pulse on an ideal resistive load is shown in Figure 3.2. Current amplitude and pulse width are defined in the same figure. Notice that there is a fixed interpulse interval of 100 μs between the two phases of the stimulation. At the end of the pulse the remaining charge on the electrodes and skin is periodically removed by an active shortcut (change of electrode polarity for 1 μs).

3.2.1. Pulse-Generation Modes

The RehaStim pro™ offers different modes of stimulation pulse generation. An Application Programming Interface (API) which enables the development of customized stimulator applications using different modes of pulse generation is provided. Moreover, a serial communication protocol is available so that the pulse generation can also be controlled by sending commands with 115200 Bauds from an external device, preferably a PC.

The following modes of pulse generation are available:

Single Pulse Mode: On an external command or an API function call the stimulator generates a single pulse on a specified channel with desired current amplitude and pulse width. The stimulator will generate the pulse immediately after processing the command. A complex stimulation pattern may be generated by sending more than one command. The application program inside the stimulator or the external device (PC) is responsible for controlling the stimulation timing, i.e. the stimulation pulse interval. Therefore, the API of the stimulator provides a 16-bit timer with 1ms resolution.

Continuous Channel List (CCL) Mode: Using this mode, the generation of complex patterns is greatly simplified. The main processor and the processors of the stimulation modules control the pulse generation by means of timer-interrupts. A list of stimulation channels has to be specified, on which pulses or even pulse groups (doublets or triplets) will be generated repeatedly. Figure 3.3 defines the main stimulation period t_1 and the interpulse time t_2 of doublets and triplets with the help of an example. The channel list is repeatedly processed with time period t_1. Pulse generation, ordered by the channel numbers, takes place on the selected channels. For each selected channel a time slot of 1.5ms is reserved, even if current and/or pulse width are zero for the channel or if the pulse width is smaller than 1.5ms. At least 1.5ms pass between the stimulation of different channels of one module. The stimulation modules A and B process the channel list in parallel with a time offset of 0.6ms. Module A generates pulses on the channels 1 to 4 if applicable, and module B generates pulses on the channels 5 to 8 if applicable. The interpulse time t_2 of doublets and triplets is fixed for all channels and is set during an initialization step. When doublets or triplets have to be generated the channel list will be processed two or three times more with period t_2. Stimulation takes

place only on the channels on which doublets or triplets have to be generated. The main stimulation frequency is specified by the period t_1. Some channels of the channel list can be assigned to a lower frequency with nt_1 activation period where n is a positive integer.

The CCL mode must be initialized by an API function call or a command (external control). Used channels, main time t_1, inter-pulse time t_2 and the maximal size of pulse groups must be chosen at this stage. The minimal possible interpulse time t_2 depends on the maximal number of channels assigned to the individual stimulation modules as follows:

$$t_2 \geq 1.5\ \text{ms} \cdot \max\left(n_{ch}^{A}, n_{ch}^{B}\right), \tag{3. 1}$$

where n_{ch}^{A} and n_{ch}^{B} are the number of selected channels of stimulation modules A and B respectively. The minimal possible period t_1 depends on t_2 and the maximal size n_{pg} of pulse groups used (n_{pg} = 1 for single pulses, n_{pg} = 2 for doublets, n_{pg} = 3 for triplets). The constraint for t_1 is then:

$$t_1 = n_{pg} \cdot t_2 + 1.5\,\text{ms}, \tag{3. 2}$$

where the 1.5 ms results from a communication between the main processor and the stimulation modules as indicated in Figure 3.3. The period t_1 can be changed in the range 3 . . . 1023.5 ms in 0.5 ms steps subject to the constraint (cf. Equation 3.2), and t_2 can be altered in the range 3 . . . 16 ms in 0.5 ms steps subject to the constraint (Equation 3.1). Using all 8 channels, a minimal group time t_2 of 6 ms can be achieved, i.e. a doublet or triplet frequency of 170 Hz. When only doublets and single pulses with a frequency of 170 Hz are applied (n_{pg} = 2), a minimal value of 13.5 ms for period t_1 is obtained, i.e. a maximal possible main frequency of 74.1 Hz.

Another API function call or external command de-activates the CCL mode. When the CCL mode is active, the pulse parameters (pulse width, current amplitude and group mode (single pulse, doublet or triplet) of the selected channels can be altered by a corresponding API function call or an external command. The new parameters will be used from the next processing of the channel list onwards.

The main processor controls the frequency $1/t_1$ by which the channel list is processed. Each time the stimulation cycle repeats, the main processor sends the actual stimulation settings to the two stimulation modules which then generate the individual pulses on the selected channels. The processors on the stimulation modules guarantee that specified pulse width and interpulse times of the doubles and triples are realized.

One Shot Channel List (OSCL) Mode: Just as in the Continuous Channel List Mode a channel list is defined by an initialization step. However, processing of the channel list is not automatically repeated so that the time period t_1 ceases to exist. Instead, the channel list will be processed once and pulses and/or pulse groups are generated, only if a special API function call or external commands are issued. Pulse parameters (pulse width, current amplitude and group mode of the selected channels) are specified by the API function call or the external command.

The OSCL mode offers the possibility to control the main stimulation frequency by an application program running in the stimulator or by an external device while the inter-pulse time of the doublets and triplets is realized by the stimulation modules.

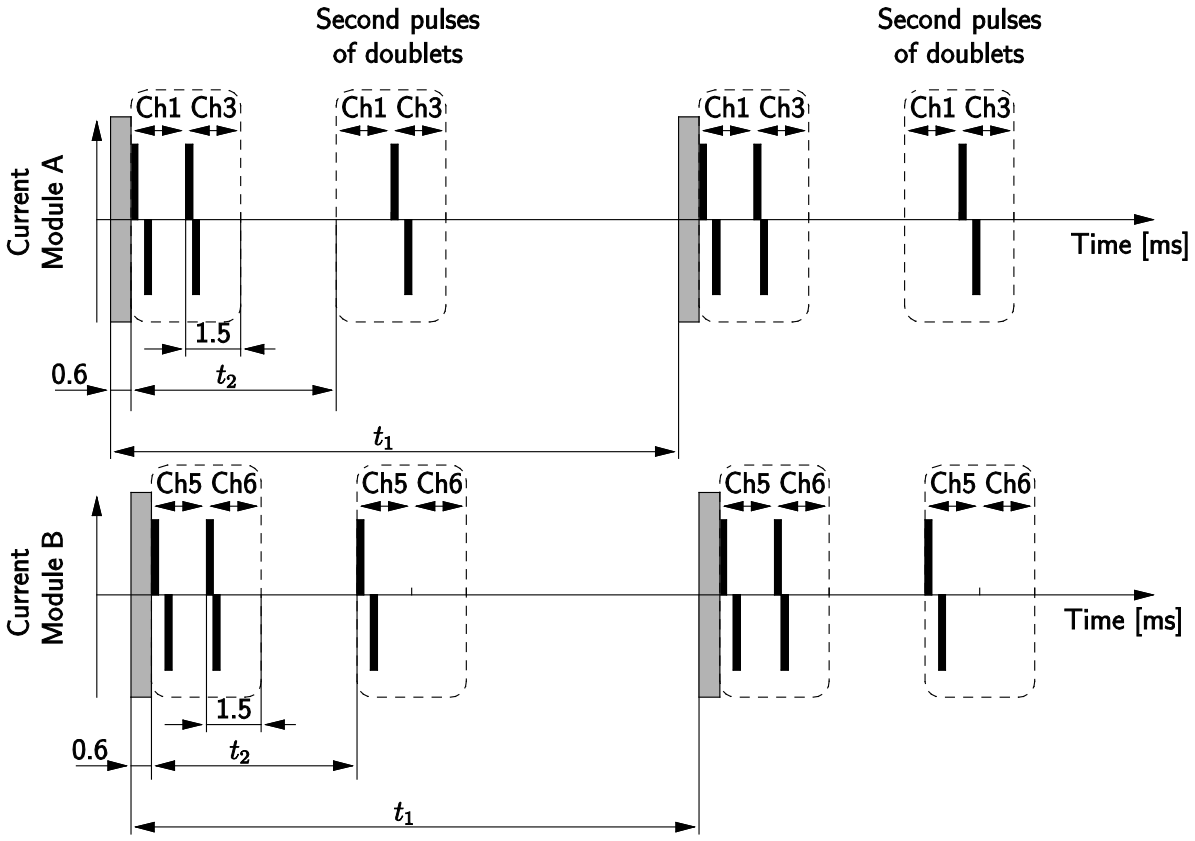

Figure 3. 3: Example showing the continuous channel list mode of the stimulator. The channel list encloses the channels 1, 3, 5 and 6. The main stimulation frequency is $1/t_1$. Doublets are generated on the channels 3 and 5 with a frequency $1/t_2$. The grey bars indicate some communication periods in which the actual stimulation settings are transferred from the main controller to the stimulation modules. Stimulation pulses are represented by black bars where the same width and amplitude have been assumed for simplicity [50].

3.3. Charge-Control Modes

The effectiveness of electrical stimulation is determined by the repetition rate and the charge of the stimulation pulses. The latter is defined by the product of current amplitude and pulse width. In this context fixed stimulation frequency of 20 Hz has been applied. The stimulator RehaStim pro™ is capable of generating stimulation pulses with current amplitudes of up to 127 mA, and pulse width of up to 500 μs. Due to residual sensation of stroke patients, only a current in the range of I_{min}= 0 mA to I_{max}= 50 mA and a pulse width in the range of PW_{min}= 100 to PW_{max}= 500 μs is applicable, this is corresponding to a charge range from zero to 25 μC. Mapping this charge to the range from zero to one yields the normalized charge that can be adjusted for each stimulated muscle.

For a given charge, the values of pulse width and stimulation current are either to be selected manually, or to be automatically determined from the normalized charge by using a predefined relation between pulse width and amplitude. This approach will be called charge control. The diagram shown in Figure 3.4 is presenting three different relations between *PW* and *I* given three different charge-control modes. Stimulation pulse width and current intensity can be calculated using one of the three charge-control modes for a given charge *Q*. In charge-control mode-0 the normalized current intensity and pulse width are equally distributed. In charge-control mode-I the normalized current is dominating the normalized pulse width. In charge-control mode-II the roles of normalized current amplitude and normalized pulse width are exchanged. The relation between stimulation intensity and pulse width in the last two modes is represented by circle sectors with centers in (1,0) for mode-I and (0,1) for mode-II.

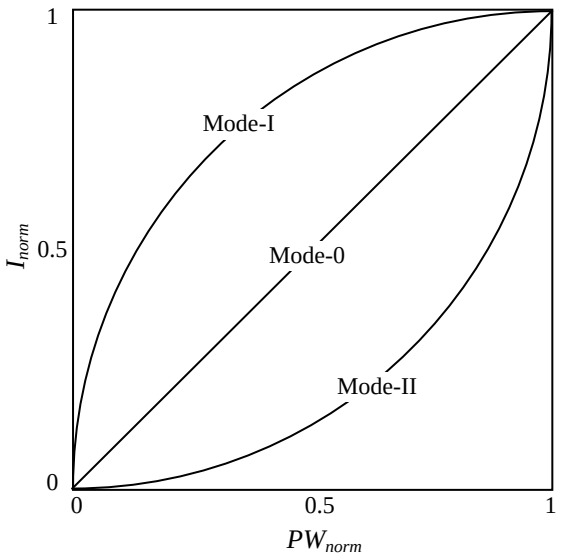

Figure 3. 4: Charge control, three charge-control modes are illustrated to allow different implementation of stimulation current and pulse width for a given charge. I_{norm} in the normalized stimulation intensity and PW_{norm} is the normalized pulse width.

All values in Figure 3.4 are normalized, where the normalized value of a certain signal, e.g. X_{norm} can be calculated as a function of its current value X and the minimum $X_{\min}$ and maximum $X_{\max}$ values by:

$$X_{norm} = \frac{X - X_{\min}}{X_{\max} - X_{\min}} \tag{3. 3}$$

The non-normalized signal is then given by

$$X = X_{\min} + X_{norm}\left(X_{\max} - X_{\min}\right). \tag{3. 4}$$

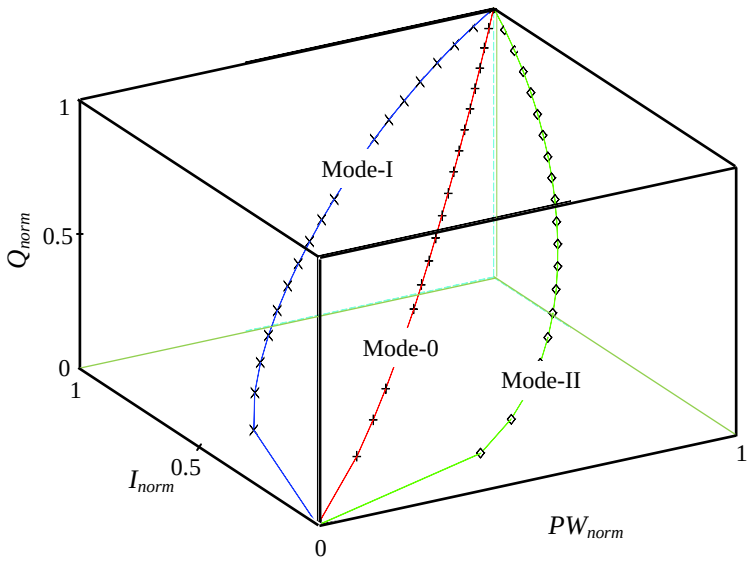

Figure 3. 5: Charge control, three dimensional illustration of the three charge-control modes.

In the sequel it will be explained how the normalized pulse width and normalized current are determined for a given charge Q. The charge Q is a function of the non-normalized current and pulse width:

$$Q = PW \cdot I \tag{3. 5}$$

Equation (3.4) can be employed here to express the charge as a function of I_{norm} and PW_{norm}:

$$Q = \left(PW_{norm}\left(PW_{\max} - PW_{\min}\right) + PW_{\min}\right)\cdot\left(I_{\min} + I_{norm}\left(I_{\max} - I_{\min}\right)\right) \quad (3.6)$$

The solution of (3.6) depends on the relation between PW_{norm} and I_{norm}. Three different relations between PW_{norm} and I_{norm} are forming different charge-control modes. To uniquely determine I_{norm} and PW_{norm} one has to use additionally the relation between I_{norm} and PW_{norm} given by the curves in Figure 3.4.

3.3.1. Mode-0 "Equally distributed normalized- pulse width and normalized current"

In charge-control mode-0 the relation between I_{norm} and PW_{norm} is a straight line ($I_{norm} = PW_{norm} = N$) as shown in Figure 3.4.

Equation (3.6) can be rewritten as follows:

$$Q = \left(N\left(PW_{\max} - PW_{\min}\right) + PW_{\min}\right)\times\left(I_{\min} + N\left(I_{\max} - I_{\min}\right)\right) \quad (3.7)$$

Equation (3.7) is solved to find the value of N for a given charge Q. There are two solutions:

$$N_{1,2} = \frac{A \pm \left(\left(I_{\max} - 2I_{\min}\right)PW_{\min} + I_{\min}PW_{\max}\right)}{\left(2I_{\max} - 2I_{\min}\right)\left(PW_{\max} - PW_{\min}\right)} \quad (3.8)$$

with

$$A = \sqrt{\left(4I_{\max} - 4I_{\min}\right)\left(PW_{\max} - PW_{\min}\right)Q + \left(I_{\max}PW_{\min} - I_{\min}PW_{\max}\right)^2} \quad (3.9)$$

The solution that gives the normalized values of I_{norm} and PW_{norm} is

$$I_{norm} = PW_{norm} = \frac{A + \left(2I_{\min} - I_{\max}\right)PW_{\min} - I_{\min}PW_{\max}}{\left(2I_{\max} - 2I_{\min}\right)\left(PW_{\max} - PW_{\min}\right)}. \quad (3.10)$$

3.3.2. Mode-I "The Dominating Current Mode"

As shown in Figure 3.4, the curve determining the relation between I_{norm} and PW_{norm} in charge-control mode-I is part of the circle described by

$$I_{norm}^2 + \left(PW_{norm} - 1\right)^2 = 1. \quad (3.11)$$

The solution of this equation for I_{norm} is:

$$I_{norm} = \pm\sqrt{2PW_{norm} - PW_{norm}^{2}} \tag{3. 12}$$

By substituting the positive solution of I_{norm} into (3.6) we obtain:

$$Q = \left(PW_{norm}\left(PW_{\max} - PW_{\min}\right) + PW_{\min}\right)\left(I_{\min} + \left(I_{\max} - I_{\min}\right)\sqrt{2PW_{norm} - PW_{norm}^{2}}\right) \tag{3. 13}$$

To solve Equation (3.13) for PW_{norm} the nonlinear equation solver routine gsl_root_fsolver_brent of the GNU Scientific Library[5] is applied in real time during stimulation. It uses the Brent-Dekker method (Brent's method)[6]. It combines an interpolation strategy with the bisection algorithm. This One-dimensional root finding algorithm is available online and distributed under the GNU General Public License. The solution of Equation (3.13) will give the value of PW_{norm} as a function of a given charge Q. Normalized current can be obtained from Equation (3.12) using the calculated value of PW_{norm}.

3.3.3. Mode-II "The Dominating Pulse width Mode"

The curve determining the relation between PW_{norm} and I_{norm} in charge-control mode-II is part of the circle described by

$$\left(I_{norm} - 1\right)^{2} + PW_{norm}^{2} = 1. \tag{3. 14}$$

The solution of this equation for $\mathrm{PW}_{\mathrm{norm}}$ is:

$$PW_{norm} = \pm\sqrt{2I_{norm} - I_{norm}^{2}} \tag{3. 15}$$

By substituting the positive solution of PW_{norm} into (3.6) it follows

$$Q = \left(\sqrt{2I_{norm} - I_{norm}^{2}}\left(PW_{\max} - PW_{\min}\right) + PW_{\min}\right) \times \left(I_{\min} + I_{norm}\left(I_{\max} - I_{\min}\right)\right) \tag{3. 16}$$

To obtain the values of PW_{norm} and I_{norm} (3.15) and (3.16) have to be solved using the GNU Scientific Library. As the resolution of PW and I is limited on the stimulation device to 1 µs and 2

[5] http://www.gnu.org/software/gsl/

[6] http://linux.math.tifr.res.in/manuals/html/gsl-ref-html/gsl-ref_31.html

mA respectively, the physically applied *PW* and *I* are chosen to have the smallest Euclidean distance to the ideal values calculated before.

3.4. Experimental Evaluations

This section will introduce the experimental assessment of charge-control mode-I and mode-II. The two charge-control modes are experimentally compared with respect to the minimum charge required for maintaining a desired muscular contraction and with respect to muscular fatigue due to FES.

3.4.1. Experimental procedure

A simple experimental study had been performed to evaluate the differences between the charge-control mode-I and mode-II. Mode-0 was not included in this study since its performance should be in between the other two modes.

Investigated was the charge required for each mode to maintain a desired muscle contraction over a certain period of time. It is preferred to use a charge-control mode which requires lower stimulation charge, because this will leave smaller charge under FES/EMG electrodes after the stimuli. This will minimize the electrode polarization effects and allows the StiMyo device to measure longer periods of EMG. Another criterion for selecting the preferred charge-control mode will be the observed muscle fatigue (measured by the increase of the feedback controlled stimulation charge over time to keep the desired contraction), which should be minimized.

The experimental study involved 5 neurologically intact male volunteers (with an average age of 32.5 ± 6.5 years, weight 78.5 ± 4.5 kg and height 182.5 ± 4.5 cm)[7]. For each subject, the experiment was divided into two sessions, each lasting for 100 seconds, one for charge-control mode-I, the other for charge-control mode-II. The two sessions were separated by 10 minutes to give the muscle enough time to recover from fatigue. The order of the sessions was random.

As shown in Figure 3.6, a simple PI-controller for FES had been implemented on a laptop to stabilize the wrist-joint angle at 20^{o} by FES. The controller was realized on a laptop with real-time Linux (RTAI extension)[8]. The programs were realized using Scilab/Scicos[9] version 4.1.2 with the HART-Toolbox[10] and RTAI-Lab (part of RTAI) which offers automatic code generation from Scicos-Diagrams. For online changing of program/controller parameters and for real-time

[7] *The studies in this chapter were approved by the Local Research Ethics Committee at Charité Berlin.*
[8] *http://www.rtai.org*
[9] *http://www.scilab.org*
[10] *http://hart.sourceforge.net*

monitoring of signals the program QRtaiLab[11] was used. The laptop periodically triggers the stimulator RehaStim pro™ stimulation device (HASOMED GmbH, Germany) via an optically-isolated USB interface. Two reusable self-adhesive hydrogel electrodes (Type: RehaTrode – oval 60 x 40 mm, HASOMED GmbH, Germany) were used to deliver the 20 Hz stimulation pulses to the extensor carpi ulnaris, extensor carpi radialis and extensor digitorum muscles. A controllable normalized charge (Q_{norm} from 0 to 1 which corresponds to 10-400 µs pulse width and to 5-20 mA current amplitude) was used. One ENG single-use electrode (Ambu Blue Sensor NF, Ambu, Denmark) of size 28x20 mm was used as a reference electrode and placed on the elbow.

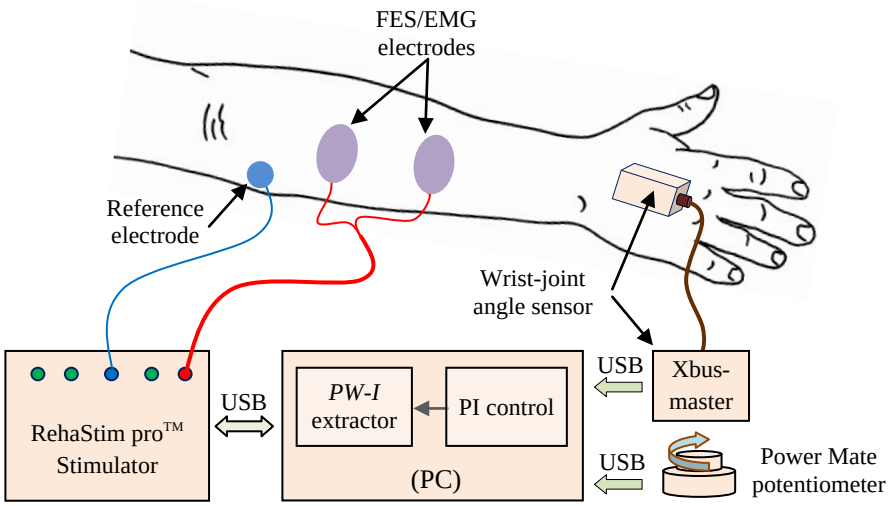

Figure 3. 6: Experimental setup for evaluating different charge-control modes. The PI wrist-joint control is applying FES to maintain a given wrist-joint angle of 20°. For each charge-control mode, the *PW-I* extractor is calculating pulse widths and current amplitudes.

An USB potentiometer (PowerMate, Griffin Technology) was used to manually set the desired wrist-joint angle, or to activate the different charge control modes. A full inertial sensor (MT9-B, Xsens Motion Technologies, The Netherlands) was used to detect the wrist-joint angle. The inertial sensor includes a gyroscope, an accelerometer and a magnetic field sensor, which are all three-axial. The MT9-B is connected to a laptop though one digital signal processing unit (Xbus-Master, Xsens Motion Technologies, The Netherlands) using an USB interface. By using a Direction Cosine Matrix (DCM)-based orientation estimation algorithm [93], the wrist joint-angle can be determined from the calibrated sensor signals on the laptop. The forearm was lying on the table. Hence, the extension angle of the wrist joint can be measured using only one inertial sensor mounted on the back of the hand (cf. Figure 3.6). The subject had to relax during the experiment, and didn't volitionally control his wrist joint. The charge-control modes were implemented on the laptop. The

[11] *http://qrtailab.sourceforge.net*

current/pulse-width extractor was extracting pulse width and current amplitudes for each mode. The calculated pulse widths and current amplitudes were periodically sent to the stimulator via the USB interface.

3.4.2. Results

Figure 3.7 shows the feedback controlled wrist-joint angle θ and the corresponding charge Q for mode-I and mode-II for one subject. The ongoing increase in stimulation charge is clearly indicating muscle fatigue for both modes. Compared to charge-control mode-II, charge-control mode-I is requiring less charge, which makes it preferred to be used.

Figure 3.8 represents the calculated fatigue index F% of the two modes, which is defined as

$$F\% = \frac{\Delta Q}{Q_o}, \tag{3. 17}$$

where Q_o is the average charge which is calculated over the Q_o-band (over 150 recording samples) as shown in Figure 3.7. This interval was selected during the initial steady state phase just before the onset of visible muscle fatigue. The value ΔQ is representing increase in stimulation charge:

$$\Delta Q = \frac{1}{N - s_0} \sum_{i=s_0}^{N} (Q_i - Q_o) \tag{3. 18}$$

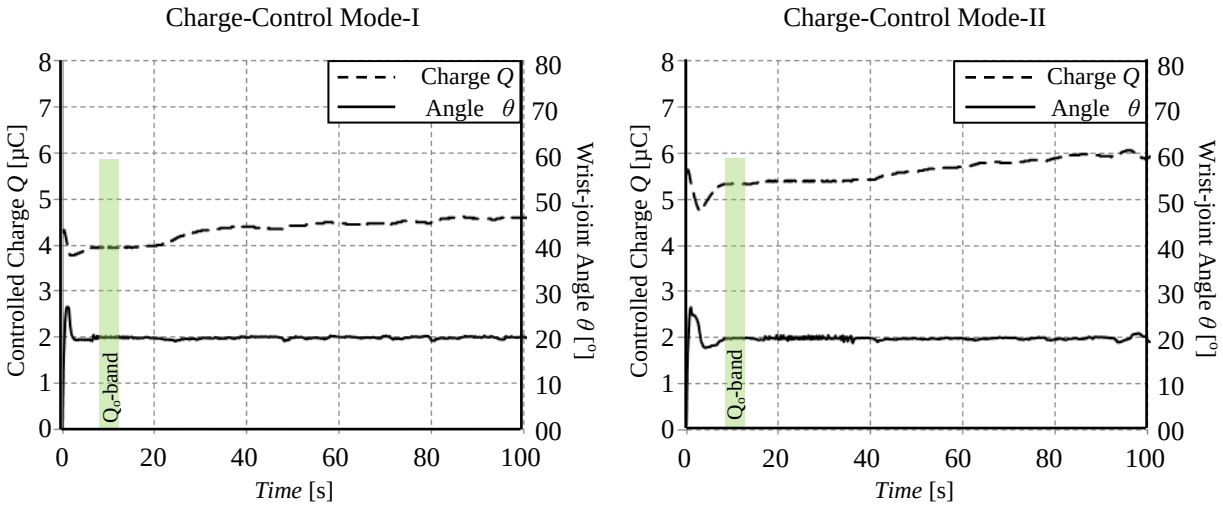

Figure 3. 7: PI controlled wrist-joint angle for one subject. Shown are the controlled angle θ[°] and the applied charge Q [µC] for charge-control mode-I and charge-control mode-II. For both charge-control modes, a clear muscular fatigue can be observed from the increase in applied charge.

In Equation (3.18), S_o is the first sample of the Q_o-band. N is the entire number recorded samples (N = 2000) and Q_i is the applied charge at the i^{th} sample.

Figure 3.8 show the mean fatigue index over all subjects. Charge-control mode mode-I exhibits slightly better fatigue resistance compared to mode-II.

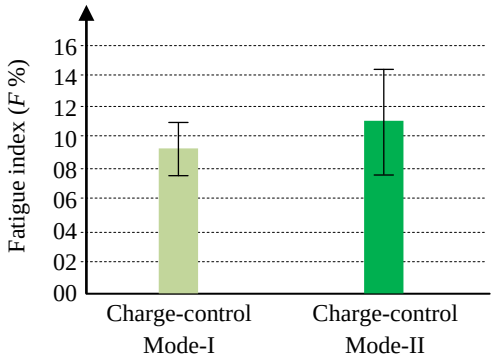

Figure 3. 8: the percentile fatigue index (F%) over all subjects of the two charge-control modes. Mode-I shows slightly better fatigue resistance compared to mode-II.

Table 3.2 shows the average stimulation charge and the average fatigue index for all subjects for mode-I and mode-II. It is clearly visible that charge control-mode-I requires much lower charge to produce the desired muscle contraction (20^o wrist extension) compared to charge control-mode-II. Charge control-mode-I is also causes slightly less fatigue compared to charge control-mode-II.

Table 3. 2: The average stimulation charge Q_o^{AV} and the fatigue index $F\%_{AV}$ for all subjects using charge-control mode-I and Mode-II.

Charge-control Mode	Q_o^{AV} [µC]	$F\%_{AV}$
Mode-I	2.785	9.21
Mode-II	4.442	11.03

3.5. Conclusions and Discussion

The RehaStim pro™ stimulator provides bipolar current pulses with controllable current amplitude and pulse width. In this work a fixed stimulation frequency of 20 Hz has been applied. The objective was to identify settings of stimulation amplitudes and pulse widths that maximize the force induced by FES for a given stimulation charge Q, and to increase fatigue resistance under FES. In [94], Crago et al. have investigated the relationship between the intramuscular electrical stimulation

parameters (*PW* and current amplitude) and the generated force from cat soleus, human finger and thumb muscles. The results demonstrated that using the same stimulation charge, the muscle force depends on the internal distribution of current amplitudes and pulse widths. Selecting high current amplitude and short *PW* is generating higher force compared to selecting lower current amplitude and wider pulses. However the effect on fatigue resistance was not investigated.

From the EMG measurement perspective, the current amplitude and pulse width settings that require the minimal charge to produce a desired force are preferred. This should leave less residual charge under FES/EMG electrodes after the delivery of stimulation pulses. This will enhance the discharging process of the electrode/skin contacts, and will reduce the chance of amplifier saturation. Selection of current amplitudes and *PW* setting which provides less muscle fatigue is a secondary aim.

The control realization of stimulation charge by three different distributions modes of *PW* and current amplitude has been investigated (equally distributed pulse width and current, the dominating current amplitude distribution and the dominating pulse width distribution). An experimental study with 5 neurologically intact subjects confirmed the observation by Cargo et al. [94] that pulses with high current amplitude and short *PW* produce stronger muscle contraction than wider pulses with lower current amplitude. Thus less charge is needed for obtaining a desired muscle contraction. In addition to the work in [94], the study also showed less fatigue for the high current amplitude and short *PW* pulses compared to other distributions.

A deeper understanding of the underlying physiology principles of the electrical stimulation of nerves is required at this point to physiologically interpret these observations [95].

In summary the charge-control mode-I (high current and short pulse width) will be recommended for use in EMG-controlled stimulation. The automatic extraction of current amplitude and *PW* for a given charge *Q* simplifies the selection of stimulation settings (current amplitude and *PW*).

Further studies are required to study the acceptance of different current amplitudes and *PW* distributions by the patient in term of induced pain. For arm stimulation all setting were tolerated equally. For stimulation of the leg a recent study by Ambrosini [96] reports high pain for high current/shorter pulse width compared to other distributions. For this reason, charge-control mode-0 may be a good compromise when stimulating the lower limbs to increase tolerance by the patient while still having an acceptable low value of charge with respect to the produced muscle contraction.

Chapter 4

4. EMG-Amplifier Design and Electrode Discharging

4.1. Introduction

This chapter introduces the design and implementation of a 4 channel EMG amplifier named “StiMyo”. StiMyo is an EMG recording device which is able to detect the residual muscle activity from the patients’ paretic muscles. The main advantage of StiMyo over other devices existing in clinical rehabilitation centers is that StiMyo can measure the residual vEMG also from an electrically stimulated muscle between stimulation pulses. This chapter briefly introduces the basic requirements of bio-potential amplifiers, and shows how does these requirements were fulfilled by the StiMyo device. A preliminary experimental evaluation of the StiMyo device will be presented.

This chapter is organized as follows: Basic requirements of EMG amplifiers are stated in Section 4.2. Section 4.3 explains the design of the different amplifier components such as the pre-amplifier circuit, switching circuit and the analog signal processing. A great emphasis is put on fast electrode/skin discharging techniques. Section 4.4 is showing the experimental evaluation of the StiMyo amplifier. In Section 4.5, EMG suppression due to electrode polarization and the muscle contractions (action potentials) caused by the electrode/skin discharging are discussed. Conclusions are given in Section 4.6.

4.2. Basic Requirements of EMG-Amplifiers

In the typical EMG pre-amplifier two electrodes are picking up the EMG signal from the target muscle and a third electrode is providing the reference potential. The input signal to the amplifier consists of four components; the desired bio-potentials (EMG), the 50/60 Hz power line interference signal, interference signals generated by the skin/electrode interface (e.g. movement artifacts), and noise.

There are several important issues to be considered during the design of an EMG-amplifier such as:

- The amplifier has to offer full protection of the user from any electrical shock.
- The desired (EMG) signals should not be influenced by the amplifier itself.
- The best separation of EMG signal from all other interferences should be provided.
- The amplifier inputs have to be protected against damages that might result from high FES voltages.

In addition to these general issues, the pre-amplifier should reject any common mode interferences by means of high Common Mode Rejection Ratio (*CMRR*) and high input impedance (R_{in}). A good EMG-amplifier should provide a high Signal to Noise Ratio (SNR) and a strong DC signal suppression. The next subsections are discussing the effects of each of these amplifier properties on the quality of EMG measurement.

4.2.1. Common Mode Rejection Ratio

The first stage in any bio-potential amplifier is the differential pre-amplifier (cf. Figure 4.1). The main task of this differential amplifier is to reject the power line frequency interferences (50/60 Hz) that are electrostatically or magnetically coupled into the subject skin and appear at the both pre-amplifier inputs. The interferences from the power lines show a very small difference in amplitude and phase between the two amplifier inputs. This causes approximately the same potential at the two amplifier inputs and is thus called common mode signals [97]. In contrast the EMG signals at each amplifier input are different and will be amplified [98]. Such signals are known as differential mode inputs. A strong rejection of common mode inputs is one of the most important characteristics of a good designed amplifier.

The CMRR of an amplifier is defined as the ratio of the differential mode gain over the common mode gain.

4.2.2. Input Impedance

Furthermore, it is very important for EMG pre-amplifiers to possess high input impedance. The surface electrode/skin impedance is typically in the range of several kΩ with gel-electrodes and proper skin preparation. In order to accurately measure a desired signal the input resistance of the measurement device should be considerably larger than the impedance of the electrode/skin interface (at least ten times). If not, the signal will be attenuated and distorted due to the loading effect of the low amplifier input impedance. For EMG amplifiers with gel-electrode recording, input impedance in the tens of MΩ range is sufficient.

4.2.3. Signal to Noise Ratio

Noise at the input terminals of the pre-amplifier is usually caused by power lines, other electrical devices, surrounding radio frequencies and cable movements. The Signal to Noise Ratio (SNR) of the pre-amplifier strongly depends on the parasitic capacitance of the measurement cables and the input impedance of the amplifier. The parasitic capacitance increases as the length of EMG cables increases. Long cables combined with a high input impedance of the amplifier will reduce the signal to noise ratio. The SNR is also affected by unbalanced electrode/skin impedances. If the impedances of both electrodes become too different, common mode noise signals will be seen by the amplifier as differential input signals and will be amplified [98].

4.2.4. DC Signal Suppression

It is important to have a pre-amplifier circuit with strong suppression of DC components within the differential mode input signal. Such DC components could arise due to asymmetry in the electrodes-skin impedances and/or due to unbalanced stimulation pulses during FES. Any DC potential difference between the two electrodes will be seen by the amplifier as a differential signal and will be amplified. This could drive the pre-amplifier into saturation or instability if no sufficient DC suppression is present.

4.3. Typical EMG Pre-Amplifier

The typical configuration of an EMG pre-amplifier is shown in Figure 4.1. The both potentials (V_{IN}^{-} and V_{IN}^{+}) at the pre-amplifier inputs (A_2 and A_1) are amplified and fed respectively to the inverting and the non-inverting inputs of a differential amplifier (A_{diff}). The entire gain G can be set by the resistor R_G. The output voltage of the entire pre-amplifier is given by $V_o = G\left(V_{IN}^{+} - V_{IN}^{-}\right) + V_R$ where V_R is a reference voltage.

The Pre-Amplifier Gain: In this section, standard linear system theory has been used to analyze the pre-amplifier circuit shown in Figure 4.1 [99]. To calculate the entire gain G, an ideal operational amplifier case will be considered. This assumption means that the input current for each operational amplifier (A_1, A_2 and A_{diff}) is assumed to be zero (i.e. $I_{IN_1} = I_{IN_2} = 0\,\text{A}$). Thus the potential difference between the operational amplifier inputs will be zero Volt (i.e. $V_{IN}^{+} = E_1^{-}$ and $V_{IN}^{-} = E_2^{-}$, etc.).

At the operational amplifier A_1, the potential E_1^- can be calculated from the voltage divider formed by R_2 and R_G such that:

$$E_1^- = E_2^- + \left(\frac{V^+ - E_2^-}{R_2 + R_G} \right) R_G \,. \tag{4. 1}$$

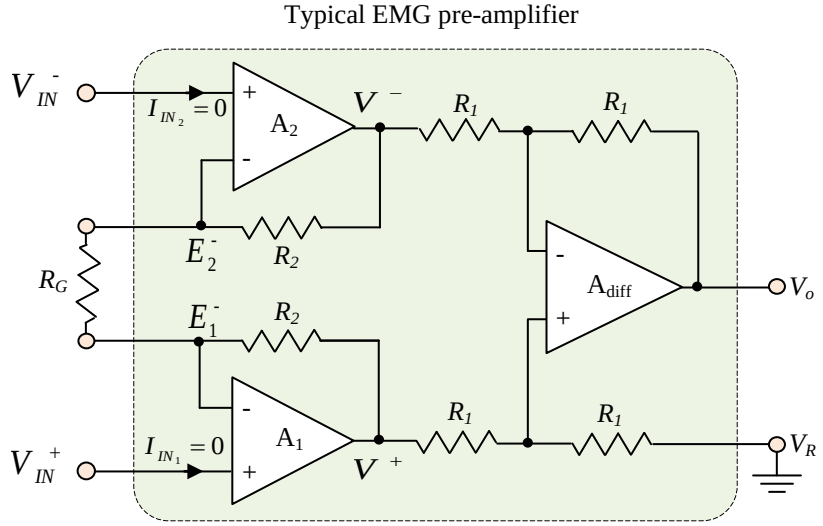

Figure 4. 1: Circuit diagram of the typical EMG pre-amplifier: The output voltage of the entire pre-amplifier is given by $V_o = V_R + \left(V_{IN}^+ - V_{IN}^- \right) \left(2R_2 + R_G \right) / R_G$.

Substituting V_{IN}^+ for E_1^- and V_{IN}^- for E_2^-, Equation (4.1) becomes

$$V_{IN}^+ = V_{IN}^- + \left(\frac{V^+ - V_{IN}^-}{R_2 + R_G} \right) R_G \,. \tag{4. 2}$$

Solving (4.2) for the output voltage of the operational amplifier A_1 gives:

$$V^+ = \left(\frac{R_2 + R_G}{R_G} \right) V_{IN}^+ - \left(\frac{R_2}{R_G} \right) V_{IN}^- \tag{4. 3}$$

Similarly, at the operational amplifier A_2, using the voltage divider formed by R_2 and R_G, the voltage E_2^- is calculated as

$$E_2^- = E_1^- + \left(\frac{V^- - E_1^-}{R_2 + R_G}\right) R_G . \tag{4. 4}$$

Substituting V_{IN}^- for E_2^- and V_{IN}^+ for E_1^-, Equation (4.4) becomes

$$V_{IN}^- = V_{IN}^+ + \left(\frac{V^- - V_{IN}^+}{R_2 + R_G}\right) R_G \quad . \tag{4. 5}$$

Solving (4.5) for the output voltage of the operational amplifier A_2 gives:

$$V^- = \left(\frac{R_2 + R_G}{R_G}\right) V_{IN}^- - \left(\frac{R_2}{R_G}\right) V_{IN}^+ \tag{4. 6}$$

The output voltage of the unity gain differential amplifier A_{diff} is $V_o = V_R + \left(V^+ - V^-\right)$. Where V_R is a reference voltage that can be used to modulate the mean value of the amplifier output V_o.

$$V_o = V_R + \frac{1}{R_G}\left(\left(R_2 + R_G\right) V_{IN}^+ - R_2 V_{IN}^- - \left(R_2 + R_G\right) V_{IN}^- + R_2 V_{IN}^+\right) \tag{4. 7}$$

$$= V_R + \left(\frac{2R_2 + R_G}{R_G}\right)\left(V_{IN}^+ - V_{IN}^-\right) \tag{4. 8}$$

Nowadays, the EMG pre-amplifiers circuit shown in Figure 4.1 is typically available in form of an integrated circuit (instrumentation amplifier). Usually datasheets give the value of R_2 while the reference voltage V_R and the gain resistor R_G should be selected during the design process to set the mean value of V_o and the gain G respectively, where

$$G = \frac{2R_2 + R_G}{R_G}. \tag{4. 9}$$

To increase the amplifier's ability to suppress the DC inputs, the low frequent contents of the output signal V_o could be used as reference voltage V_R and negatively fedback to the reference terminal of the pre-amplifier. This technique is known as AC-coupled amplifier.

4.4. Design of the EMG-Amplifier "StiMyo"

This section is showing the design of the 4-channel EMG amplifier (named "StiMyo") which is able to detect the volitional activity from stimulated paretic muscles. The EMG detection is possible in synchronization with FES. This means; the stimulation pulses will be sent at a certain rate (e.g. 20 Hz) to produce a desired muscle contraction, and parallel to this StiMyo is measuring the EMG between stimulation pulses.

Figure 4.2 is showing one channel of the StiMyo amplifier. The diagram illustrates amplifier protection circuits, electrode/skin discharger as well as amplification and analog signal processing stages.

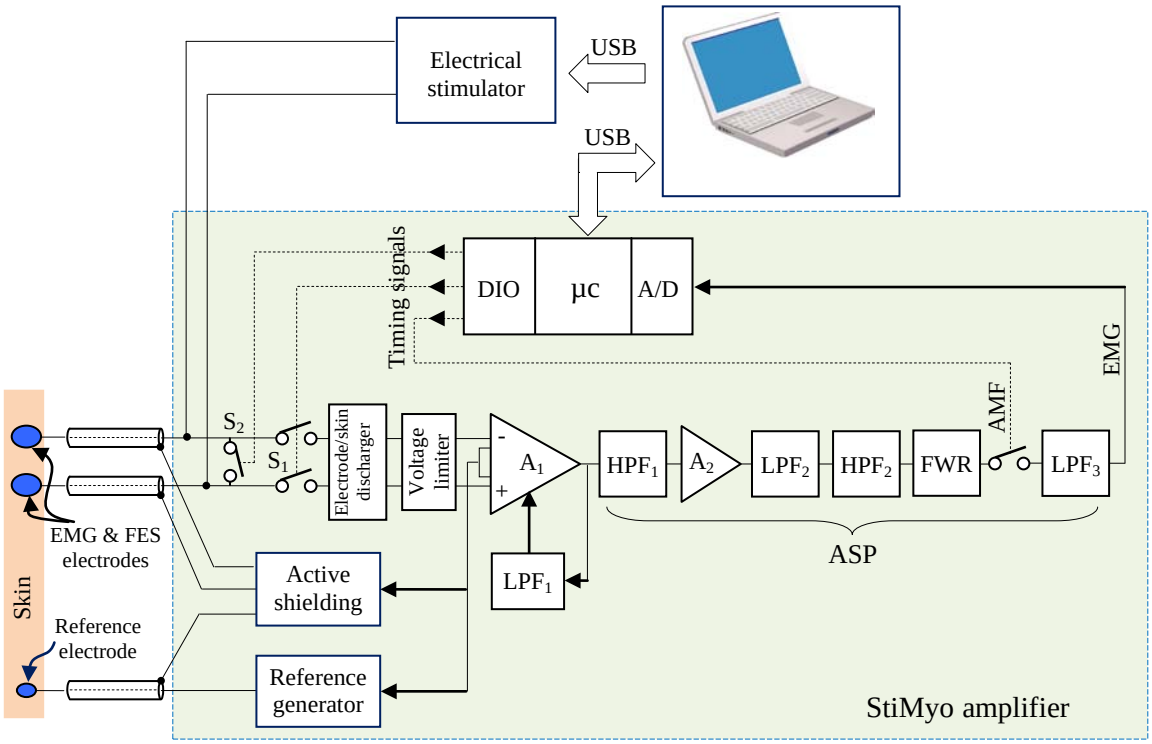

Figure 4. 2: Block diagram showing one channel of the EMG StiMyo amplifier in connection with FES. StiMyo is using shared FES/EMG electrodes.

4.4.1. EMG Pre-amplifier

As shown in Figure 4.2, the first amplification stage A_1 utilizes the instrumentation amplifier INA129 (Texas Instruments, Dallas, Texas, USA) as an EMG pre-amplifier. The amplifier INA129 possesses a very low offset voltage (50 µV). INA129 is furthermore supplemented with integrated over-voltage protectors at the input circuit terminals. This inherent protection can withstand only up to ± 40 V without damage. Protection against stimulation pulses of up to 160 V is therefore introduced by the later described switching circuit. Furthermore, a resistor diode circuit (voltage limiter) is additionally clamping the input signal from electrodes to the ± 5V supply voltages provided by 8 AA batteries [67]. This feature is very useful as it protects the pre-amplifier in case of an unwanted direct connection of stimulator outputs and amplifier inputs. Such an event could be caused by a failure in the switching circuit. The voltage protection circuit (resistor diode circuit shown in Figure 4.3) consists of diodes (BAV199, NXP Semiconductors; Netherlands) with very low leakage current (typically 9pA, max. 5nA) and thin-film precision chip resistors (Tyco Electronics, USA) with 0.1% tolerance. The amplifier INA129 has at least 100 dB Power Supply Rejection Ratio (PSRR) for power supply changes up to 60 Hz. No variations in the supply voltage above this 60 Hz frequency are expected as batteries operate the amplifier.

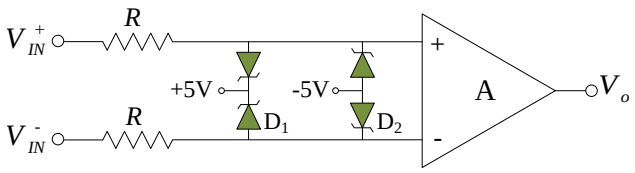

Figure 4. 3: The resistor diode circuit is clamping the input signals from electrodes to the ± 5V supply voltages provided by 8 AA batteries.

To fulfill the DC suppression requirements mentioned earlier, the pre-amplifier with a gain of 10 dB was designed as an AC-coupled amplifier with first order high-pass characteristics (cutoff frequency of 35 Hz) as shown in Figure 4.4. This also suppresses the low-frequent movement and stimulation artifacts from the input signal. This AC-coupling has been realized by feeding the output of the instrumentation amplifier through a first order 35 Hz low-pass filter LPF1 back to the reference terminal of the INA 129 as proposed in the data sheet[12].

12 Texas Instruments, “Precision, Low Power Instrumentation Amplifiers,” 2005.

Frequency response of the AC-coupled amplifier: As shown in Figure 4.2, the AC-coupled amplifier is representing a closed-loop circuit formed by A_1 and LPF_1. To check the operation and the stability of the feedback loop, the equivalent circuit shown in Figure 4.4 (b) was analyzed using standard linear system theory [99].

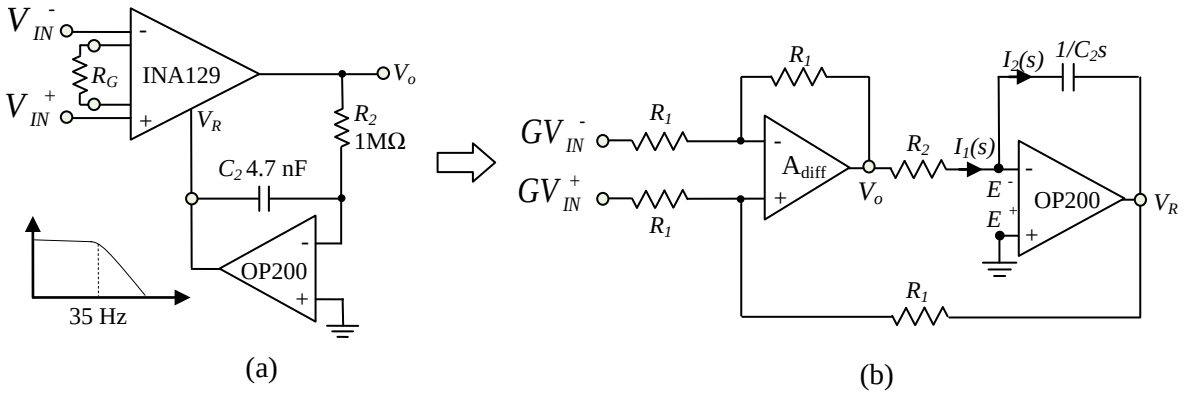

Figure 4. 4: Analysis of the AC-coupled instrumentation amplifier: Subfigure (a) is showing the circuit diagram. The equivalent circuit (in s-domain) of the output stage of INA129 and the feedback LPF is shown in subfigure (b). The amplifier A_{diff} and the four resistors R_1 are representing the output stage of the differential amplifier shown in Figure 4.1.

The output V_o of the instrumentation amplifier INA129 has been obtained by Equation (4.8). Considering the ideal operational amplifier case, the output of OP200 can be obtained as follows:

The input current of OP200 is considered to be zero, so that the input currents $I_1(s)$ and $I_2(s)$ are equal and $E^+ = E^-$. Using the nodal analysis at the E^- node, the current $I_1(s)$ and $I_2(s)$ are obtained as

$$I_1(s) = \frac{V_o - E^-}{R_2}, \tag{4. 10}$$

and

$$I_2(s) = \frac{E^- - V_R}{1/C_2 s}. \tag{4. 11}$$

Setting $I_1(s) = I_2(s)$ and $E^- = 0$ yields

$$V_R = -\frac{V_o}{R_2 C_2 s}. \tag{4. 12}$$

Using (4.12) in (4.8) and solving the result for the pre-amplifier (INA129) output V_o we get

$$V_o = GR_2C_2\left(\frac{s}{R_2C_2s+1}\right)\left(V_{IN}^{+} - V_{IN}^{-}\right), \tag{4. 13}$$

where G = 3.16 (10 dB) is the pre-amplifier gain. From (4.13) the closed loop transfer function T_{pre} of the AC-coupled pre-amplifier is.

$$T_{pre} = \frac{V_o}{\left(V_{IN}^{+} - V_{IN}^{-}\right)} = GR_2C_2\left(\frac{s}{1+R_2C_2s}\right) \tag{4. 14}$$

With the nominal values of the gain G, R_2, and C_2 we obtain

$$T_{pre} = 0.0148\left(\frac{s}{1+0.0047s}\right). \tag{4. 15}$$

The frequency response of T_{pre} is shown in Figure 4.5 (a).

The closed-loop system shown in Figure 4.5 (a) with the open loop transfer function $L(s) = 1/(R_2C_2s)$ = (212.76/s) is stable with 90^o phase margin and infinite gain margin. The frequency response of the AC-coupled pre-amplifier is depicted in Figure 4.5 (b) and shows HPF characteristics.

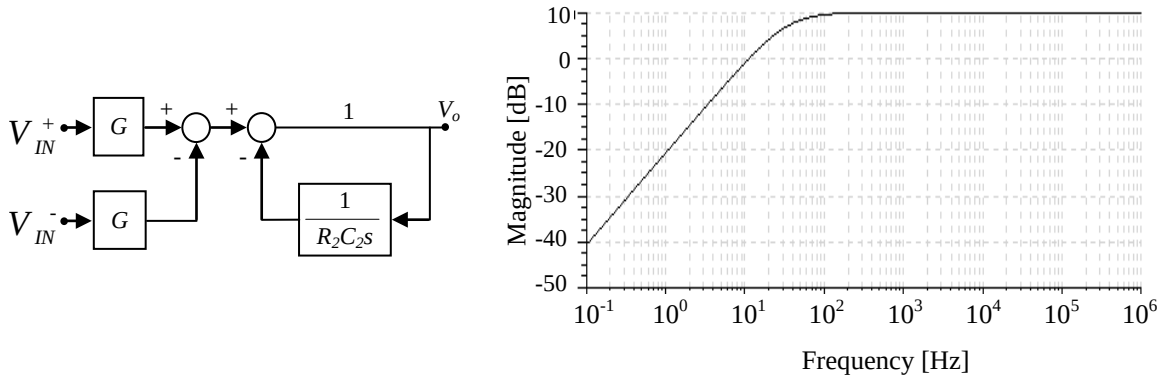

(a) (b)

Figure 4. 5: AC-coupled pre-amplifier: (a) Block diagram which represents the circuit diagram of Figure 4.4, (b) Frequency response showing high pass characteristics.

The next section is investigating the protection of the amplifier inputs against any possible damage which could be caused by the stimulation pulses.

4.4.2. Amplifier Protection and Electrode/Skin Discharging

As shown in Figure 4.2, for each amplifier channel two sets of photo-MOS switches AQV253 (Matsushita Electric Works, Ltd., Osaka, Japan) have been implemented at the amplifier front-end (S1 & S2). The photo-MOS (Metal-Oxide Semiconductor) switch AQV253 was used due to its capability to control an extremely high load voltage, up to 250V, using a low forward LED (Light Emitting Diode) current (typically 0.9 mA) and due to its very low on-resistance (typically 5.5 Ohm). This low on-resistance insures fast discharging of the charge under EMG electrodes via S_2. Furthermore, this switch type possesses a high-speed switching behavior (worst case measured switching times: 0.8 ms turn-on and 0.06 ms turn-off time).

Amplifier Protection: The first set S_1 protects the input circuit of the EMG pre-amplifier from any damage by the electrical stimulation pulses having up to 160 Volt amplitude and reduces the transient artifact by completely isolating the amplifier input from both the current controlled stimulator as well as the target muscle during the delivery of stimulation pulses. The used stimulator possesses two current sources which are multiplexed to four stimulation channels each. For the applications considered in this thesis, the stimulated muscles could be connected to one stimulation module or to two stimulation modules. Stimulation of the second modules starts with 0.6 ms time delay compared to the first module (cf. RehaStim pro^{TM} stimulator in Chapter 3). Channels of one stimulation module cannot be activated simultaneously; a latency of 1.5 ms is separating the activation of each channel from the prior one.

Frequently Electrode/Skin Discharging: The second switch S_2 (cf. Figure 4.6) is normally OFF. For each stimulation cycle and after the delivery of the latest stimulation pulse, S_2 connects the FES/EMG electrodes together to repeatedly relieve the remaining charge under electrodes. The remaining charge at the electrode/skin contact has to be repeatedly reduced. Otherwise, the amplifier could be saturated due to the DC voltage difference between electrodes. The remaining charge may also lead to electrode polarization which could dramatically suppress the level of the detected EMG signals.

The general timing chart of the StiMyo amplifier is shown in Figure 4.6. The operation of each switch is synchronized with the stimulation pulses. Only one stimulation period of 50 ms is presented.

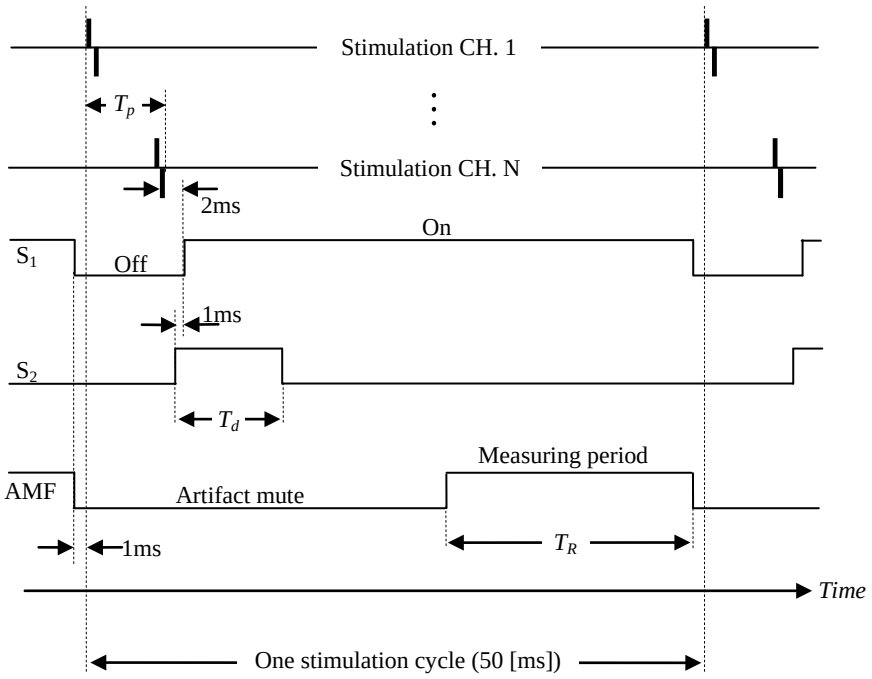

Figure 4. 6: Timing chart showing the operation of the different photo-MOS switches in synchronization with stimulation pulses.

To set the timing chart for the different switches the time T_p which the stimulation device needs to deliver the required stimulation pulses must be determined at first. This time depends on the number of active stimulation channels and whether these channels are belonging to one stimulation modules or to two modules.

Each stimulation channel has a time slot of 1.5 ms to generate the biphasic stimulation pulse. Hence, the time needed for multichannel stimulation using a one stimulation module is

$$T_p = 1.5\text{ms} \cdot N_{CH} \,. \tag{4. 16}$$

Where N_{CH} is the number of active stimulation channels.

The time needed for multichannel stimulation using two stimulation modules is

$$T_p = \max\left\{(1.5\text{ms} \cdot N_{CH}^{1}) \,,\ (0.6+1.5\text{ms} \cdot N_{CH}^{2})\right\} \tag{4. 17}$$

where; N_{CH}^{1} is the number of active channels from the first stimulation module, and N_{CH}^{2} is the number of active channels from the second stimulation module.

Taking the stimulation pulses delivery time T_P into account, the Off-period of S_1 should be set to be at least T_P+3 ms. To assure full protection of the StiMyo amplifier, the Off-period of S_1 starts 1ms before the onset of the first stimulation pulse. The Off-period of S_1 is extended by at least 2 ms beyond the end of the T_P period. During this extension period the switch S_2 starts the electrode/skin discharging process.

One millisecond before the S_1 Off-period, the switch S_2 starts to connect the two electrodes together; this creates a high-current path to permit fast electrode/skin discharging in order to minimize the length of the device blinding period due to saturation and to prevent electrode polarization. The electrode/skin discharging period T_d should provide enough discharging time for all stimulation channels. The last switch, the artifact mute filter (AMF), will be described in the next section.

All switches are controlled by external control signals generated on a micro controller ATmega328 (Atmel Corporation, San Jose, USA). In order to prolong the allowed measurement period and to achieve a high signal to noise ratio, an experimental optimization of the timing charts well be discussed in Chapter 6.

Permanent Electrode/Skin Discharging: Unfortunately the discharging through S_2 is limited to a few milliseconds every stimulation period. The reason for this is that S_2 must be released as soon as possible to give the amplifier the opportunity to measure the desired EMG signals before the onset of the next stimulation pulse. Under good stimulation conditions (symmetrical biphasic pulses and well prepared skin with good electrode-skin contact), the frequent discharging via S_2 should be sufficient. However, this measure is not able to prevent electrode polarization when asymmetrical biphasic pulses are applied and/or in presence of bad electrode/skin connection. In such situation, longer discharging periods via S_2 are needed. Unfortunately, this period cannot be extended so much as mentioned above. One alternative to the extension of the S_2 On-period is to apply a permanent discharger in form of a resistor between the measurement lines after the S_1 switches. A permanent discharging also during the EMG-measurement takes place. This will reduce the level of remaining charge under electrodes and in turn reduce electrode polarization. More details about this type of electrode discharging will be discussed in Section 4.6.

4.4.3. Signal Processing

As shown in Figure 4.2, the output signal from the AC-coupled pre-amplifier A_1 passes through a chain of Analogue Signal Processing (ASP) stages containing: filtering, scaling, and muting components. These ASP stages were implemented using the dual operational amplifier OP200 (Analog Devices, Norwood, USA). Advantages of using this amplifier are its low noise and its high stability when driving a large capacitive load. The pre-amplifier A_1 is followed by a Chebychev

configuration second order active high-pass filter (HPF_1) with unity gain and selectable cutoff frequency F_{CL} in the range 150 Hz ~ 250 Hz. The Chebychev configuration has been selected to achieve a fast roll-off in the frequency response. The design and analysis of the HPF1 are shown in Appendices A1.1. The high-pass filtered signal is then rescaled by a gain of 55 dB through the amplification stage A_2. High frequency noise is suppressed by a first order low-pass filter (LPF_2) with cutoff frequency of 700 Hz (cf. Appendix A1.3). The signal is then again high-pass filtered through HPF_2 that have the same characteristics as HPF_1. The purpose of HPF_2 is to assure elimination of the signal's DC-part before feeding it to the analogue full wave rectification.

Thus the StiMyo amplifier shown in Figure 4.2 has an entire gain of about 65 dB, before the Full Wave Rectifier (FWR) block, and a total band-pass characteristics of (F_{CL} ~ 700 Hz), where F_{CL} was the selectable cut-off frequency of HPF_1 and HPF_2in the range 150 ~ 250 Hz. Additional analogue signal processing is performed via a precision FWR followed by another photo-MOS switch AQV257 acting as an Artifact Muting Filter (AMF). Figure 4.6 shows the timing signal to drive the AMF which introduces a muting period during the delivery of stimulation pulses and the switching artifact periods. This AMF period starts 1ms before the onset of the first stimulation pulse. As shown in Figure 4.6 the time T_R is representing the signal recording period which is considered to be an artifact free period. Finally, the average (integrated) value of the detected volitional/reflex muscle EMG activity is obtained by a first order active low-pass filter (LPF3) having 5 Hz cut-off frequency.

The StiMyo output is sampled at 20 samples per second by a micro-controller ATmega328 (Atmel Corporation, San Jose, USA) with 10 bit ADC. Within with last filter stage (LPF3), also signal amplification by the factor 3.5 is performed to fully exploit the input range (0 ~ 5 V) of the A/D converter. The obtained digital signal is transmitted via an optically isolated USB-link to a PC (cf. Figure 4.2). Synchronization of the stimulation and EMG-measurement (timing of switches and sampling) is in the responsibility of a PC program running under real-time Linux (RTAI extension[13]) which periodically triggers the stimulation device and the micro-controller of the StiMyo via commands sent over the optically-isolated USB interfaces at the stimulation frequency of 20 Hz.

4.4.4. Active shielding and Reference Generator

Active shielding of cables is commonly used in the EMG amplifiers to reduce the effects of external noise and electrostatic interferences as well as parasitic capacitances of the shielded cables. In the case of active shielding, the outer conductor (shielding) is simply driven at the same potential as the

[13] *http://www.rtai.org*

inner conductor by using a buffer amplifier [100], [101]. Using active shielding, the external interferences are suppressed through the low output impedance of the unity gain amplifier shown in Figure 4.8. The parasitic capacitance C_p has no effect on the EMG measurement because both the shield and the inner conductor are at the same potential, i.e. the potential of C_p is equal to zero [102]. Parasitic capacitances of the shielded cables for differential mode signals are not problematic as the measurement of EMG signals has restricted frequency content [103]. Ideally, parasitic capacitances do not affect the measurement of EMG signals since both cable conductors are at the same potential. Each EMG channel has its own active shielding.

A single reference-signal generator (driven-right leg system [104]) is used for all EMG channels to compensate common mode disturbances at the measurement electrodes up to several volts of the amplifier's power supply. Input to this reference driver is the average of the input signals of the first channel.

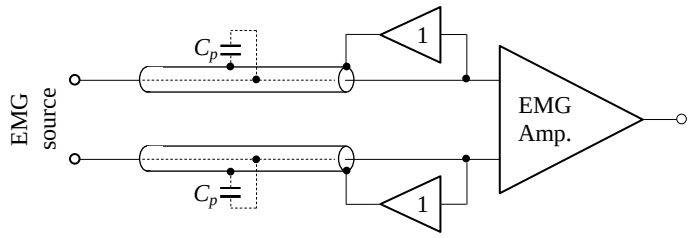

Figure 4. 7: Active shielding, the outer conductor is driven at the same potential as that of the inner conductor by using a buffer amplifier.

For EMG-measurement, carbon coated shielded cables (Mind Media BV, Roermond-Herten, The Netherlands) have been used.

4.5. Experimental Evaluation of the StiMyo Amplifier

The *CMRR*, the input resistance R_{in} of the StiMyo amplifier as well as the signal to noise ratio have been experimentally evaluated in order to assure the fulfillment of the EMG amplifier requirements.

4.5.1. Common Mode Rejection Ratio

The common mode rejection ratio of a differential amplifier was already defined as the ratio between the differential mode gain A_{dm} and the common mode gain A_{cm}, thus

$$CMRR = 20\log\left(\frac{A_{dm}}{A_{cm}}\right) \quad [\text{dB}]. \tag{4. 18}$$

A sinusoidal signal of 800 mV amplitude and variable frequency over the range of (50 Hz – 700 Hz) has been used to calculate the *CMRR* of the pre-amplifier stage. At selected frequencies in the range given above, the amplifier was operated at first in common mode connection and then in differential mode connection. The calculated *CMRR* over the entire frequency range has been recorded (cf. Table 4.1). Figure 4.8 is showing as well the *CMRR* of the StiMyo amplifier. A *CMRR* of at least 80 dB has been experimentally determined for common mode disturbances up to 700 Hz.

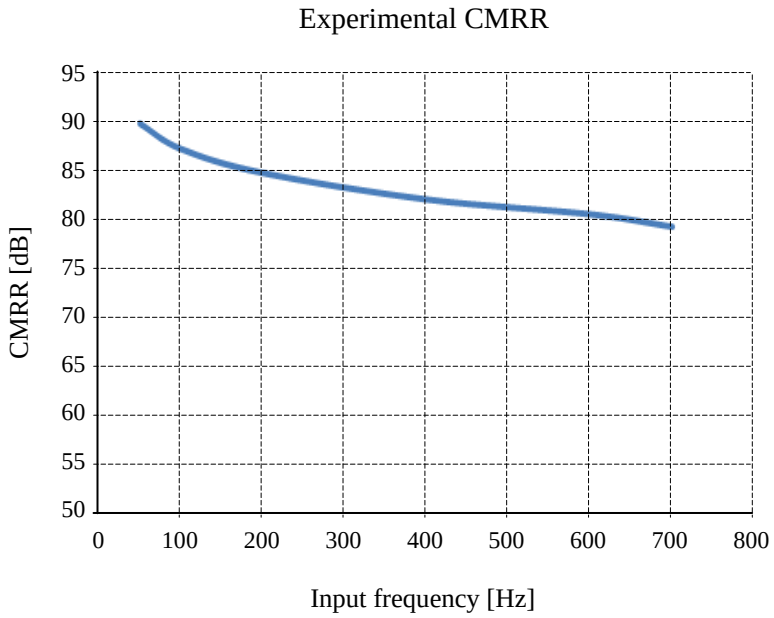

Figure 4. 8: Measured *CMRR* of the pre-amplifier versus input frequency.

Table 4. 1: *CMRR* of the pre-amplifier calculated at different frequencies.

Frequency [Hz]	50	100	200	400	600	700
CMRR [dB]	90.048	87.506	85.073	82.401	80.902	79.637

4.5.2. Input Resistance of the Amplifier (R_{in})

Measurement technique: To measure the input resistance R_{in} of the pre-amplifier a variable resistor R_s has been connected in series with a sine wave generator V_s. This combination has been connected

to the amplifier inputs as shown in Figure 4.9. The relation between the pre-amplifier output V_o and R_s can be written as

$$V_o = GV_s \left(\frac{R_{in}}{R_s + R_{in}} \right) \tag{4. 19}$$

with

$$V_s \left(\frac{R_{in}}{R_s + R_{in}} \right) = V_{in} \cdot \tag{4. 20}$$

From (4.19), the maximum output $V_o^{\max}$ is obtained for R_s= 0 Ω, thus

$$V_o\big|_{R_s=0} = V_o^{\max} = GV_s \, . \tag{4. 21}$$

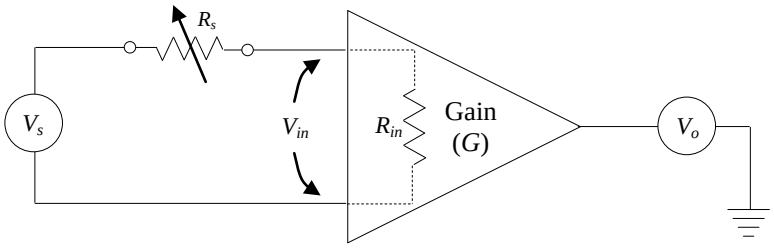

Figure 4. 9: Circuit diagram showing the experimental set-up for the evaluation of StiMyo input resistance.

If the value of R_s becomes equal to the internal resistance R_{in} of the amplifier, the output V_o will drop to the half of its maximum value. From (4.19), it follows

$$V_o\big|_{R_s=R_{in}} = V_o^{H} = G\frac{V_s}{2} \, . \tag{4. 22}$$

From (4.21) and (4.22) we obtain:

$$V_o^{H} = \frac{V_o^{\max}}{2} \tag{4. 23}$$

Experimental Procedure: The sine wave generator V_s was adjusted to an output frequency of 400 Hz and a fixed amplitude signal of 1 Volt. Starting from R_s= 0 Ω, the value of R_s was increased in 22 MΩ steps. For each step, both R_s and the corresponding value of V_o were recorded (cf. Table 4.2). The obtained data were plotted in Figure 4.10.

At R_s = 0 Ω, V_o was measured to be 3.16 V and 1.29 V was the value corresponding to R_s=154 MΩ. The relation between V_o [V]and R_s [MΩ] is almost linear, and the following equation can be obtained graphically from Figure 4.10:

$$V_o \approx 3.16 - \frac{1.87}{154} R_s \qquad (4.\ 24)$$

R_s can be written as

$$R_s \approx \frac{154}{1.87}(3.16 - V_o)\ . \qquad (4.\ 25)$$

From Table 4.2 the maximum output is $V_o^{\max} = 3.16$ V. With $V_o^H = 1.58$ V the value of R_{in}=R_s can be calculated by using Equation (4.25):

$$R_s = R_{in} \approx \frac{154}{1.87}(3.16 - 1.58) = 130.1 \ \text{MΩ}$$

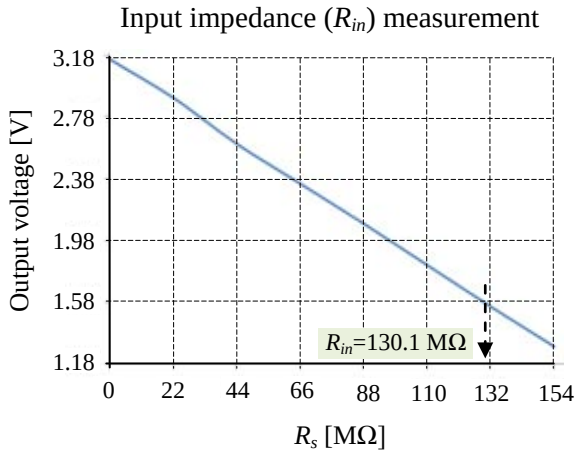

Figure 4. 10: The output signal V_o versus the value of the series resistor R_s. The experimentally measured R_{in} = 130 MΩ.

Table 4. 2: Measurement of input resistance, V_{out} vs. R_s.

R_s [MΩ]	0	22	44	66	88	110	132	154
V_o [V]	3.16	2.91	2.61	2.35	2.09	1.82	1.55	1.29

4.5.3. Signal to Noise Ratio (SNR)

In this section, the signal to noise ration of the entire amplifier will be investigated; and the estimated range of input signal will be calculated.

Input Range: To estimate the input range of StiMyo amplifier the simplified block diagram shown in Figure 4.11 has been used. The diagram is showing the signal flow from the input V_{in} to the output V_o, passing through the amplified and bandpass filtered signal V_1, the full-wave rectified signal V_2, the muted signal V_3 and the integrated signal V_4.

To calculate the range of the input signal, the following simplifications were assumed:

- Switching artifacts are not present.
- The input signal is a sine wave of 400 Hz so that the distortion effect from the band-pass filter can be ignored.
- The recording period T_R is an integer multiple of the period T_{V_3} of the rectified signal V_3.
- The averaging filter (LPF_3) is approximated by an integrator, which is reset at the beginning of each stimulation period, and the output value of the amplifier V_o is sampled at the end of each stimulation period.

The recording period T_R can be extended up to 25 ms from a stimulation period of 50 ms (cf. Figure 4.11).

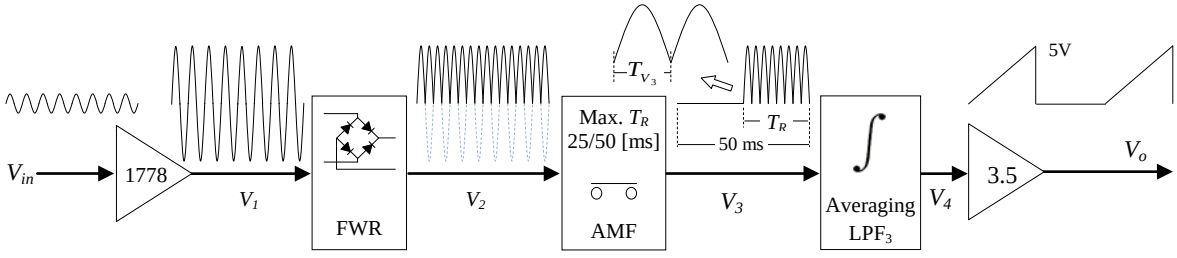

Figure 4. 11: Block diagram showing the signal flow from the input V_{in} to the output V_o. The internal signals are the amplified and band-pass filtered signal V_1, the full-wave rectified signal V_2, the muted signal V_3 and the integrated signal V_4.

Assuming, that the assumptions hold, the signal V_3 is defined for each stimulation period to be

$$V_3(t) = \begin{cases} 1778\left|V_{in}(t)\right| & during \quad T_R \\ 0 & otherwise \end{cases} \quad \text{V}. \tag{4. 26}$$

It is assumed that the EMG measurement period T_R exactly fits to an integer number of periods of the rectified signal V_3:

$$T_R = n \cdot T_{V_3} \tag{4. 27}$$

where *n* is an integer number and T_{V_3} is the period of the rectified signal V_3.Thus for any periodical input signal the value of the integrated signal portion is always the same at the end of each stimulation interval as indicated in Figure 4.12 (a).

When the condition (4.27) is satisfied, the value of the sampled outputV_o^s, which is determined at the end of each integration periodT_R, is

$$V_o^s = 3.5\left(\frac{T_R[ms]}{50}\right)\left(\frac{2V_3^P}{\pi}\right) \quad \text{V} \tag{4. 28}$$

where V_3^P is the peak value of the rectified signal.

If the condition (4.27) is not satisfied, the value of V_o^s will slightly change from one stimulation cycle to the other. This variation in the V_o^s level is related to the shift of the recorded signal with respect to the measuring window T_R as shown in Figure 4.12 (b). This variation will appear in V_o^s as fluctuations. It should be noted, that these fluctuations are not a kind of high frequency noise which is produced by the amplifier itself.

In the later calculated SNR_{dB} (cf. Figure 4.13) such fluctuation in the sampled output voltage V_o^s will not be taken into account when calculating the SNR.

The maximum allowed level of V_o^s is $V_{o-\max}^s = 5\,\text{V}$ and for the maximum T_R period it follows

$$V_{o-\max}^{s} = 3.5\left(\frac{25}{50}\right)\left(\frac{2V_3^P}{\pi}\right) = 5 \text{ V} \tag{4. 29}$$

$$V_3^P = V_{3-\max} = 4.89 \text{ V} \tag{4. 30}$$

where $V_{3-\max}$ is the maximum allowed value of V_3^P .

Hence the estimated maximum allowed amplitude of the input signal is

$$V_{in-\max} = \frac{V_{3-\max}}{1778} = 2.75 \quad \text{mV} \tag{4. 31}$$

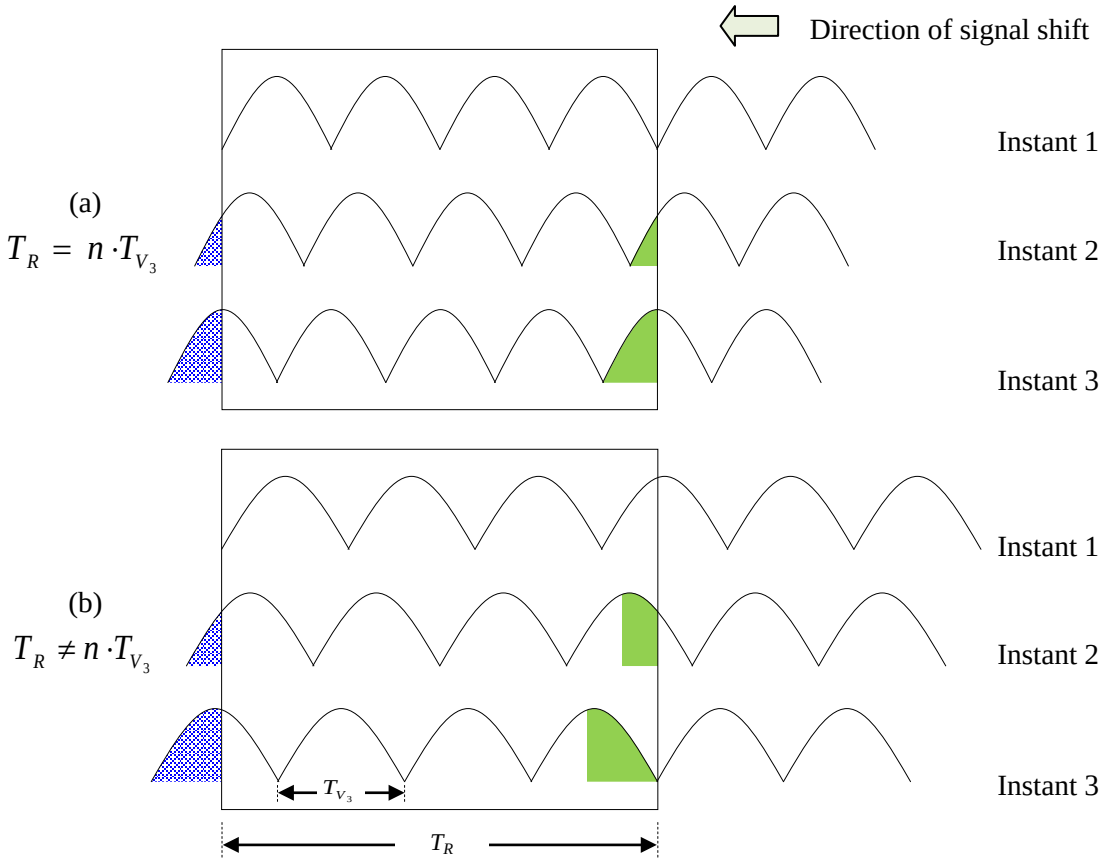

Figure 4. 12: Interaction between the measuring window T_R and the period of the measured signal T_{V_3} . In (a), the window size is fitting to an integer number of the signal periodT_{V_3} . It is clear that the portion of signal entering the window is exactly equal to that leaving it. Thus the value of the integrated signal is always the same at the end of the window. Subfigure (b) is indicating that the value of the integrated signal will vary from cycle to cycle when the condition (4.27) is not satisfied.

SNR: Noise signals and not completely removed switching artifacts are adversely affecting the EMG measurement. These signals are not desirable. The signal to noise ratio determines the amplifier capability to distinguish between the desired and the non-desired signals. An experimental assessment of SNR was carried out for 4 channels with different HPF frequencies using a measurement interval T_R 16 ms (yielding $V_{in\text{-max}}$=4 mV). The SNR has been assessed via a two steps experiment. In the first step (Sub-test A), the output signal which is related to the ambient noise is recorded; this was achieved by connecting both amplifier inputs to the power supply ground. In the second step (Sub -test B), a 4 mV amplitude, 400 Hz sine wave was used as a desired input signal. Sample output signals for the 150Hz HPF EMG-channel are shown in Figure 4.13.

For all HPF frequencies, the recorded signals were quantified through their Root Mean Square (RMS) given by

$$Y = \sqrt{\frac{1}{N}\sum_{k=1}^{N}\left(V_o^s(k)\right)^2}\,. \tag{4. 32}$$

Where $V_o^s(k)$ is the k^{th} sample of the output signal and N = 4200 is the number of recorded samples.

The SNR_{dB} is defined by

$$SNR_{dB} = 20\cdot\log\left(\frac{Y_{d+n}}{Y_n}\right). \tag{4. 33}$$

Where Y_n is the RMS of the noise-related output (measured during Sub-test A with grounded inputs), and Y_{d+n} is the RMS value of the output due to the sine wave input signal plus the contribution of the ambient noise (measured during Sub-test B).

Table 4.3 is showing the calculated SNR_{dB} for all frequencies that have been tested during StiMyo design and optimization processes. Results are showing a high SNR for all frequencies.

In Chapter 5, more general experiments will be presented in order to optimize the settings of timing charts and HPF frequencies. The aim of the optimization process is to increase the ability of the amplifier to distinguish between non-FES induced EMG and both the switching and stimulation artifacts.

Table 4. 3: Signal to noise ratio in decibel at different HPF frequencies.

HPF	250[Hz]	200[Hz]	170[Hz]	150[Hz]
Y_{d+n} [V]	3.113	3.223	4.174	4.657
Y_n [mV]	8.83	13.77	22.51	30.32
SNR_{dB}	50.944	47.387	45.363	43.729

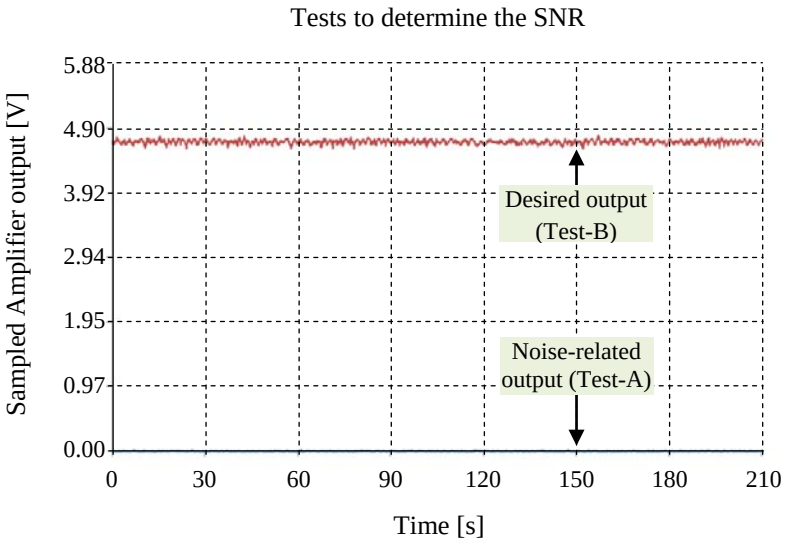

Figure 4. 13: Sample signals showing the desired and the noise related output of the StiMyo device for the channel with 150 Hz HPF. Measurement sampling frequency is 20 samples per second.

4.6. Observations on Electrode Polarization and Fast Discharging

The amplifier has been evaluated for EMG detection during two FES applications, FES-cycling on an ergometer and for FES control of the wrist-joint angle. During these evaluation processes two observations have been made: EMG Suppression due to electrode polarization and discharging induced action potentials named as D-waves

EMG Suppression: The EMG suppression is mostly related to electrode polarization. In case of bad electrode/skin contact and/or asymmetry between biphasic stimulation pulses or asymmetry between the electrode/skin impedances a large amount of charge could remain under electrodes. Under such conditions, DC potential differences will appear between the two electrodes. This will lead to electrode polarization. The conduction within the adhesive-gel layer and the stratum corneum (outermost layer of the epidermis) is considered to be of the ionic type [105], [106]. Thus, the gel layer of every electrode and the stratum corneum are representing electrolytes. Under DC bias, the electrode/skin contact will be polarized and form a depletion layer. In this case, the current passing

between the two polarized electrodes through the skin and muscle tissues will be depressed due to the lake of current carriers within the depletion layer. This will visible in form of EMG suppression. To minimize the suppression of EMG, the charge remaining under electrodes and in turn the DC voltage difference between them must be relived. At this point the need of permanent electrode/skin discharging may arise. To understand the issue of EMG suppression due to electrode polarization a model representing the interface between stimulation electrodes and skin over a stimulated muscle will be briefly presented in Section 4.6.1. The effect of applying permanent electrode discharging on electrode polarization and EMG suppression will be explained in the subsequent Section 4.6.2.

D-Wave: During FES control of the wrist-joint angle, an action potential has been sometimes observed at different stimulation levels based on the electrode types and skin preparation. This AP, which was observed for the first time, is similar to the waveform of M-wave, but with much higher latency. This AP was identified to be a second muscle action potential that is elicited by the forced electrode/skin discharging current; and to be neither F-wave nor H-wave because it was sustainable at a sequence of stimuli and showed a variable latency for different stimulation intensities. Within this thesis, the term (D-wave) is used to describe this *Discharging-related* waveform. No D-waves have been observed during FES-cycling for the applied stimulation intensities.

In Section 4.6.3, the effects of stimulation intensities and S_2 discharging time T_d on the D-wave latency will be investigated.

4.6.1. Electrode-Skin Model

A linear electrical circuit model which describes the nature of the human skin impedance during surface functional electrical stimulation has been studied by many research groups. All models were only considering the behavior of electrode/skin impedance under the application of FES; and none of them were taking the electrode polarization effects on the recorded EMG signals into account.

For example Boxtel [105] and Dorgan et al. [106] have presented the linear electrical circuit model shown in Figure 4.14.

The impedance of stratum corneum was modeled by the parallel combination of the capacitance C_p and the resistance R_p. The resistance R_s is describing the resistance of deep tissues. A series combination of the capacitor $2C_{pol}$ and resistor $R_{pol}/2$ is modeling the electrode/skin polarization at each electrode.

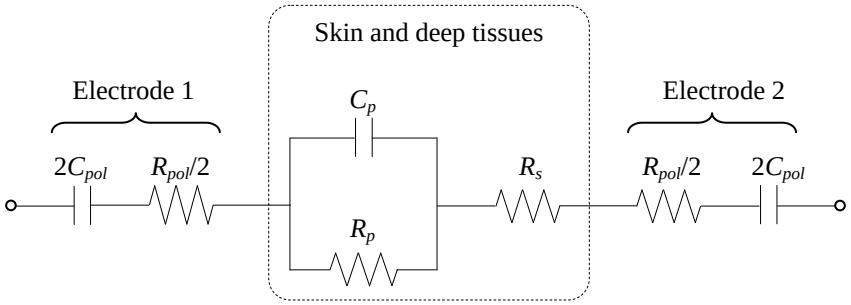

Figure 4. 14: Linear electrical model which represents the interface between electrodes/skin and deep tissues. The resistor R_s is modeling the resistance of deep tissues. The parallel combination of capacitor C_p and linear resistor R_p models the skin impedance. The electrode-skin polarization was modeled by (R_{pol}, C_{pol}).

4.6.2. Permanent Electrode/Skin Discharging

The depletion layer which the electrode polarization creates in the electrolyte (skin and the adhesive-gel layer) reduces the electrode/skin conductivity. This suppresses the bio-signals passing to the amplifier via the two electrodes, and in turn the recorded EMG will be clearly depressed. When EMG is to be measured from the stimulated electrodes (the scope of this thesis) a severe EMG suppression can be expected.

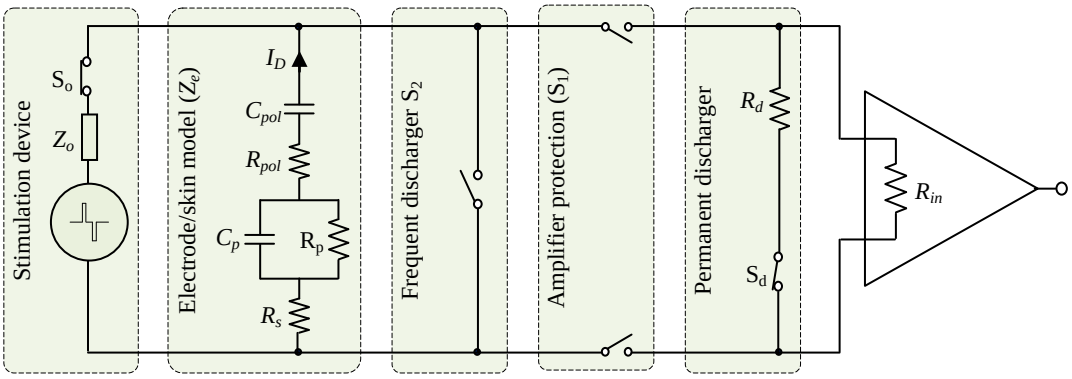

Figure 4. 15: Diagram showing the connection of the permanent discharging resistor R_d. The value of the total discharging impedance is $Z_D = Z_e + (R_d//R_{in}//S_2//Z_o)$. Where Z_e is the electrode/skin impedance and R_d is the permanent discharging resistor. R_{in} and Z_o are the amplifier input resistance and the stimulator output impedance respectively. The instantaneous value of Z_D depends on the operation of the different switches.

Under such polarization conditions the need for more efficient electrode/skin discharging arises. Permanent electrode/skin discharging also during the EMG-measuring period may reduce the DC voltage difference between electrodes and in turn reduce the electrode polarization. A resistor connecting the two EMG recording cables is a simple example of such permanent discharger as shown by R_d in Figure 4.15. The electrode/skin interface model mentioned above has been used to show the function of the permanent discharging resistor R_d.

The electrode discharging current I_D passes between the two electrodes and through the total discharging impedance Z_D. As shown in Figure 4.15, Z_D is formed by the parallel combination of the external electronic circuits (R_d, R_{in}, S_2 and Z_o) in series with the impedance of electrode/skin model Z_e. The value of Z_D is calculated as

$$Z_D = Z_e + (R_d \,//\, R_{in} \,//\, S_2 \,//\, Z_o). \tag{4. 34}$$

The current I_D depends on the DC voltage difference between the two electrodes and on the components involved in the total discharging impedance Z_D. Based on (4.34), Table 4.4 is showing the value of Z_D for all possible states of the switches S_1, S_2 and the manually-controlled switch S_d. The contribution of Z_o has been neglected since the switch S_o is connecting the stimulator to the electrodes only during the delivery of stimulation pulses. Hence,

$$Z_D = Z_e + (R_d \,//\, R_{in} \,//\, S_2). \tag{4. 35}$$

If the switch S_2 is on, Z_D is reduced to Z_e regardless R_d is connected or not. Otherwise, it follows

$$Z_D = Z_e + (R_d \,//\, R_{in}). \tag{4. 36}$$

Table 4. 4: The total discharging impedance Z_D for all possible states of the switches S_1, S_2 and S_d.

Switch	Status							
S_d	off				on			
S_1	off		on		off		on	
S_2	off	on	off	on	off	on	off	on
Z_D	» ∞	Z_e	$Z_e + R_{in}$	Z_e	» ∞	Z_e	$Z_e + (R_{in}//R_d)$	Z_e

The speed of electrode/electrolyte discharging depends on the value of the total discharging impedance Z_D. If discharging time T_d of the frequent discharger S_2 is not sufficient to reduce the remaining charge in the electrode/electrolyte capacitance C_{pol}, the assistant resistor R_d should be

manually activated (via S_d) to introduce a lower-resistance discharging path. This should relieve the charge under electrodes and mostly stop the EMG suppression. Figure 4.16 is implementing the data given in Table 4.4 and showing the effect of using R_d on the instantaneous value of Z_D over one stimulation period.

From Table 4.4, If S_1 is on and S_2 is off the value of the discharging impedance becomes $Z_D = Z_e + R_{in}$ (almost $Z_D = R_{in}$, i.e. tens of MΩ). If R_d is switched on for the same S_1 and S_2 conditions, the value of Z_D becomes $Z_e + (R_{in} // R_d)$. Since $R_{in} >> R_d$ the value of Z_D will be reduced to almost $Z_e + R_d$. Lower value of Z_D permits higher discharging current, and vice versa.

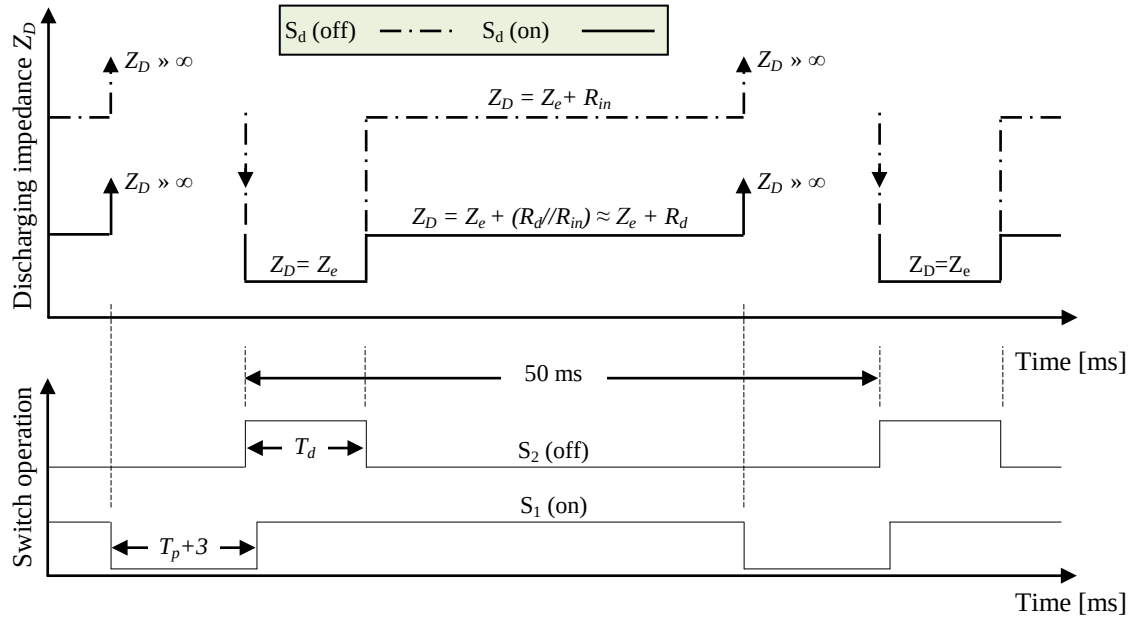

Figure 4. 16: Diagram showing the instantaneous value of Z_D. During the interval T_d the switch S_2 is on and the value of $Z_D = Z_e$. The consideration of resistors R_d and R_{in} depends on the status of the switches S_1 and S_d (cf. Table 4.4).

The disadvantage of using such R_d is that amplifier input resistance will be reduced. The value of R_d should be carefully selected. A large R_d might be not sufficiently discharge the polarization capacitor C_{pol}. On the other side, a small R_d value could dramatically reduce the amplifier input resistance. In this thesis, a resistor R_d of 100 KΩ has been applied and experimentally tested without any harmful effects on the StiMyo device performance. Such resistor is not a replacement of the frequent discharging switch; it should be used as an additional discharger.

4.6.3. Discharging-Related Action Potential (D-wave)

Fast Discharging: After the delivery of each stimulation pulse, parts of stimulation charge remain under electrodes. In normal EMG amplifiers the remaining charge is slowly reduced due to the small discharging-current I_{in} which passes through the amplifier input resistance R_{in}, as shown in Figure 4.17(a). Usually, the time between successive stimulation pulses is quite short; this may lead to sufficient and permanent electrode/skin charge which could be enough to drive the amplifier into saturation, especially when EMG is measured from FES electrodes. Due to these reasons fast discharging of the electrode/skin junction is strictly connected with the process of EMG measurement from stimulation electrodes. As mentioned above, fast elimination of electrode/skin charge is possible by inducing a high current path immediately after the delivery of stimulation pulses (cf. the automatically controlled switch S_2 in Figure 4.17(a)).

The switch current I_s is much higher than the amplifier input current I_{in}. The switch S_2 connects stimulation electrodes together, and permits a large discharging current to pass through the muscle tissues ($I_D = I_s + I_{in}$) and in turn causes a faster drop of the remaining charge. Figure 4.17(b) is showing the relation between S_2 operation and discharging current I_D.

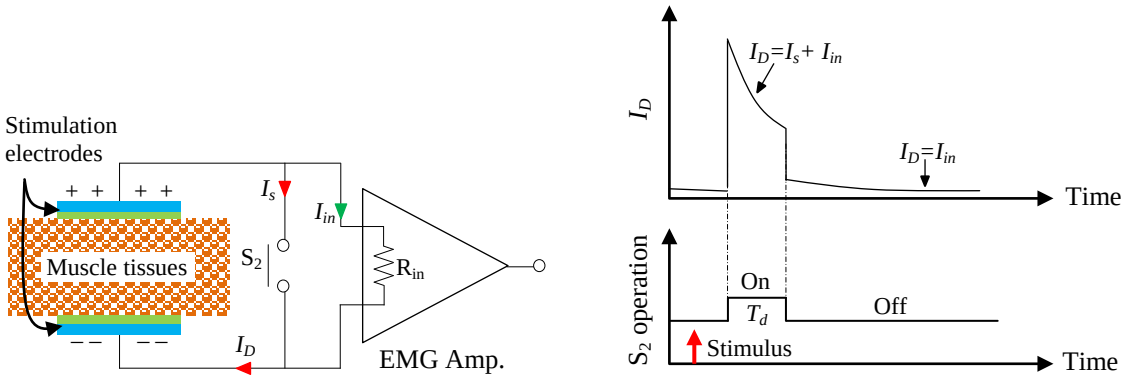

Figure 4. 17: Operation of S_2 (periodic electrode/skin discharger). I_D is the total discharging current; I_{in} is the low discharging current passing through the amplifier input resistance. The current I_s is the forced discharging current during the interval T_d.

Effect of the Discharging Current: Depending on the value of the remaining charge and Z_D, the discharging current I_D could be large enough to elicit a discharging-related muscle action potential which was named in this thesis as D-wave. A clear dependence of the D-wave latency (T_D) on the stimulation intensity Q and on the S_2 discharging time T_d has been observed. This dependency is considered to be strong evidence that the observed waveform is an AP related to the electrode discharging current I_D and not an H-reflex or F-wave triggered by the main stimulus. Based on the

level of I_D, each stimulation period could be divided into two intervals (cf. Figure 4.17 (b)). The first is the high current interval T_d in which is $I_D = I_s + I_{in}$. The second is the remaining part of the stimulation period with low discharging current $I_D = I_{in}$. The next two figures will aim to explain the relation between D-wave latency T_D and both stimulation intensity Q and T_d.

***Definition*:** The threshold charge Q_D is defined to be "the minimum charge that must be injected to the neuromuscular system during the electrode/skin discharging process in order to elicit the D-wave".

The threshold stimulation level Q_D is a function of the waveform of stimulation pulses. For simplicity it will be assumed that the dependency of Q_D on the pulse form can be ignored. The threshold charge Q_D is then calculated as

$$Q_D = \int_0^{T_D - D_n} (I_D . t)\, dt \,. \tag{4. 37}$$

where D_n is a fixed delay between the AP induced in the nerve innervating the muscle and the appearance of the resulting muscle action potential (D-wave) in the EMG.

It is clear from (4.37) that for low I_D a long integration time will be required to accumulate the threshold stimulation charge Q_D, i.e. a low discharging current will produce a D-wave with long latency and vice versa.

Figure 4.18 is showing the electrode discharging phase from one stimulation period. It explains the relation between the fast discharging interval T_d and the resulting D-wave latency T_D. Two different discharging periods ($T_{d1} < T_{d2}$) have been considered while applying the same stimulation intensity Q. Longer T_d should leave less charge under electrodes at the end of each stimulation period and results in a lower discharging current I_D in the next period, hence longer integration time to reach the Q_D level is required. I.e. longer T_d increases the D-wave latency.

Unfortunately we have to keep the fast electrode discharging although the D-wave effects. The conclusion from Figure 4.18 is using longer T_d value could increase the D-wave latency and kick it out of the EMG recording period. However the value of T_d is limited due to the reasons mentioned above. This thesis is presenting the permanent electrode/skin discharger R_d as a technical solution that kicks the D-wave out from EMG recording period. The advantage of using such permanent discharger is to avoid any additional transient that can shorten the EMG recording periods. The permanent discharger R_d will reduce the remaining charge under electrodes, this will produce less I_D current during the forced electrode discharging period T_d.

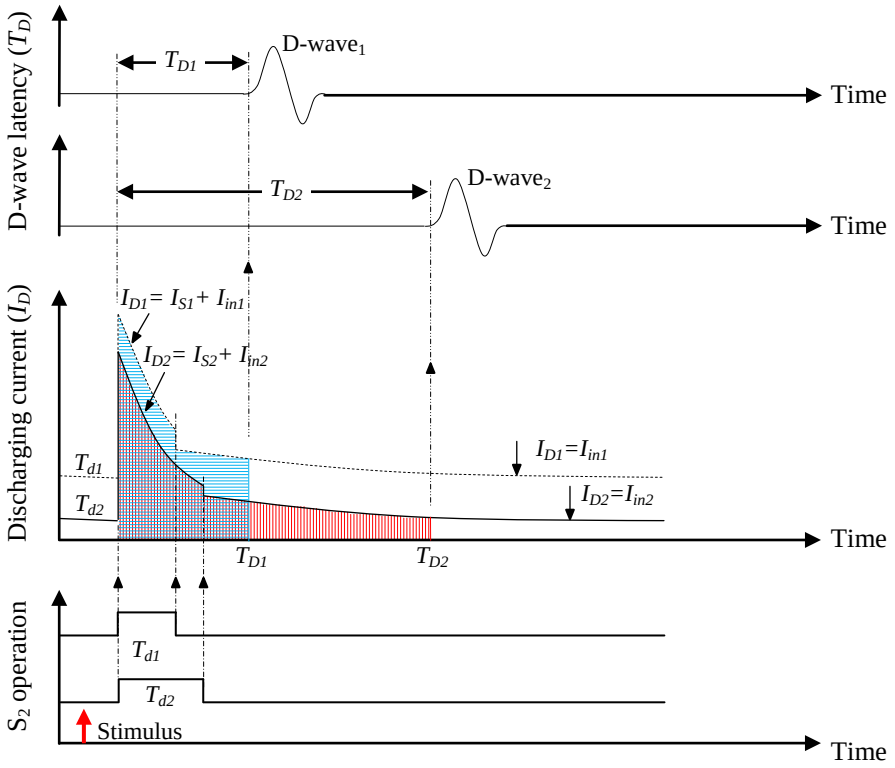

Figure 4. 18: Electrode/skin discharging phase, showing the effect of the forced discharging periods on the D-wave latency T_D. Applying the same stimulation charge, two different intervals ($T_{d1} < T_{d2}$) show that longer T_d produces D-wave with longer latency.

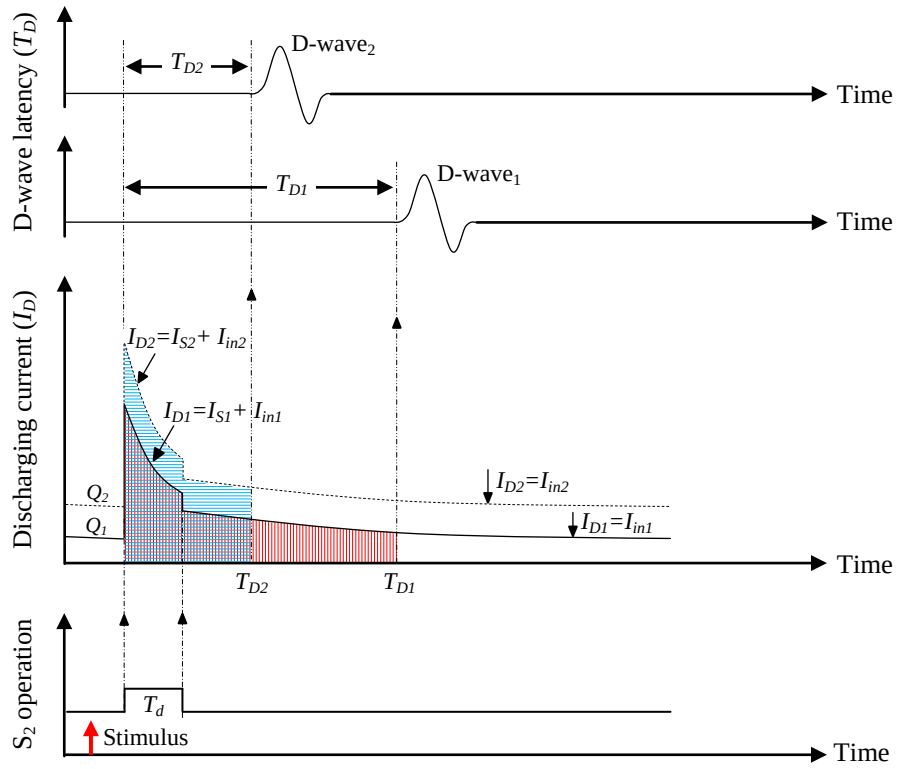

Figure 4. 19: Electrode/skin discharging phase, showing the effect of different stimulation intensities on the D-wave latency T_D. Using constant discharging time T_d, the application of two stimulation intensities ($Q_1 < Q_2$) show that larger Q causes shorter D-wave latency.

Figure 4.19 is showing the electrode discharging phase which explains the effect of applying different stimulation intensities ($Q_1 < Q_2$) on the D-wave latency T_D, when the forced electrode discharging time T_d is kept constant. Higher stimulation intensity Q_2 leaves more remaining charge under the electrodes; this yields a higher current I_{D2}. According to Eq. (4.37) shorter T_{D2} time will be required to inject the necessary charge dose Q_D to the stimulated muscle and vice versa.

The suppression of the surface EMG during FES is limiting the applicability of EMG-proportional FES. Also, an appearance of D-wave during the EMG recording period will disturb the control action because the controller cannot distinguish between D-wave and vEMG. The experimental investigation of the effect of both stimulation level Q and the fast discharging periods T_d on the latency of D-wave will be presented in the next section.

4.6.4. Experimental Setup

Figure 4.20 is showing a computer-controlled FES system in which the StiMyo was integrated. The purpose was to experimentally show the effect of stimulation charge Q and electrode discharging time T_d on the latency of D-wave. Furthermore, the aim was to investigate the EMG suppression due to electrode polarization and to demonstrate the benefits of applying the permanent electrode discharging R_d as countermeasure. All experiments in this chapter were performed with one healthy male subject[14]. The stimulator RehaStim pro™ stimulation device (HASOMED GmbH, Germany) was connected to the StiMyo amplifier. The stimulation pulses were delivered at 20 Hz frequency to the major wrist-joint and finger extensors (extensor carpi ulnaris, extensor carpi radialis and extensor digitorum) through two reusable self-adhesive hydrogel electrodes (Type: RehaTrode – oval 60 x 40 mm, HASOMED GmbH, Germany) . One ENG single-use electrode (Ambu Blue Sensor NF, Ambu, Denmark) of size 28x20 mm was used as a reference electrode and placed on the elbow. Stimulation pulses with controllable normalized charge (Q_{norm} from 0 to 1 which corresponds to 10-400 μs pulse width and to 5-20 mA current amplitude) were sent to the stimulated muscles. The charge control mode-I was applied to determine pulse widths and current amplitudes of the stimulation pulses. The inertial sensor (MT9-B, Xsens Motion Technologies, The Netherlands) was used to detect the wrist-joint angle. The inertial sensor includes a gyroscope, an accelerometer and a magnetic field sensor, which are all three-axial. The MT9-B is connected to a laptop though one digital signal processing unit (Xbus-Master, Xsens Motion Technologies, The Netherlands) using an USB interface. By using a Direction Cosine Matrix (DCM)-based orientation estimation algorithm [93], the wrist joint-angle can be determined from the calibrated sensor signals on the laptop. The forearm was lying on the table. Hence, the extension/flexion angle of the wrist joint can be measured using only one inertial sensor mounted on the back of the hand. The laptop screen is online showing

[14] *The studies in this chapter were approved by the Local Research Ethics Committee at Charité Berlin.*

the measured wrist-joint angle that can be used as a visual feedback signal. Just for a better interpretation of the processed EMG measurements (output of the StiMyo). Internal EMG amplifier signals (before rectification) The D-wave effect was monitored at 2 kHz with a 16-bit data acquisition card (NI DAQCard-6036E, National Instruments). For safety reasons the laptop was powered through an isolation transformer while using the DAQ-card. The maximum and minimum stimulation intensities are determined in a pre-experiment using an USB potentiometer (PowerMate, Griffin Technology).

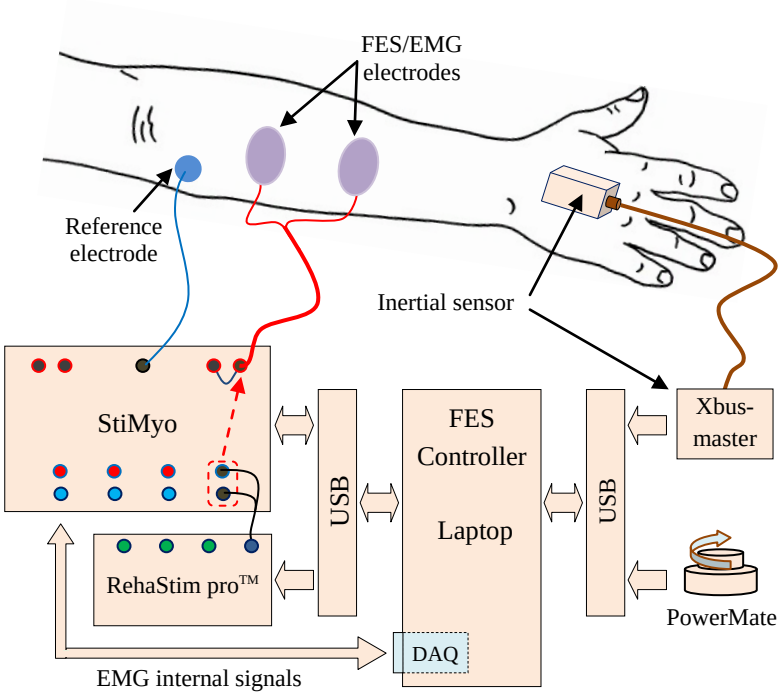

Figure 4. 20: Diagram showing the experimental setup for the investigation of the effects of the permanent electrode discharger R_d on EMG suppression. The setup was also used to show the effect of both the stimulation intensity Q and electrode discharging time T_d on the latency of the D-wave.

4.6.5. Results on EMG Suppression

Experimental protocol: A periodical trapezoidal waveform was used to for the stimulation charge Q. The maximum stimulation level was selected to produce sufficient wrist-joint extension and was expressed as a percentile of the used 10 µC maximum stimulation charge. The permanent discharger R_d was initially disconnected (off). When the stimulation reaches its maximum the subject was asked to shortly increase his wrist-joint angle by 10^o (volitionally). This volitional contribution should be repeated every new stimulation period. Also between the stimulation phases, the subject

was asked to volitionally extend the wrist-joint. After two stimulation periods the resistor R_d was manually switched on, while the subject was instructed to repeat the same volitional contribution on top of the maximum FES levels. The experiment was conducted twice. The first experiment was performed when a clear EMG suppression occurred. The second experiment was performed under normal EMG recording conditions where no electrode polarization and no clear EMG suppression were observed. The same protocol was applied in both experiments. In both experiments, the recorded data were the stimulation intensity, the wrist-joint angle and the electromyogram (output of the amplifier).

In the Figures 4.21 and 4.22, the left sub plots show results for the disabled resistor R_d while the right sub plots contain results for the connected resistor R_d. It can be observed from Figure 4.21 what a clear EMG suppression was present in case of the unconnected resistor. The detected volitional EMG-level during stimulation significantly increases by the activation of the resistor. Also the EMG-activity related to the T-reflex (caused by sudden drop of the hand at the end of stimulation) can be better seen after the polarization was stopped by the connected resistor. Under normal EMG recording conditions (no polarization) no effect can be observed by connecting or disconnection the resistor R_d (cf. Figure 4.22).In Figure 4.21, for the non-connected resistor, disturbances in EMG due to the D-wave (D-wave effect) can be observed. By enabling the resistor, these disturbances could be removed as the D-wave was moved outside the EMG-measurement period.

One drawback of using R_d is an increase of the base EMG level as seen in Figure 4.21.

A numerical performance index *PI* has been defined as the ration between the average value of *vEMG* and the corresponding average wrist-joint angle. (cf. the shaded bands in Figures 4.21 and 4.22). *PI* is calculated as

$$PI = \frac{vEMG_{av}}{\theta_{av}} \quad \text{[V/rad].} \tag{4. 38}$$

where $vEMG_{av}$ is the average vEMG and θ_{av} is the average angle of the wrist-joint.

The performance index *PI* was used to evaluate the degree of EMG suppression with and without the application of the permanent electrode discharging resistor R_d (cf. Table 4.5).

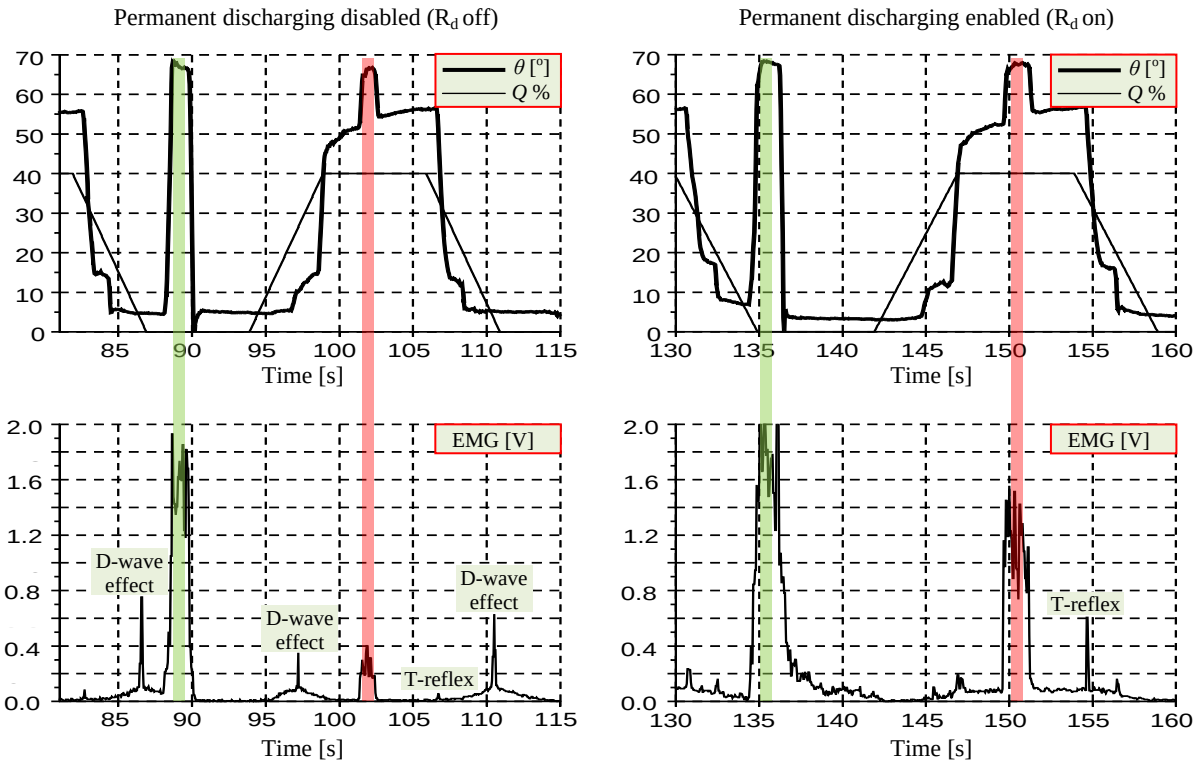

Figure 4. 21: The left side shows EMG suppression due to electrode polarization when permanent discharging is off. The right side shows that the application of the permanent electrode discharging reduces the electrode polarization.

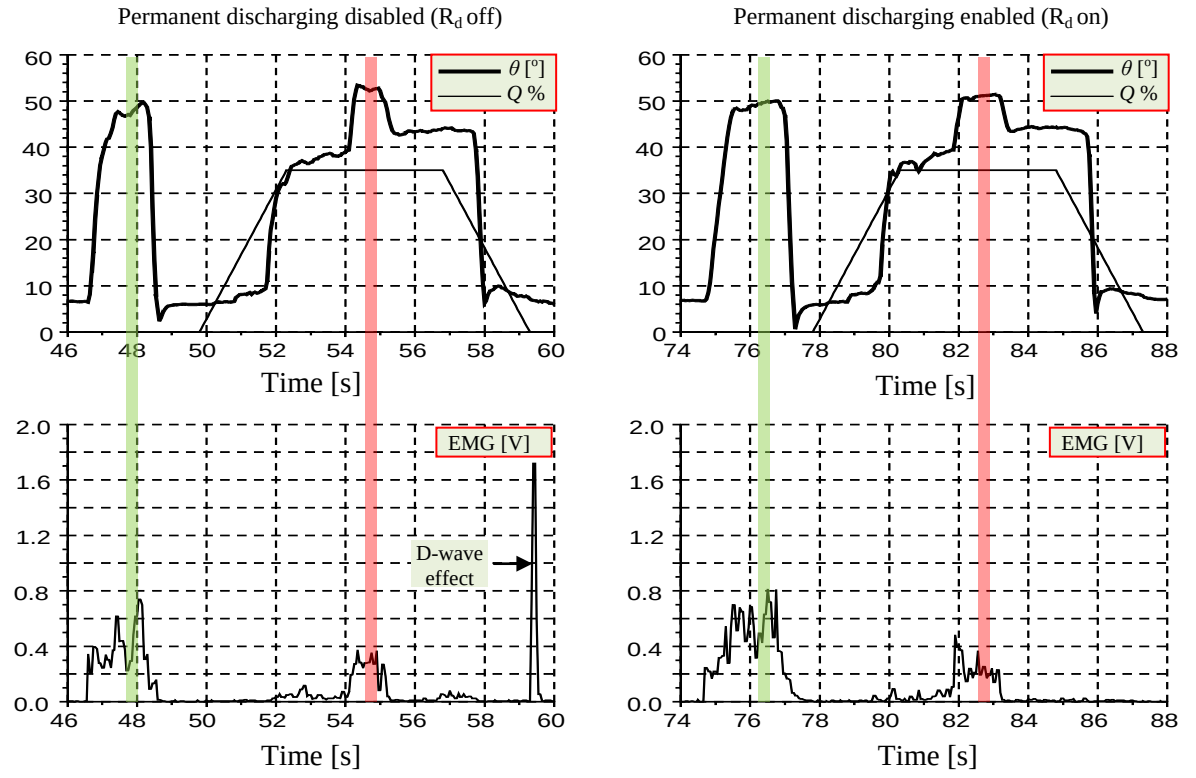

Figure 4. 22: The effect of the resistor R_d under normal EMG recording conditions (no electrode polarization).

Table 4. 5: Performance index *PI* representing the ratio between $vEMG_{av}$ and the average wrist-joint angle θ_{av}.

	Clear EMG suppression				No EMG suppression			
FES	off		on		off		on	
R_d	off	on	off	on	off	on	off	on
PI [V/rad]	1.57	1.74	0.25	1.17	0.41	0.55	0.23	0.22

4.6.6. Observations on the Latency of D-wave

The experimental results in this section are showing the relation between the D-wave latency T_D and both the stimulation charge Q and the forced discharging intervals T_d. Figure 4.23 illustrates the effect of stimulation intensity on the D-wave latency. The plot shows superposed the raw (none rectified) EMG signal (internal amplifier signal) of three stimulation periods with different stimulation intensities ($Q_1<Q_2<Q_3$). In agreement with the explanation in Section 4.6.3, (cf. Figure 4.19), the experimental data show that higher stimulation intensity leads to shorter T_D and vice versa. The shaded area in Figures 4.23 to 4.25 is representing the AMF period.

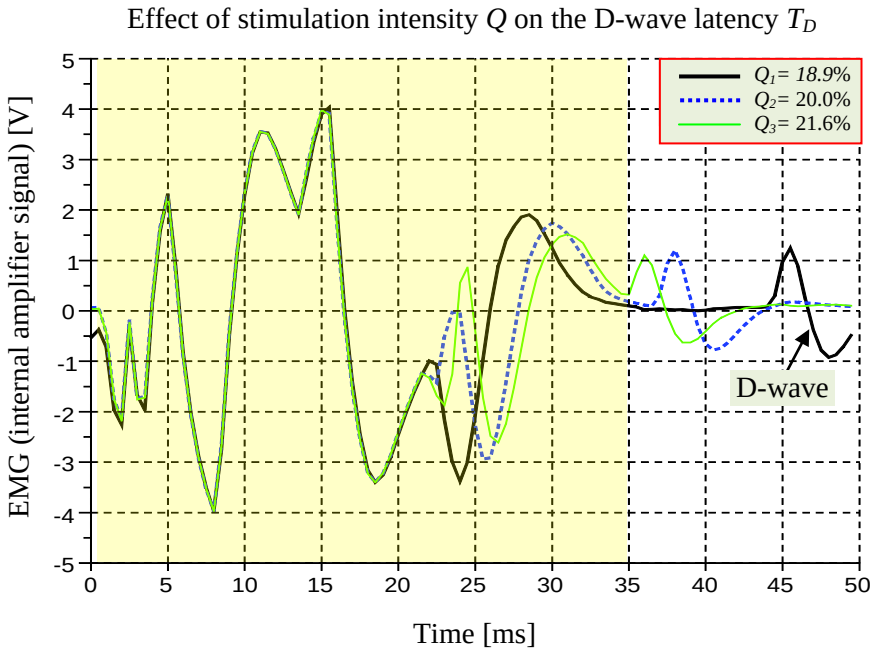

Figure 4. 23: Superposed internal amplifier signals (before rectifier) for three stimulation periods with constant T_d and different stimulation intensities ($Q_1<Q_2<Q_3$). Higher stimulation intensity leads to shorter T_D, such that ($T_{D1}>T_{D2}>T_{D3}$) are corresponding to ($Q_1<Q_2<Q_3$) respectively.

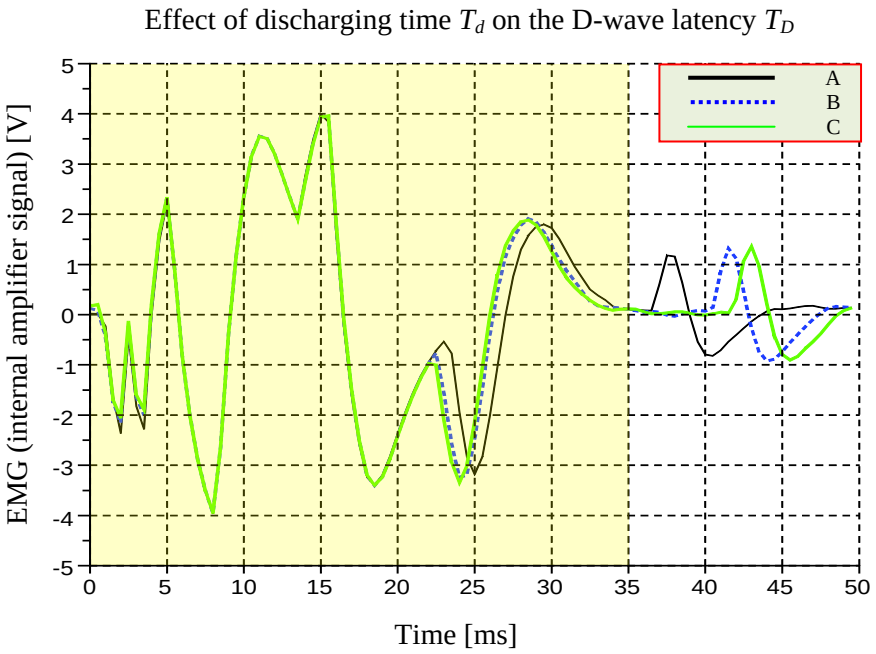

Figure 4. 24: Superposed internal amplifier signals (before rectifier) for three successive stimulation periods with constant *Q*. The plots are showing three different T_D latencies produced due to sudden change in the T_d period from 6 ms to 7 ms. The time order for those periods is A → B → C, which means that the D-wave starts at certain position and shifts to the right side.

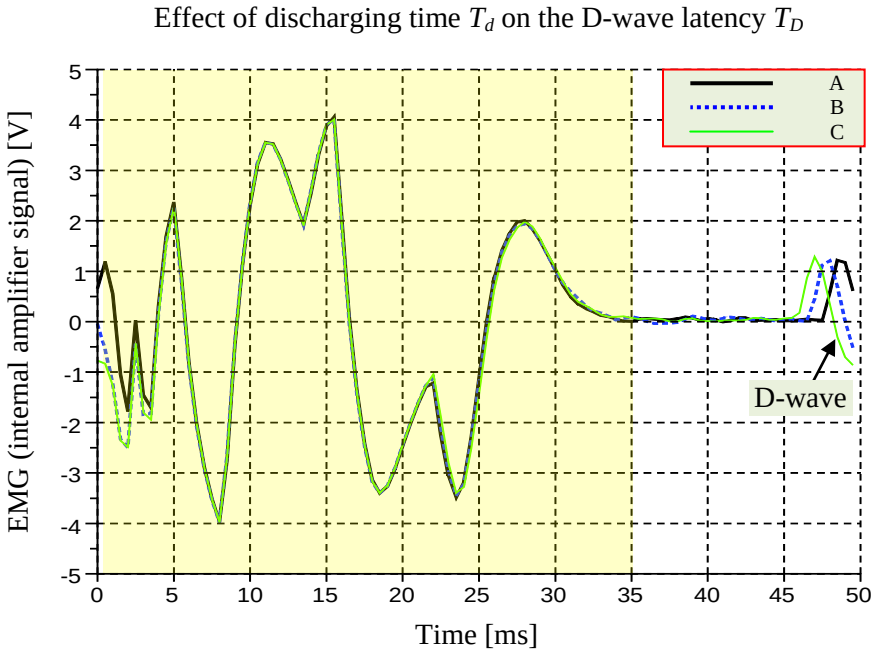

Figure 4. 25: Superposed internal amplifier signals (before rectifier) for three successive stimulation periods with constant *Q*. The plots are showing three different T_D latencies produced due to sudden change in the T_d period from 8 ms to 7 ms. The time order for those periods is A → B → C, which means that the D-wave starts at certain position and shifts to left side.

Figures 4.24 and 4.25 are illustrating the effect of the forced discharging time T_d on T_D when the stimulation intensity Q is kept constant. Internal amplifier EMG signals were recorded during three successive stimulation periods. Figures 4.24 is showing three different T_D latencies produced due to sudden change in the forced discharging time T_d from 6 ms to 7 ms. And Figures 4.24 is showing three different T_D latencies produced due to sudden change in the T_d period from 8 ms to 7 ms. The results approved the explanation discussed in Section 4.6.3 (cf. Figure 4.18), i.e. longer T_d period causes D-waves with higher latency, and vice versa.

4.7. Discussion and Conclusions

It is a big challenge to use stimulation electrodes to measure non FES-related EMG between stimulation pulses. A very limited number of articles describing EMG-recording systems from stimulation electrodes using switching circuits have been reported as outlined in Chapter 2. The reported devices by other research groups have only been applied for stimulation of muscles which require moderate stimulation intensity (dorsiflexor in [61], [62], and upper limb in [79], [80], [107]). It is therefore questionable, if the previously described EMG amplifiers work adequately for higher stimulation intensities applied, for example, during FES-cycling in stroke patients.

This chapter introduced the design process and the experimental evaluation of the StiMyo device which is a 4-channel EMG amplifier. The investigated device shows a good capability of detecting residual volitional EMG signals from stimulation electrodes during FES. It is suitable for EMG detection from small muscles when it is too difficult to use separate electrodes for stimulation and EMG recording. By reducing the number of electrodes and connected wires costs related to this will also be minimized. Compared to the similar devices in literature, StiMyo is able to measure a wider range of EMG frequencies during higher stimulation intensities. This makes it usable for EMG detection during FES-cycling as later shown in Chapter 5. A switching network was applied to protect the amplifier input circuitry and to introduce fast electrode/skin discharging. Two important issues related to EMG recording from stimulation electrodes have been addressed. The first is the electrode polarization leading to EMG suppression. The suppression of EMG was sometimes observed in experiments with healthy subjects. The second issue is the observation of a new EMG waveform. The new observed wave form is a second action potential related to the the electrode/skin discharging process. This wave form was named as D-wave in this thesis. To deal with electrode polarization and D-waves, a permanent electrode/skin discharging resistor has been proposed as a technical solution. This countermeasure reduces the effect of EMG suppression and it also moves the D-wave out from EMG recording intervals.

Inability to measure M-wave due to the relatively long mute periods is considered to be the main disadvantage of such EMG amplifier. To remove non-desired switching artifacts, stimulation artifacts and the low frequency part of electrode discharging, a limited frequency bandwidth had to be applied. The frequency bandwidth is ranged from 150 Hz to 700 Hz. Other devices in literature applied even narrower frequency bands. For example Muraoka [64] developed a device that detects a volitional EMG frequency band of 330 Hz to 460 Hz. Also the limited EMG recording interval (at least 15 ms recording period of each 50 ms stimulation period) due to artifact mute periods is another limitation.

To optimize the StiMyo performance for detecting volitional EMG activity during FES, an experimental tuning of the timing chart for the switches and of the HPFs frequency will be presented in Chapter 6. The Chapters 5 and 6 will describe possible applications of the StiMyo device in detail.

Chapter 5

5. Application of EMG in FES-Cycling

5.1. Introduction

Functional electrical stimulation leg cycle ergometry (FESLCE), which is often used as exercise for people with spinal cord injury (SCI), has recently been applied in the motor rehabilitation of stroke patients. The first completed studies show controversial results, but with a tendency to positive training effects. Currently used technology is identical to that applied in FES-LCE for SCI, whereas the pathology of stroke differs strongly. Most stroke patients with hemiparesis are able to drive an ergometer independently. Depending on the degree of spasticity, the paretic leg will partially support or hinder movements. Electrical stimulation increases muscle force and endurance and both are pre-requisites for restoring gait. However, the effect of FES-LCE on improving impaired motor coordination is still unclear.

To assess motor coordination during FES-LCE, it is important to monitoring non FES-induced EMG during FES-cycling. In this chapter the StiMyo EMG-amplifier is evaluated during FES-cycling on healthy subjects. The purpose is to investigate the feasibility to monitor vEMG or spasticity induced muscle activity during FES. The technology presented here can be used to monitor the effects of FES-LCE to adapt the stimulation strategy or to realize EMG-biofeedback training.

This chapter is organized as follows: In Section 5.2, a brief review about the use of FES-cycling in stroke rehabilitation will be presented. Section 5.3 describes the experimental setup of the computer-controlled FES-cycling ergometry system and explains the applied stimulation pattern generator as well. Section 5.4 is showing the experimental procedure. The experimental results are given in Section 5.5. The discussion of the obtained results, the conclusions and an outlook for future work are given in Section 5.6.

The results presented in this chapter are already published in a journal article [108].

5.2. FES Cycling in Stroke Rehabilitation

Normal cycling exercises: The recovery of gait is one of the main goals of motor rehabilitation after stroke. Within this chapter, cycling on an ergometer represents an often used training modality to establish prerequisites for successful gait training. Nearly all people know how to cycle and do so in a very consistent and stereotyped fashion. Most patients, even those who are not fully ambulatory, can pedal on an ergometer at zero or light resistance. Such cycling exercises can also be safely performed from a wheelchair before gait training is possible. Modern ergometer systems possess electrical drives to support or hinder the cycling movement depending on the abilities of the patient. In one study [34], a cycling wheelchair is described which can be driven by pedaling with the legs. Using this wheelchair practical locomotion for the hemiplegic patients without walking ability is possible at least when moving on a straight line. Another advantage of cycling is that the active Range of Movement (ROM) at the hip or the knee is greater for cycling than for walking. Thus the effect of stretch may reduce the muscle spasticity, if present. Cycling may even prevent contractures of the leg joints and delay or prevent the onset of spasticity when it is directly preformed after the acute phase of stroke. Active cycling exercises also lead to an increase in endurance and muscle strength of both legs. These improvements lead to an increase of walking speed as reported in several studies [109-112]. However, locomotor coordination does not improve post-intervention, as shown by Kautz et al. [109], for most of the patients. Only a very limited number of studies describe specialized cycling exercises for retraining of motor coordination.

Brown and DeBacher [113] proposed an EMG biofeedback cycling exercise to train muscle coordination in patients with spastic hemiparesis. The aim of the training was to increase the activity of the flexors in the paretic leg while decreasing spastic reactions of the leg extensors during flexion phases. The resistance of the ergometer is increased until the patient can control his/her paretic muscles in such a way that the 180^{o} phase shifted reciprocal muscle activity of the healthy leg can be reproduced by the paretic leg. A case study illustrated this approach.

Commercially available ergometers with motor assistance sometimes offer a symmetry training to balance the effort of paretic and healthy leg. A symmetry index is calculated from the motor torque and displayed to the patient who can adjust his/her cycling accordingly. However, because only the motor torque is used to determine the symmetry index and not individual force sensors at each pedal, the accuracy of such a symmetry index is questionable. Pulling and pushing with the healthy leg can equally lead the patient to believe the symmetry between both legs is perfect, whereas the paretic leg might not be active at all.

FES cycling exercises:

The application of functional electrical stimulation (FES) via surface electrodes to the lower limbs, with FES synchronized to the cycling movement, can enhance the rehabilitation progress of the patients. FES directly activates the paretic muscles. This prevents muscle atrophy and helps to build up muscle mass and strength. The possible gain in induced force due to FES in the paretic leg is generally limited because residual sensation limits the stimulation intensity. Therefore, a complete compensation for motor deficits by FES might not be possible in all stroke patients.

FES induced afferent-efferent stimulation together with cutaneous and proprioceptive inputs could be important in ‘‘reminding’’ subjects how to perform the movement properly. Indeed, this complete afference of the task could enhance the synaptic controls and modify the excitability of specific motor neurons, thus facilitating the reorganization of the motor schemes and accelerating the process of functional recovery. Such effects of FES have already been described in the literature concerning the stimulation of the upper extremity and FES for drop foot treatment in stroke survivors [17].

Several clinical studies [37-39], [114], [115] evaluating the effects of FES leg cycle ergometry (FES-LCE) in gait rehabilitation of stroke patients have already been performed. Some of the studies report statistically significant positive effects on muscle force and statistically non-significant positive effects on some mobility measurements compared with standard rehabilitation [38] or cycling exercise without FES [114], [115]. Janssen et al. [39] could not observe improvements in the training effects by adding FES to cycling exercises in stroke patients. The stimulation and training protocols differ much for all reported studies. This reveals that no standard protocols for FES cycling currently exist. Eigler [114], Ferrante et al. [38] and Ambrosini et al. [115] used motorized ergometers and stimulated both legs (also the non-paretic), whereas Janssen et al. [39] used an isotonic cycle ergometer (Ergys2) with flywheel stimulating only the paretic leg. Patients were allowed to cycle voluntarily on the resistance controlled ergometers (isotonic mode) in studies by Eigler [114] and Janssen et al. [39], whereas Ferrante et al. [38] and Ambrosini et al. [115] instructed the patients to be passive during the exercise. In the latter case, a movement of the legs was solely induced by the motor and FES. Stimulated muscles in all studies have been the quadriceps, hamstring and M. gluteus maximus (cf. Figure 5.1). In [38], [114], [115] M. tibialis anterior was also electrically stimulated. In summary, recent studies show that FES assisted cycling exercise can have positive effects in stroke patients.

While muscle strength and endurance can be increased by such therapy forms, the effects on motor relearning and muscle coordination remain unclear. By extrapolating results from training programs

with intensive ergometer exercises without stimulation, no positive effects could be expected. Changes in muscle coordination due to the FES cycling rehabilitation program have not been evaluated using electromyograms (EMGs), neither during cycling nor during gait. Incorrect muscle activation patterns caused by spastic hemiplegia might be manifested by repeating such impaired movement patterns. In the studies of Ferrante et al. [38] and Ambrosini et al. Ambrosini et al. [115], the symmetry in the task was the aim of the therapy. Therefore, both legs were stimulated and no voluntary muscle activity was requested from the patients. Using this approach, no incorrect movement patterns are elicited, which can yield good motor relearning and muscle coordination, as indicated by the presented results of a sit-to-stand test in [38]. Existing clinical FES cycling systems do not observe the immediate effect of the intervention on movement symmetry, muscle coordination, and spasticity. There is also no method to check if muscle fatigue is present or not. Ambrosini et al. [116] investigated the use of individual force sensors on both legs to exactly assess symmetry in the driving torques produced by FES. Based on this information, a feedback control strategy is proposed to individually adjust stimulation intensity applied to both legs with the aim of maintaining symmetry in torque generation.

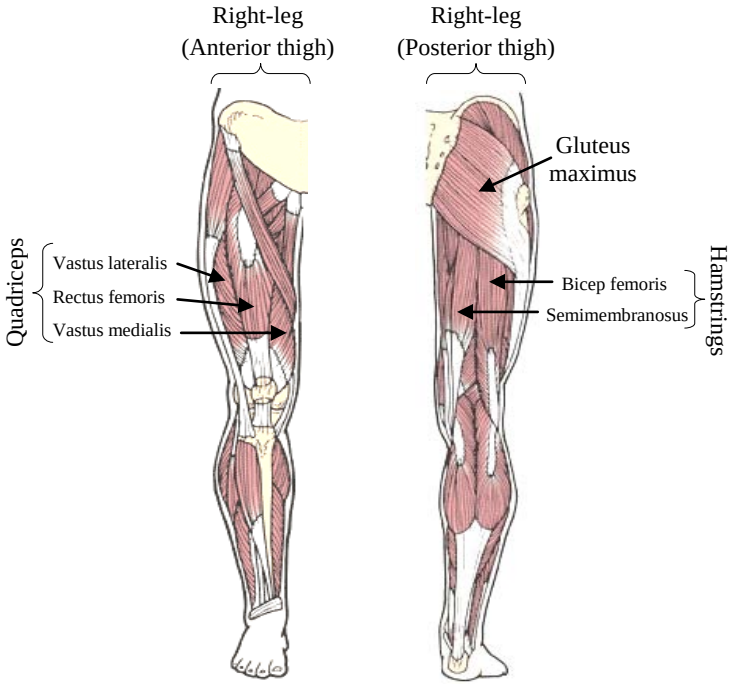

Figure 5. 1: Anatomy of the right leg showing the quadriceps (anterior thigh), hamstrings and gluteus maximus (posterior thigh). These muscles and the corresponding muscles in the left leg are stimulated during FES-cycling from the same muscles; EMG activity is recorded via the stimulation electrodes between the stimulation pulses.

Chen et al. [83] present an EMG driven stimulation system for FES cycling. The stimulation intensity is controlled proportionally to the detected vEMG activity. The latter is measured from separate EMG electrodes located on the muscle belly along its longitudinal axis at mid-distance between the stimulation electrodes. This approach, however, considerably increases the number of electrodes to attach. It should be noted that the proposed method simply distinguishes between correct and incorrect muscle activation by comparing the activities of both legs to avoid activation of electrical stimulation due to incorrect muscle activation.

A monitoring of EMG directly from the stimulation electrodes will be very useful to assess muscle coordination during FES cycling. The gained information on motor coordination can be used to adjust parameters in FES-LCE or to provide a visual biofeedback to the patient. In the latter case, electrical stimulation is indicating the ‘‘correct’’ intervals during which the patient should control his/her muscles. The feasibility of using StiMyo for EMG recording in FES cycling will be demonstrated below.

5.3. Experimental Setup

The StiMyo device has been integrated into a computer-controlled FES cycling ergometer as shown in Figure 5.2. Basis of the system is a commercially available cycling ergometer with functional electrical stimulation (RehaMove, HASOMED GmbH, Magdeburg, Germany), which consists of a motor assisted ergometer (MOTOmed Viva2, RECK-Technik GmbH & Co. KG, Betzenweiler, Germany) and an eight-channel neuro-muscular electrical stimulator (RehaStim, HASOMED GmbH). Stimulated muscles are the hamstrings and quadriceps on both legs. Large reusable self-adhesive stimulation electrodes (type: RehaTrode, HASOMED GmbH) of size 7.5*13 cm are used to activate these muscles. The electrodes for the quadriceps were mainly placed to cover M. rectus femoris and M. vastus lateralis, whereas the hamstring electrodes are mainly located over the M. biceps femoris and M. semimembranosus (cf. Figure 5.1). The charge control mode-0 has been applied to determine the pulse widths and current amplitudes of the stimulation pulses. The timing of the switches used inside the StiMyo amplifier were empirically tuned taking into account that each leg is served by a separate RehaStim stimulation modules and that a maximum of 2 pulses might be delivered to each leg within one stimulation period in a worst case. Figure 5.3 illustrates the applied timing of the switches and their synchronization with respect to stimulation pulses for 20 Hz stimulation frequency. For discharging of the stimulation electrodes only the repeated discharging via the switch S_2 was applied; no permanent discharging resistor R_d was used. The ergometer can be parametrized externally via a serial link and provides periodic readings of cadence, crank angle and motor torque. Possible modes of exercise are isokinetic (constant cadence) and

isotonic (constant resistance) cycling. The stimulator can be controlled from a laptop via an optically isolated USB interface using the ScienceMode protocol[15] (cf. Section 3.2.1).

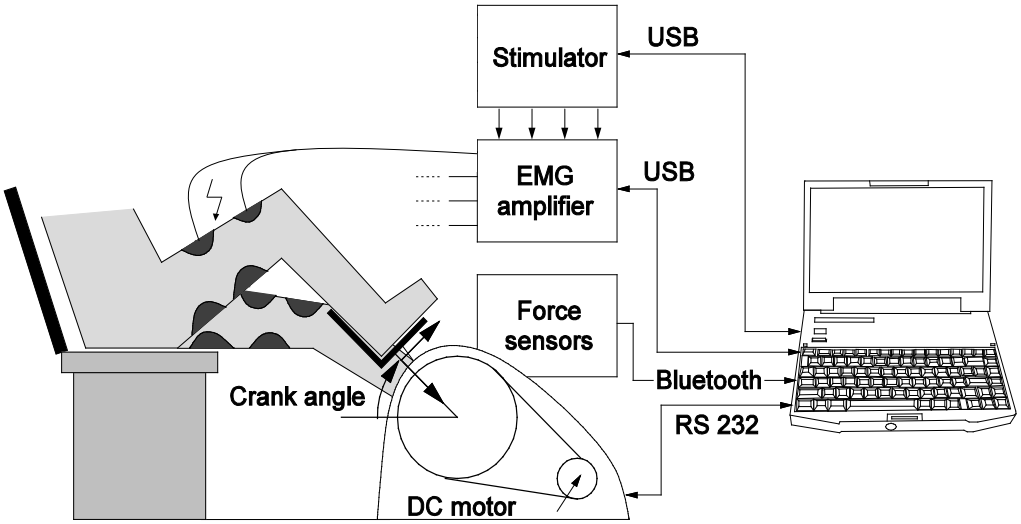

Figure 5. 2: Computer-controlled FES cycling ergometer system with integrated EMG measurement from stimulation electrodes.

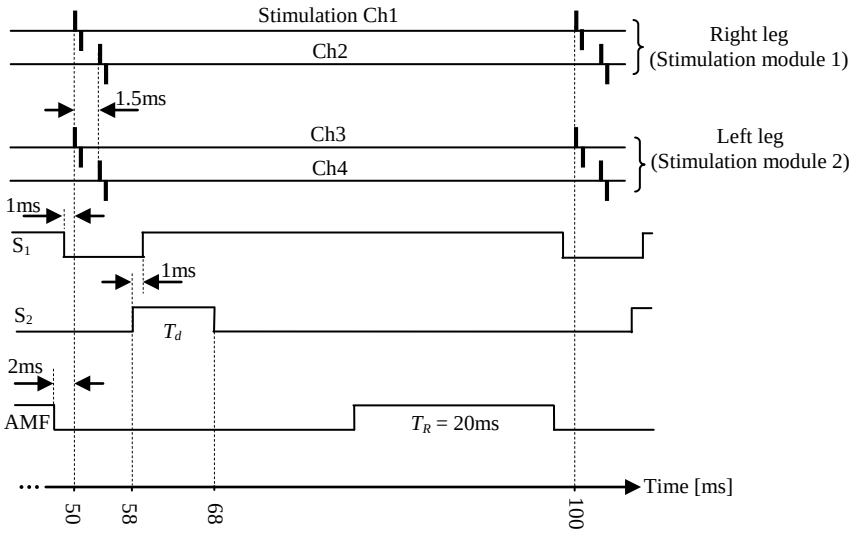

Figure 5. 3: One stimulation period showing stimulation pulses for the stimulated muscle groups and the timing charts of the different photo-MOS switches that utilized during FES-Cycling. Overlapping stimulation ranges for both legs are assumed as this represents the worst case for the EMG-measurement due to longer stimulation artifacts.

15 http:\\sciencestim.sf.net

The ergometer is equipped with two force sensors [117] (PowerTec, o-tec GmbH, Bensheim, Germany) to obtain measurements of radial and tangential forces acting on both crank arms in real time. Two OEM Bluetooth modules (Bluesense AD, Corscience GmbH & Co. KG, Erlangen, Germany) are used for wireless data transmission of the force measurements. After each mounting of the forces sensors a calibration is required due to misalignment of the sensor axes and the coordinate system assigned to the crank arm. The calibration is performed by mounting cylindrical weights with known mass at the pedal threads and measuring the resulting forces for different constant cadences. Based on the expected force components for this load, the calibration is performed using the least squares method to calculate the scaling and bias as well as the rotation of the sensor coordinate system with regard to the crank arm for each sensor.

In the case of a constant cadence, controlled by the electrical motor, one can easily calculate the ‘‘active’’ forces at the crank arms produced by the leg muscles from the calibrated force recordings. This is achieved by subtracting the ‘‘passive’’ forces, i.e., mainly gravitational forces due to the mass of the legs, from measured radial and tangential forces. These forces which are dependent on the crank position must be determined initially during a phase of passive cycling where the legs are solely moved by the motor. Once determined the force profiles are stored in a look-up table.

FES-pattern Generator: As shown in Figure 5.4, the stimulation of the individual muscle groups is switched on and off depending on crank angle and cadence. Figure 5.2 shows the definition of the crank angle. A ‘‘static’’ stimulation pattern is defined which describes angular ranges in which a certain muscle will produce a positive tangential force at the crank arm. During cycling the muscles have to be activated earlier than defined in the static pattern as a time delay between stimulation and force generation of approximately 200 ms must be taken into account. The static stimulation pattern is therefore shifted proportionally with regard to the cadence to obtain a ‘‘dynamic’’ stimulation pattern. The starting and stopping angles of the dynamical stimulation pattern (θ_{dy}^{start} and θ_{dy}^{stop}) are obtainable by adding a correction value to the corresponding angles of the static stimulation pattern (θ_{st}^{start} and θ_{st}^{stop}), such that

$$\theta_{dy}^{start} = \theta_{st}^{start} + \Delta\theta \tag{5. 1}$$

and

$$\theta_{dy}^{stop} = \theta_{st}^{stop} + \Delta\theta \tag{5. 2}$$

where $\Delta\theta$ is the cadence-base correction value and given by

$$\Delta\theta = -kv \ . \tag{5. 3}$$

with the correction factor k = 0.8 deg/rpm.

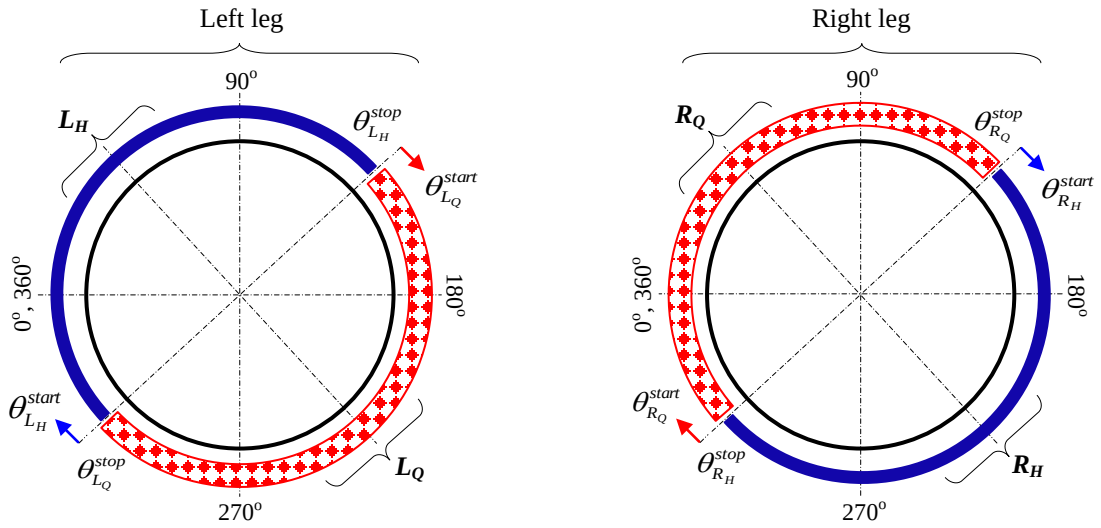

Figure 5. 4: Static stimulation pattern showing the angular ranges in which a certain muscle shall produce a positive tangential force at the crank arm at zero cadence. L_H and R_H are the hamstrings in the left and right leg respectively; L_Q and R_Q are the quadriceps in the left and the right leg respectively. Angles θ_m^{start} and θ_m^{stop} are showing starting and stopping angles of the muscle m.

Within the activation ranges, an arbitrary stimulation profile, with the crank angle as argument, can be assigned. The stimulation profiles shown in Figure 5.5 are used in this work. The profiles are trapezoidal with ramps over 50° crank angle. The stimulation conditions are updated at a time interval of 50 ms corresponding to the stimulation frequency. The entire stimulation control is realized on a laptop running real-time Linux (RTAI extension[16]) under open Frameworks[17] which is an open source C++ toolkit for creative coding with OpenGL for graphics. This allows an almost effortless implementation of visual biofeedback strategies in FES cycling based on EMG.

16 http://www.rtai.org

17 http://www.openframeworks.cc

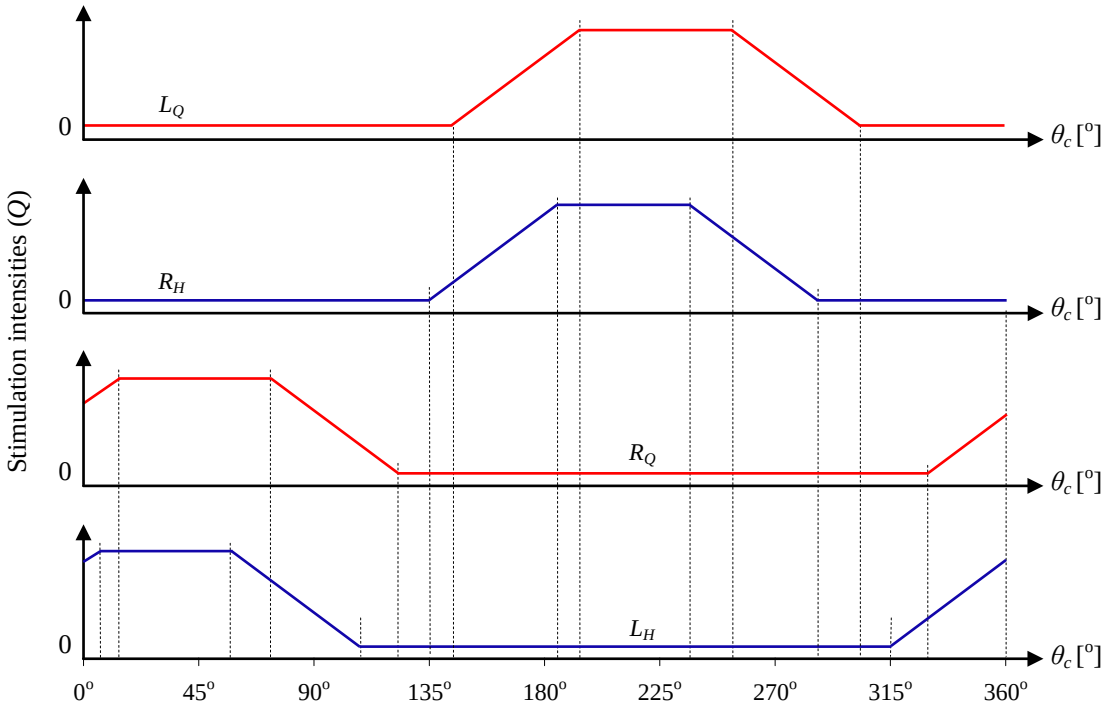

Figure 5. 5: Trapezoidal stimulation patterns with up and down ramps over 50 degree crank angle θ_c.

5.4. Experimental Procedure and Data Analysis

The StiMyo amplifier was verified in cycling experiments with a healthy male subject[18]. Tests were performed under isokinetic conditions at a motor controlled cadence of 30 rpm and each test contained around 15 crank revolutions. For each test, EMG profiles over the crank angle were computed together with confidence intervals (68%). The EMG of each muscle was normalized between 0 (base line) and 1 (maximum EMG value during volitional cycling). Passive forces were initially measured while the subject was neither volitional cycling nor being stimulated but just being moved by the motor.

The experimental procedure is carried out through five sub-tests marked as (A, B, C, D, and E), see Table 5.1. For all sub-tests, the calculated active tangential forces at the crank arms were displayed in real time to the cyclist who was instructed not to exceed 40 N when cycling volitionally. This corresponds to a maximum crank torque of 8.8 Nm. Low FES levels in table 5.1 means a normalized charge Q_{norm} of 0.5 which corresponds to 382 µs pulse width and 35 mA current amplitude. High FES levels means Q_{norm} of 1.0 which corresponds to 500 µs pulse width and 50 mA current amplitude.

[18] *The studies in this chapter were approved by the Local Research Ethics Committee at Charité Berlin.*

Table 5. 1: Different sub-testes which are carried out during FES cycling experiments.

Sub-test	A	B	C	D	E
Description	Volitional cycling	Low FES levels	Low FES + vol. cycling	High FES levels	High FES levels + vol. cycling

Sub-test A: In Sub-test A, the subject was asked to cycle volitionally. During this test the dynamic stimulation ranges and measured EMG activation profiles were plotted in real time over the crank angle. The experimenter could adjust the start and stop angles of the stimulation pattern in steps of 5^o in order to make the stimulation pattern visually fit to the volitional EMG activation ranges while avoiding overlapping muscle activations.

Sub-test B: In this sub-test, low-intensity stimulation was applied using the selected stimulation pattern while the subject was passive. Stimulation intensities of all muscles were set to 50% of the maximal stimulation intensity (normalized charge: 0.5, pulse width: 382 ms, current amplitude: 35 mA).

Sub-test C: During Sub-test C, the subject was asked to cycle voluntarily while the low level stimulation was still active.

Sub-test D: After Sub-test C, the stimulation intensity was increased to the maximum level (normalized charge: 1.0, pulse width: 500 ms, current amplitude: 50 mA) for all muscles while the subject was not actively cycling.

Sub-test E: Finally, while keeping maximum stimulation intensity, the subject was instructed to cycle additionally by himself.

5.5. Results

The obtained stimulation pattern from the Sub-test A at a cadence of 30 rpm is given in Table 5.2.

Table 5. 2: Stimulation pattern defined by angular ranges of the crank for a cadence of 30 rpm.

	Left leg		Right leg	
Muscle	Start angle [^{o}]	Stop angle [^{o}]	Start angle [^{o}]	Stop angle [^{o}]
Quadriceps	145	305	325	125
Hamstring	315	105	135	285

Below, only data from the left leg are reported.

Figure 5.6 is showing the internal EMG amplifier signal (after rectification). The upper subplot displays the EMG signal recorded during Sub-test E when the muscle was activated by FES and volitional effort. The lower subplot reports the EMG signal measured during Sub-test D when only FES was active and the patient behaved passively.

In Figure 5.7, the normalized EMG profiles are presented for all sub-tests A to E. The EMG-aligned dynamic stimulation ranges, chosen by the experimenter in Sub-test A, are additionally shown in Figure 5.7. In Figure 5.8, recorded tangential forces are reported.

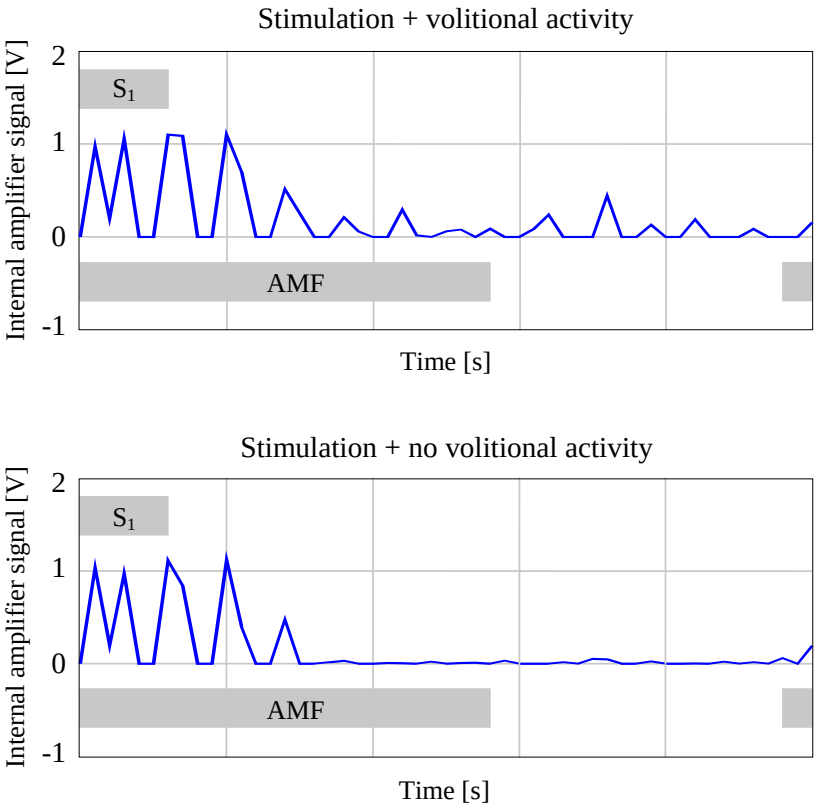

Figure 5. 6: The internal EMG amplifier signals (after rectification) over one stimulation period during sub-tests E (upper graph) and D (lower graph).

Table 5.3 provides the average EMG of the hamstring and quadriceps for all tests and mean tangential forces during the extension and flexion phase of the knee, all compared to the values obtained during Sub-test A.

Table 5. 3: Average EMG values for the left quadriceps (EMG_{LQ}) and left hamstring (EMG_{LH}) as well as average tangential forces at the left crank during knee extension (F_{EXT}) and flexion phase (F_{FLEX}). All variables are normalized with regard to the average values of Sub-test A (volitional cycling without stimulation).

Sub-test	EMG_{LQ} (%)	EMG_{LH} (%)	F_{EXT} (%)	F_{FLEX} (%)
A	100	100	100	100
B	2	2	8	-2
C	48	106	87	99
D	5	2	44	-3
E	37	80	95	80

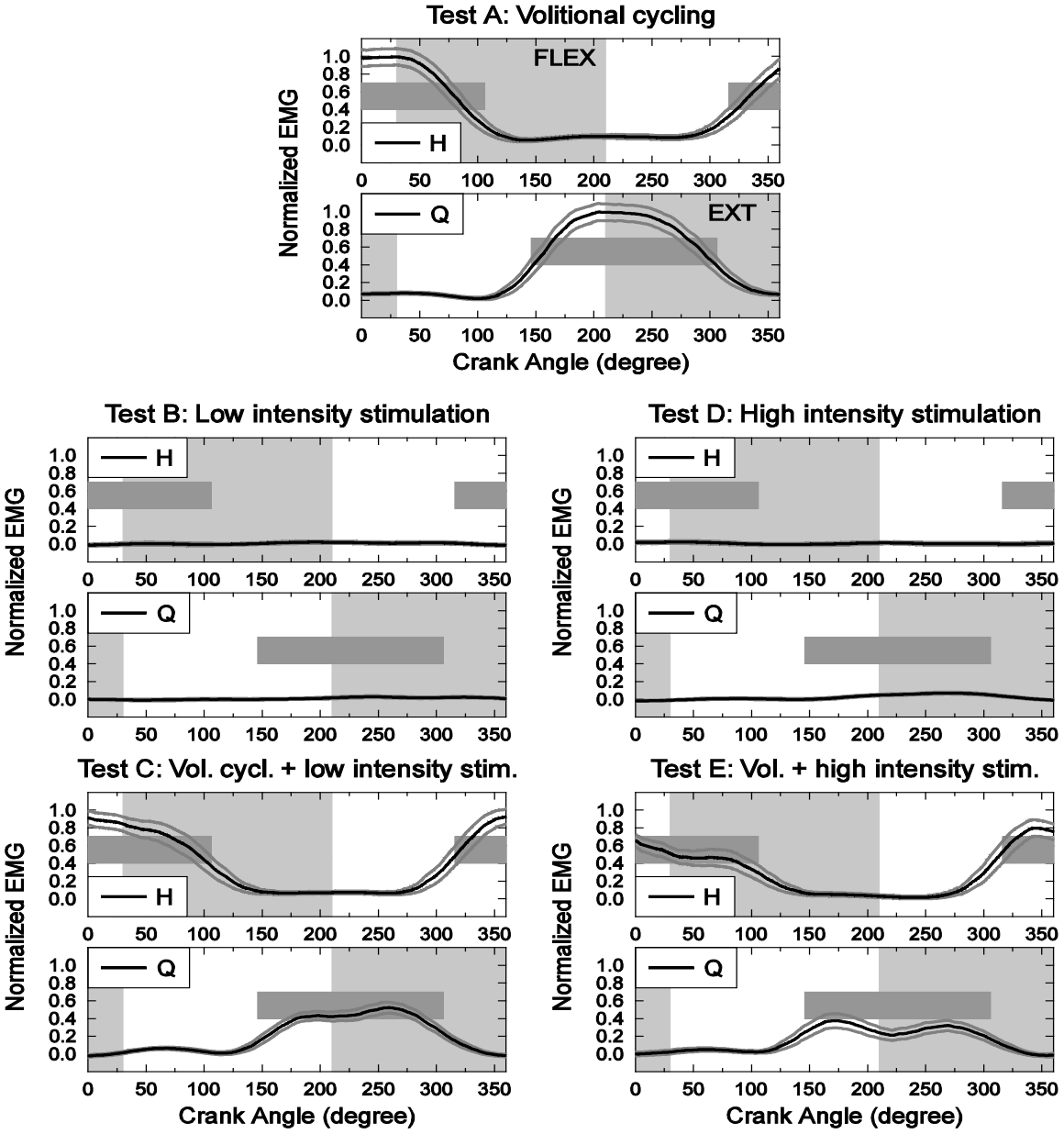

Figure 5. 7: EMG profiles of the hamstring (H) and quadriceps (Q) of the left leg for all cycling tests (A to E). The ranges of knee flexion and extension are shown in light gray. The used stimulation pattern at a cadence of 30 rpm is drawn in dark gray.

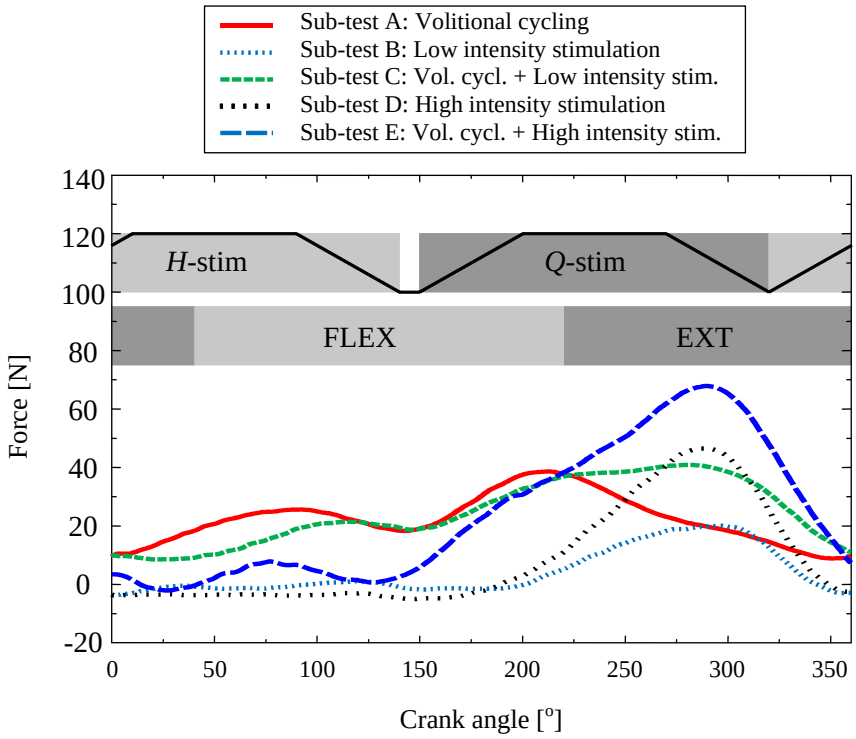

Figure 5. 8: Tangential forces recorded at the left crank arm for all cycling tests (A–E).

5.6. Discussion and Conclusions

The presented illustrative results show that a multichannel EMG measurement from stimulation electrodes is feasible during FES cycling. Also, under active superimposed electrical stimulation, muscle activity can be clearly detected. The EMG profiles obtained during volitional cycling (both with and without stimulation) are typical for cycling, showing a reciprocal activity fitting to extension and flexion of the knee joint. The phase advance of the EMG activities compared to the extension and flexion of the knee joint is due to time delay between muscle activation and force generation. The observed small overlapping of the EMG activities of hamstring and quadriceps can furthermore be explained by the fact that M. rectus femoris also flexes the hip and both stimulated hamstring muscles also extend the hip. In addition, a significant reduction in volitional EMG activity of the quadriceps can be observed under stimulation (more than 50% decrease). Electrical stimulation of the quadriceps clearly contributes to the force generation, so that with stimulation the subject needs less effort to achieve force levels comparable to Sub-test A (purely volitional cycling). Not much force generation was observed during hamstring stimulation (see results of Sub-tests B and D), so that no strong change in EMG activity related to electrical stimulation was present.

The effectiveness of suppressing stimulation artifacts can be assessed from Sub-tests B and D. Ideally, no EMG activity should be recorded during these Sub-tests. The observed average EMG values (see Table 5.3) of 2% - 5% are acceptable and might be caused by remaining minor stimulation artifacts or unintended muscular activities of the subject. Relaxing perfectly under stimulation is practically impossible. The aim of this study was to prove the feasibility to measure volitional/reflex related EMG during FES cycling. Recruiting a healthy subject was the preferred option for this aim, as such a subject can relax better during stimulation than a stroke patient and should not show disturbing reflexes. For these reasons, one can assume that recorded EMG activities during the stimulation tests without volitional cycling (Sub-tests B and D) are mostly linked to stimulation artifacts. Following the instructions given during tests might also be a problem for some stroke patients. However, more crucial is the fact that the developed amplifier will later be used in therapy only with stroke patients in whom EMG activities of weak muscles are lower than in healthy subjects. To address this fact, the healthy subject was asked to generate low volitional tangential forces (<40 N) during the tests comparable to the values observed in stroke patients [109].

In a next step the EMG amplifier must be extensively used during FES cycling with stroke patients to monitor volitional activities and reflexes while performing the exercise. First successful tests have already been performed. Based on the results, biofeedback training should be developed for treatment of muscle imbalance in patients with spastic hemiparesis similar to the approach described in [113] but extended by FES. One currently unsolved problem is to distinguish crosstalk and co-contraction for patients with thin legs when using the presented amplifier.

No electrode polarization effects were observed during this single case study. However, such effects might occur in some patients under certain conditions so that additional measures like applying the permanent discharging resistor or changing the charge control mode are necessary. Also D-waves have not been observed so far during FES cycling under the applied stimulation intensities and for used discharging technique. If D-waves occur under other conditions in different persons, the discharging process must be adapted (timing, permanent discharging resistor, charge control mode); in order to move the D-waves out of the EMG-measurement interval.

When interpreting the EMG recordings, it must be taken into account, that these EMG signals are measured through large electrodes covering muscle groups rather than individual muscles. Only a net EMG from several muscles is available which does not allow drawing precise conclusions on the activity of individual muscles. On the other hand such an EMG recording from the healthy leg might be more suitable to tune the stimulation ranges in FES cycling than EMG patterns taken from individual muscles using standard electromyographic kinesiology. Our preliminary results indicate

that such an approach might work at least for the quadriceps. A positive drive torque at the crank was measured for the EMG-tailored stimulation range. However, using the stimulation range determined from hamstring EMG activity did not produce much force despite the fact, that the EMG recorded from the same electrodes shows clearly visible EMG profiles.

Using smaller electrodes will improve the EMG measurement from stimulation electrodes as less charge will be accumulated after stimulation and therefore a reduction of muting periods will be possible. However, decreasing the electrode size will increase stimulation current densities below the electrodes making the stimulation maybe more unpleasant for the patient.

In stroke patients, the recorded EMG from the healthy could also be used to reciprocally control the intensity of FES for the paretic leg. The activity of the paretic leg muscles can be estimated by shifting the recorded EMG signals from the healthy hamstrings and quadriceps by 180^{o}. Two control methods can be applied. The first is to control the intensity of FES in proportion to the estimated paretic leg activity. The second is to apply the estimated muscle activity to trigger trapezoidal stimulation patterns which were applied during this chapter (cf. Figure 5.5). In the second method the stimulation pattern for each muscle has to be centered on the estimated activity interval of the same muscle. Triggering the stimulation of the paretic leg based on the locally measured EMG might be another form of FES control for patients with weak, but good coordinated, muscular control in both legs. The observed crank angle should to be used in all methods to avoid wrong stimulation patterns and overlapping stimulation.

Chapter 6

6. EMG-driven FES of Wrist–joint and Finger Extensors

6.1. Introduction

After stroke the dysfunction of the paretic limbs impairs the performance of many daily activities such as walking, dressing, bathing, self-care, and writing, thus reducing the patient independency. Because of the limited rehabilitation time in clinic, walking is considered to be the primary goal of rehabilitation, while restoration of arm and hand functions often takes a secondary priority. In contrast to the legs, it is possible to compensate the lost function of the paretic arm by the healthy arm and the use of some special tools. Although the partial compensation of some arm functions, the paretic arm still remains problematically in daily live. Assistance is still needed especially for dressing and health care. Many stroke survivors can partially control the paretic arm muscles when leaving clinic. However, the residual motor functions are not sufficient enough to perform the daily activities mentioned above.. The weakness of the arm muscles forces the patient not to use his/her arm/hand. Therefore the paretic arm/hand functions get worse with time. These facts push for better rehabilitation techniques of arm and hand functions after stroke.

As already outlined in Chapter 2 (cf. Section 2.4.1), EMG-driven FES can be used to support the patients by amplifying the residual motor functions of the paretic arm/hand. Beside this functional aspect, FES has several therapeutic benefits such as the prevention or reduction of muscle atrophy [41-44].

This chapter describes the use of StiMyo amplifier for realizing an EMG-driven FES of the wrist-joint and finger extensor muscles. This shall amplify the still present residual motor control in stroke patients. This is first time that the performance of an EMG-driven FES system with combined stimulation and measurement electrodes is investigated using quantitative measurements. Experiments with healthy subjects have been carried out to estimate the theoretically achievable performance.

At the beginning of this chapter, the tuning of the StiMyo amplifier performance will be introduced The amplifier will be optimized to improve the signal to noise ratio for the detection of volitional muscle activity from the wrist-joint and finger extensors. Such a sophisticated tuning procedure was not described for other EMG-amplifiers in the literature.

Then the tuned amplifier is used to investigate two EMG-driven FES approaches. The first approach is the EMG-proportional FES. This method is aiming to exploit as much as possible the residual motor control of the patient by quasi linear amplification of the detected vEMG. Therefore, a stimulation charge which is proportional to the detected volitional muscle activity is applied. The ability of the subjects to track given wrist-joint angles with and without EMG-proportional FES will be investigated.

The EMG-proportional FES control may fail if the patient is not able to relax during FES or cannot control his/her residual EMG activity in a smooth way (without excessive oscillations). In this case one might apply the second control approach which is named EMG-carried FES. This method can be seen as a compromise between EMG-triggered FES and EMG-proportional FES. The stimulation is initiated as soon as the volitional muscle activity exceeds a predefined threshold level, and stays active until the volitional muscle activity drops below a second lower threshold.

This chapter is organized as follows: Section 6.2 describes the experimental setup which is used during the tuning of the StiMyo amplifier and the tests of the EMG-driven FES approaches. Section 6.3 deals with the tuning of StiMyo's timing-charts and HPF frequency. Section 6.4 explores the EMG-proportional stimulation while the EMG-carried stimulation will be analyzed in Section 6.5. Conclusions and outlook for future work are given in Section 6.6.

6.2. Experimental Setup

As shown in Figure 6.1, the StiMyo amplifier is integrated into a computer-controlled FES system. A full inertial sensor (MT9-B, Xsens Motion Technologies, The Netherlands) was used to detect the wrist-joint angle. The inertial sensor includes a gyroscope, an accelerometer and a magnetic field sensor, which are all three-axial. The MT9-B is connected to a laptop though one digital signal processing unit (Xbus-Master, Xsens Motion Technologies, The Netherlands) using an USB interface. By using a Direction Cosine Matrix (DCM)-based orientation estimation algorithm [93], the wrist joint-angle can be determined from the calibrated sensor signals on the laptop. The forearm was lying on the table. Hence, the extension/flexion angle of the wrist joint can be measured using only one inertial sensor mounted on the back of the hand (cf. Figure 6.1). For tuning of the EMG-amplifier and for FES-driven control the processed volitional EMG of the amplifier was used (cf.

Chapter 4), which was sampled at the 20 Hz stimulation frequency and transmitted via USB from the StiMyo device to the Laptop. Just for a better interpretation of the processed EMG measurements (output of the StiMyo). Internal EMG amplifier signals (before rectification) were monitored for all channels at 2 kHz with a 16-bit data acquisition card (NI DAQCard-6036E, National Instruments). This signal was used for discussing the possible sources of EMG modulation during FES (inability to relax, presence of F-waves and/or D-waves). For safety reasons the laptop was powered through an isolation transformer while using the DAQ-card. An USB potentiometer (PowerMate, Griffin Technology) was used to manually control of the stimulation intensity of the RehaStim pro™ stimulation device (HASOMED GmbH, Germany) or to activate the different EMG-driven control schemes. Two reusable self-adhesive hydrogel electrodes (Type: RehaTrode – oval 60 x 40 mm, HASOMED GmbH, Germany) were used for transcutaneous FES of the extensor carpi ulnaris, extensor carpi radialis and extensor digitorum (major wrist-joint extensors and finger extensors, cf. Figure 6.2) and to measure the net vEMG from these muscles. One ENG single-use electrode (Ambu Blue Sensor NF, Ambu, Denmark) of size 28x20 mm was used as a reference electrode and placed on the elbow.

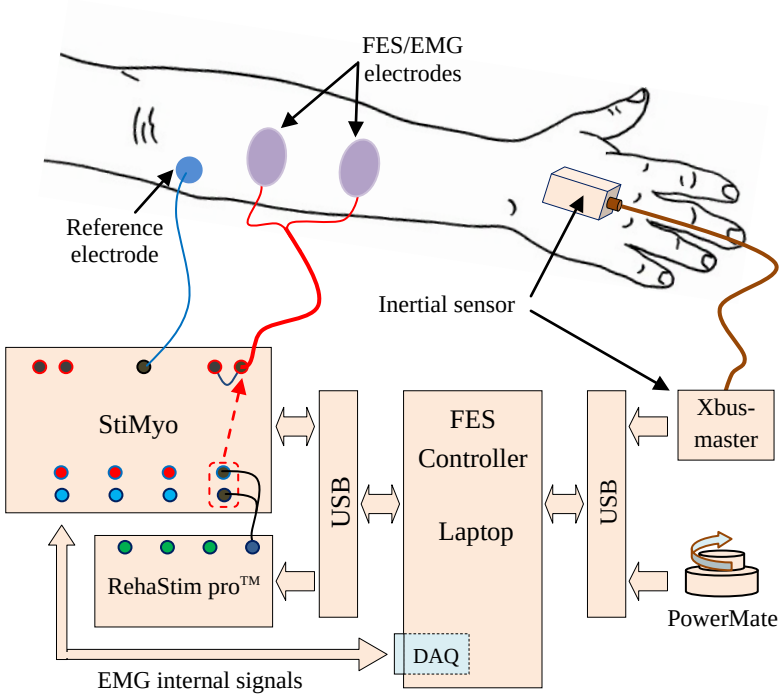

Figure 6. 1: The experimental setup showing the integration of StiMyo EMG-amplifier into a computer-controlled FES system.

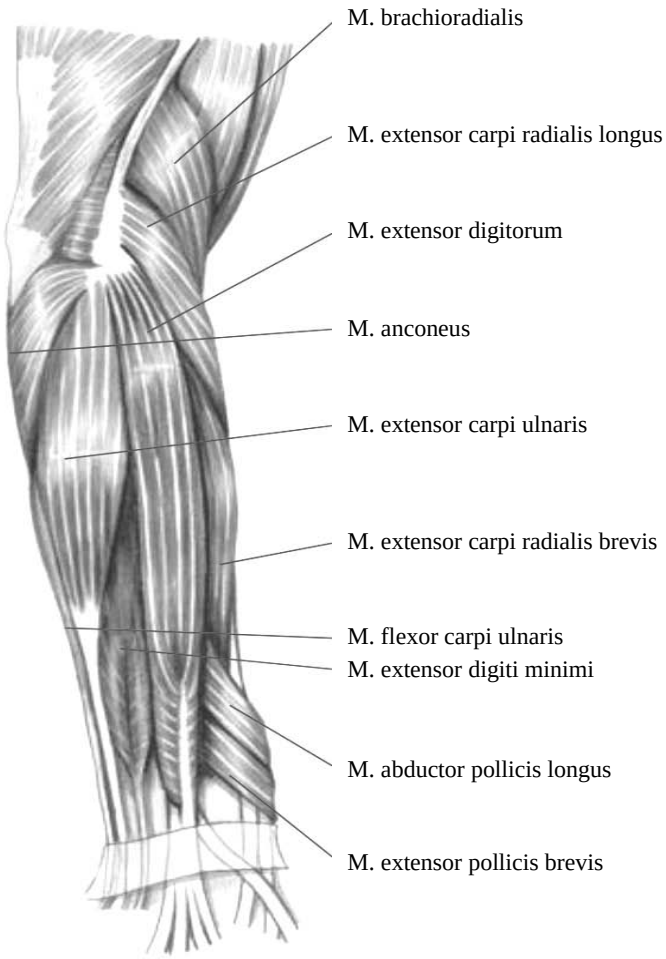

Figure 6. 2: Anatomy of the posterior forearm muscles (modified from [118]).

The charge control mode-I was applied to determine pulse widths and current amplitudes of the stimulation pulses. Stimulation pulses with controllable normalized charge (Q_{norm} from 0 to 1 which corresponds to 10-400 μs pulse width and to 5-20 mA current amplitude) were sent to the stimulated muscles. The FES control algorithms and the data acquisition were running on a laptop with real-time Linux (RTAI extension)[19]. The programs were realized using Scilab/Scicos[20] version 4.1.2 with the HART-Toolbox[21] and RTAI-Lab (part of RTAI) which offers automatic code generation from Scicos-Diagrams. For online changing of program/controller parameters and for real-time monitoring of signals the program QRtaiLab[22] was used.

[19] *http://www.rtai.org*
[20] *http://www.scilab.org*
[21] *http://hart.sourceforge.net*
[22] *http://qrtailab.sourceforge.net*

This setup was used during the experimental tuning of both HPF frequency and timing-chart of the StiMyo switching circuits and for testing of the EMG-driven FES approaches.

6.3. Tuning of Timing-chart and High-Pass Filter Frequency

The optimization of the StiMyo amplifier aims to prolong the allowed recording period T_R for the volitional EMG from the stimulation electrodes as much as possible without negatively affecting the suppression of stimulation and switching artifacts as well as of FES-induced action potentials. . This goal can be achieved by tuning of the HPF frequency and the timing-chart which controls the StiMyo switching circuits (cf. Figure 4.6). Adjustable parameters of the timing chart are the time intervals T_d and T_R.

A performance index PI_{Amp} was defined and used to assess the quality of volitional EMG detection during FES. This index was used to select the optimal combination of HPF frequency, T_d and T_R. To carry out the tuning of the StiMyo device, the frequency of the HPF were set differently for all four channels (150, 170, 200 and 250 Hz). In order to compare the performance of the EMG-amplifying channels with different HPF frequencies, all channels were connected together to the same pair of electrodes. Timing instructions were applied simultaneously to all channels, i.e. T_p, T_d, and T_R were the same for all channels.

As explained in Chapter 4, T_p is the time interval needed for delivering the stimulation pulses. The Switch S_1 safely isolates (protects) the pre-amplifier inputs during the delivery of pulses. This value of T_p is solely defined by the number of active channels/modules within one stimulation period and is defined by Equations (4.17). As only one channel was used here, the value of T_p was bound to 1.5 ms.

Two values (6 and 10 ms) have been tested for the discharging period T_d during which the switch S_2 connects the stimulation electrodes together to relieve the residual charge under electrodes. The permanent discharging resistor was deactivated during the experiments.

The AMF is responsible to mute stimulation and switching artifacts. In order to allow a long EMG recording period T_R the AMF should start the EMG recording immediately after the end of artifacts. The possible range of T_R depends on many parameters such as frequency of HPFs as well as the settings of T_p and T_d. Three values (25, 20 and 15 ms) have been tested for T_R during the tuning process.

6.3.1. Experimental Procedure and Data Analysis

The experimental sessions involved 5 neurologically intact volunteers (32.5 ± 6.5 years old, weight of 78.5 ± 4.5 kg and height of 182.5 ± 4.5 cm)[23]. For each subject, the experiment was divided into 6 sessions during which different combinations of T_d and T_R were applied in the order presented in Table 6.1. A rest time period of 5 minutes followed each session to allow fatigue-recovery of the stimulated muscles.

Table 6. 1: Experimental sessions together with the applied time periods T_d and T_R.

Session number	1	2	3	4	5	6
S_2 (T_d [ms])	6			10		
AMF (T_R [ms])	25	20	15	25	20	15

Session Instructions: Figure 6.3 explains the protocol of a single session which volunteers should follow. The subjects were asked to start with relaxed wrist-joint and fingers. As the hand was lying on the table, the relaxed wrist-joint angle was almost 0^o (Region A, cf. Figure 6.3). Then, in Region B, while stimulation was still off, the subjects should voluntarily extend their wrist-joint to 20^o with fully extended fingers and to maintain this position for about 5 seconds. After that they were asked to relax again (Region C). In Region-D, the subjects should keep relaxing and the PowerMate potentiometer was turned slowly to increase the stimulation intensity until a wrist-joint extension of 60° was achieved with no volitional support; after 5 seconds the applied stimulation stopped.

The following performance index was applied:

$$PI_{Amp} = \frac{EMG_V - EMG_S}{EMG_V - EMG_B} \tag{6. 1}$$

Here EMG_B is the average base-line of the amplifier output, which is measured during Region A when stimulation is off and the muscle at rest. EMG_V is the average volitional muscle activity with regard to 20^o wrist extension (region B). EMG_S is represents the modulated base-line due to the application of FES in Region C. Ideally, EMG_s and EMG_B should be equal. In practice EMG_s will be larger than EMG_B for the following possible reasons: remaining switching or stimulation artifacts, FES-induced action potentials (F-wave or D-wave) or inability of the subject to relax under FES. To evaluate the specific reasons of an increases EMG_S level, the internal EMG-amplifier signal has to

[23] *The studies in this chapter were approved by the Local Research Ethics Committee at Charité Berlin.*

be investigated. All averaged EMGs values are calculated over the shaded bands shown in Figure 6.3.

The chosen index describes how good moderate EMG levels (corresponding to 20^o wrist-joint angle) can be detected. The index compares the level of volitional EMG to the disturbance in EMG base level which is produced at maximum stimulation (corresponding to 60° wrist-joint angle). The best value of PI_{Amp} is 1, which reflects the perfect cancellation of all artifacts and shows no presence of F-waves and/or D-waves during the EMG recording period T_R. The index will be smaller than one for $EMG_B < EMG_s < EMG_v$ and zero for $EMG_s = EMG_v$. Negative values of PI_{Amp} correspond to $EMG_s > EMG_v$.

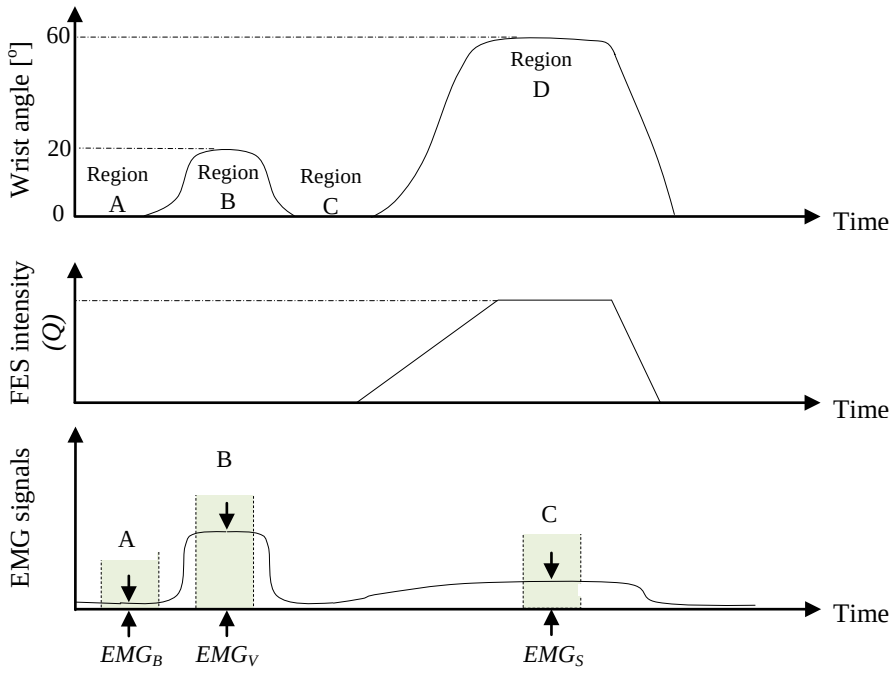

Figure 6. 3: Protocol for a single experimental session during the tuning process of the StiMyo device. The upper subplot presents the wrist-joint angle. The middle subplot shows the applied stimulation level. In the lower graph the expected muscle activity (amplifier output) is illustrated.

6.3.2. Results and Discussion

The index PI_{Amp} has been calculated for different HPF frequencies and different time periods T_R and T_d. Table 6.2 is showing the calculated PI_{Amp} for all possible 24 combinations. The 24 crosses in Figure 6.4 are showing the average values of PI_{Amp} for all subjects during different sessions.

Table 6. 2: StiMyo performance index for different HPF filter frequencies combined with different timings of the electrode/skin discharging time T_d and EMG recording time T_R.

HPF Frequency	T_d [ms]	T_R [ms]	Amplifier performance index (PI_{Amp})					
			Subj. 1	Subj. 2	Subj. 3	Subj. 4	Subj. 5	Average
250 Hz	6	25	0.59	0.59	-0.06	0.84	0.71	0.53
		20	0.82	0.46	0.00	0.72	0.87	0.57
		15	0.80	0.83	0.64	0.82	0.92	0.80
	10	25	0.16	-0.37	-0.20	0.35	0.03	0.00
		20	0.69	0.44	-0.05	0.26	0.59	0.38
		15	0.86	0.28	0.65	0.76	0.71	0.65
200 Hz	6	25	0.51	0.37	-0.16	0.82	0.62	0.43
		20	0.77	0.47	0.01	0.74	0.90	0.58
		15	0.82	0.84	0.67	0.84	0.95	0.82
	10	25	-0.61	-1.14	-0.30	-0.29	-0.64	-0.60
		20	0.64	0.35	-0.02	0.24	0.58	0.35
		15	0.89	0.30	0.67	0.79	0.74	0.68
170 Hz	6	25	-0.48	-0.76	-0.72	0.55	-0.06	-0.29
		20	0.71	0.40	-0.06	0.72	0.80	0.51
		15	0.81	0.83	0.68	0.82	0.87	0.80
	10	25	-2.92	-2.73	-0.82	-1.81	-2.80	-2.22
		20	0.05	-0.66	-0.08	-0.09	0.18	-0.12
		15	0.93	0.32	0.66	0.81	0.67	0.68
150 Hz	6	25	0.01	0.12	-0.66	0.77	0.46	0.14
		20	0.71	0.37	-0.06	0.72	0.78	0.50
		15	0.86	0.85	0.62	0.87	0.87	0.81
	10	25	-1.85	-1.45	-0.75	-0.59	-0.99	-1.13
		20	0.47	0.11	-0.07	0.27	0.36	0.23
		15	0.94	0.19	0.61	0.90	0.73	0.67

From the determined PI_{Amp} (cf. Figure 6.4), the following facts can be extracted:

- Independent of the HPF frequency, the best combination of the time intervals are T_d = 6 ms and T_R = 15 ms. This setting will guarantee a good amplifier performance index for all subjects. Unfortunately, the measurement interval T_R is very limited.
- Independent of the HPF frequency and the timing of AMF, the best discharging interval is T_d = 6 ms. When using extended measurement periods (T_R = 25 or 20 ms) the performance index varied strongly for the different subjects.

Figure 6.5 shows in the internal EMG-amplifier signal for one subject during the Region C (maximum stimulation). The used measurement interval T_R (indicated by the active AMF in Figure 6.5) was 15 ms. During the last shown stimulation period, an action potential (probably a F-wave) can be seen just before the begin of the T_R interval. It is clear, that an extended measurement interval would partly or even completely include this action potential. This would dramatically modulate the EMGs level. The appearance of such action potentials during the EMG recording period will make the application of EMG-proportional FES impossible. The FES controller cannot distinguish between vEMG and FES-induced EMG. This will disturb the control performance and may produce unwanted muscle contractions.

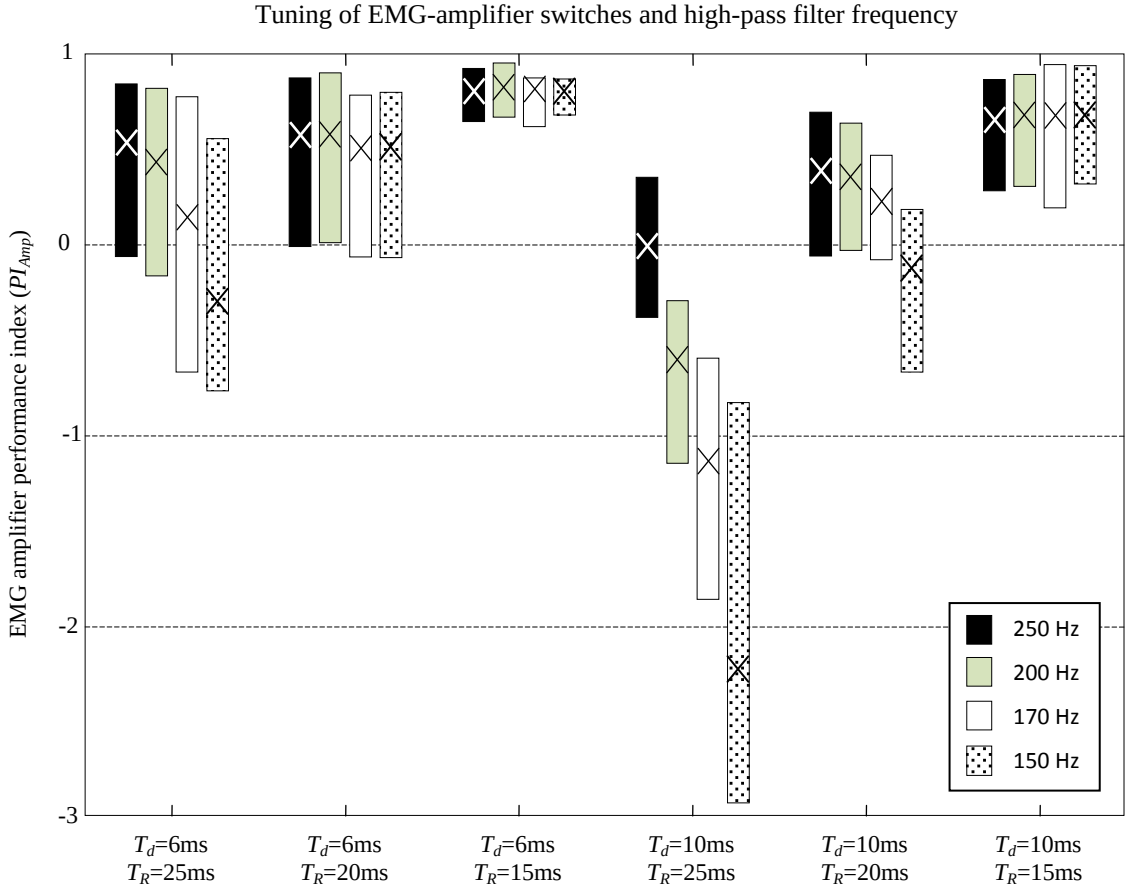

Figure 6. 4: Performance index PI_{Amp} for different settings of the StiMyo amplifier. Crosses indicate mean values while the bars illustrate the range of obtained indexes for all 5 subjects.

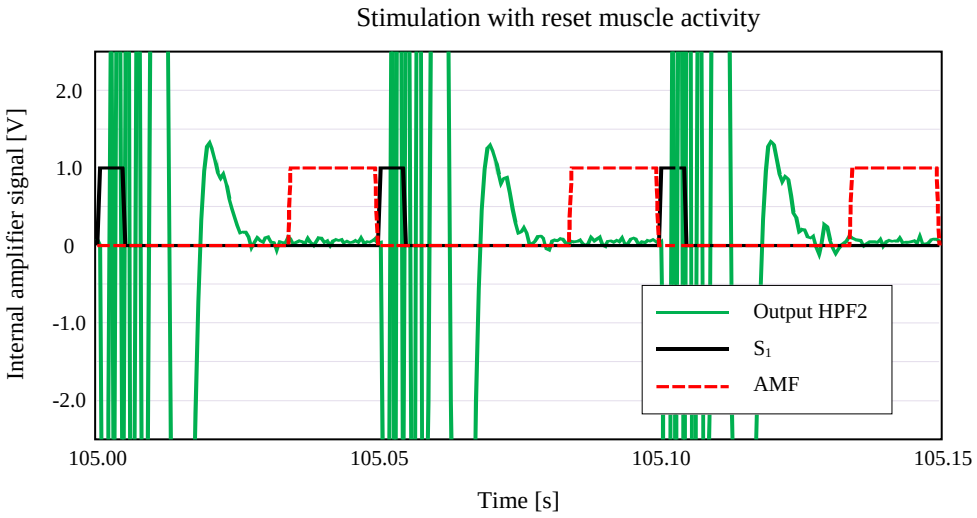

Figure 6. 5: Internal amplifier signals during maximal stimulation without volitional muscle activity (from Region C of the experimental session). The third stimulation period is showing the appearance of an action potential (probably a F-wave), immediately before the AMF gets high.

In summary, the best values for the time intervals are T_d = 6ms and T_R = 15 ms. These values are utilized during EMG-driven FES of the wrist and finger extensors. For the HPF a value of 200 Hz has been chosen due its slightly better performance index when applying the above chosen settings for T_d and T_R.

The resistor R_d was not on during this study. An active R_d would improve the discharging process which would allow shorter T_d time intervals and therefore T_R interval might be extended. It is expected that the performance index will improve. However, as the input impedance of the amplifier is dramatically reduced by the resistor R_d, it will be used only in case of strong EMG depression due to electrode polarization or to modulate the latency of D-waves. A low input impedance of the amplifier would increase the high-frequency noise which will lead to an increase in EMG_B. As EMG_B is contained also in EMG_V and EMG_S, the used performance index will not be affected.

Only a very limited measurement interval of 15 ms could be achieved. This might cause more fluctuations of the later recorded volitional EMG. An additional low-pass filtering of the amplifier output will be required before applying EMG driven FES controllers. As the results of this study indicate, extended measurement intervals might be possible for some subjects. However, this would require a patient and maybe session specific tuning of the amplifier. This is not applicable in clinical environments.

Finally, it should be noted that this amplifier optimization was application specific and must be repeated for other applications.

6.4. EMG-Proportional FES

In the EMG-proportional FES considered here, the residual muscle activity is measured from the paretic fingers and wrist-joint extensors. In order to apply an EMG-proportional FES, the sampled amplifier output must be digitally low-pass filtered on the laptop. A first order filter with a cut-off frequency of 1 Hz was used to obtain a smooth control signal. The filtered volitional EMG is then normalized and used to control the intensity of stimulation in proportion to the weak motor control. The calculated stimulation charge is then delivered to the same muscle. Figure 6.7 shows the block diagram of the EMG-proportional FES system.

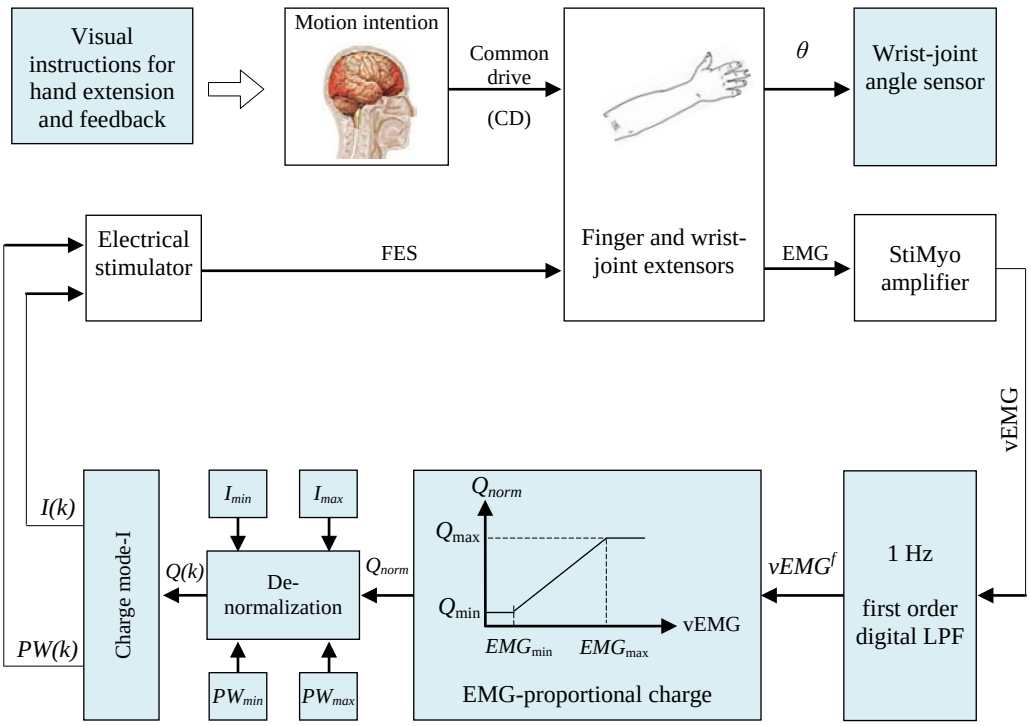

Figure 6. 6: Block diagram of EMG-proportional FES, applied to the finger and wrist-joint extensors.

The normalized volitional muscle activity $vEMG_{norm}(k)$ is obtained by

$$vEMG_{norm}(k) = \begin{cases} 0, & vEMG^{f}(k) < vEMG_{\min} \\ \dfrac{vEMG^{f}(k) - vEMG_{\min}}{vEMG_{\max} - vEMG_{\min}} & vEMG_{\min} \le vEMG^{f}(k) \le vEMG_{\max} \\ 1, & vEMG^{f}(k) > vEMG_{\max} \end{cases} \quad (6.2)$$

where $vEMG^{f}(k)$ is the low-pass filtered instantaneous volitional muscle activity (sampled at stimulation frequency with k being the sample index). The constants $vEMG_{\max}$ and $vEMG_{\min}$ are the maximum and the minimum volitional muscle activity respectively.

The controller determines the value of normalized stimulation charge $Q_{norm}(k)$ in proportion to the normalized vEMG:

$$Q_{norm}(k) = Q_{\min} + (Q_{\max} - Q_{\min}) vEMG_{norm}(k) \quad (6.3)$$

In Eq. (6.3), $Q_{\max}$ and $Q_{\min}$ are the maximum and the minimum normalized stimulation levels respectively. The controller parameters $vEMG_{\max}$, $vEMG_{\min}$, $Q_{\max}$ and $Q_{\min}$ are identified in a pre-experiment which will be explained in the next section. The controller continuously sends each stimulation period the obtained charge $Q(k)$, obtained by de-normalization,, to the charge mode-I calculation which delivers the corresponding stimulation current-amplitude $I(k)$ and pulse width $PW(k)$ to the stimulation device.

6.4.1 Experimental Procedure and Data Analysis

The test of EMG- proportional FES was divided into two experiments. The first was a pre-experiment by which the controller parameters of the Equations (6.2) and (6.3) were determined. In the second experiment, the feasibility and the performance of the tuned EMG –proportional controlled were investigated. The protocol was applied to the same healthy subjects who participated in the tuning study of the StiMyo device (cf. Section 6.3.1).

The **pre-experiment** involved two sub tests as illustrated in Figure 6.7.

The aim of the first sub test (A) was to determine $vEMG_{\max}$. The remaining controller parameters were identified during the second sub test (B). The test B was furthermore used to monitor if a clear EMG-suppression due to electrode polarization or D-waves were present in order to decide on the use of the permanent discharging resistor R_d as a countermeasure. Sub test A started with zero stimulation intensity and subjects were instructed to volitionally achieve 20^{o} wrist-joint extension.

The corresponding muscle activity was defined as $vEMG_{max}$ in order to be comparable with the expected performance of the paretic muscles in stroke patients.

During sub test B, the subjects should keep the wrist joint relaxed, while the stimulation intensity was slowly ramped up from zero to the level producing the maximum desired wrist-joint angle (50^o). The normalized level of stimulation charge which produced 50^o wrist-joint extension without volitional contribution was defined as Q_{max}. The value of Q_{min} was set to the minimal normalized stimulation level at which an initial extension of the wrist joint could be observed. During the ramping up of charge, the experimenter was also monitoring the appearance of D-wave effects (cf. Figure 6.7, Sub test B). After the stimulation level reached Q_{max}, the subjects were instructed to volitionally extend the wrist-joint by 10^o more (from 50^o to 60^o) shortly. The corresponding muscle activity ($vEMG_s$) was observed. The application of Q_{max} modulates the detected vEMG base level. The mean modulated base level was marked as $vEMG_{min}$.

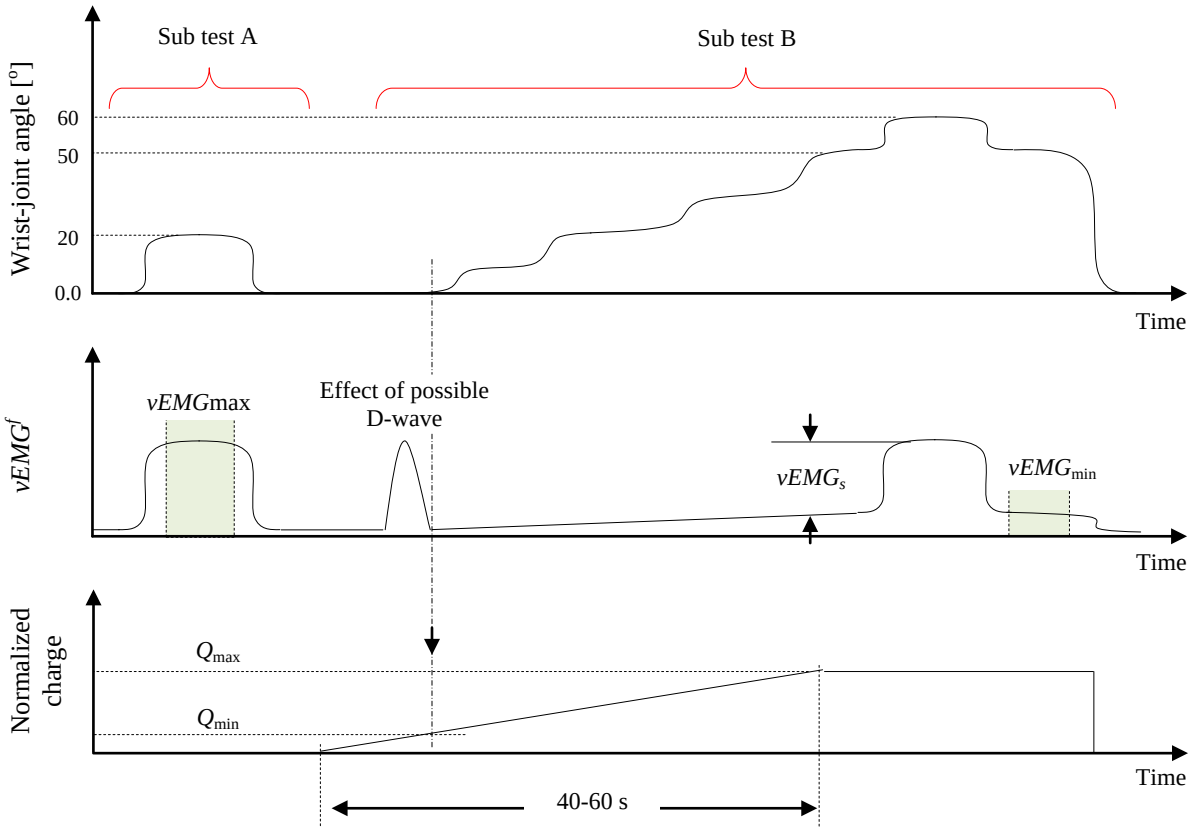

Figure 6. 7: Experimental protocol to determine Q_{min}, Q_{max}, $vEMG_{min}$ and $vEMG_{max}$. This protocol also examines the appearance of D-wave effects and EMG suppression. Average values were calculated over the shaded bands.

The permanent discharging resistor R_d was activated when unwanted D-wave effects occurred at stimulation levels higher than Q_{min} or when EMG suppression was present ($vEMG_s < 0.2\ vEMG_{max}$).

The **experiment for evaluation of the EMG-controlled FES** was divided into two sub tests V (volitional) and C (controlled) as illustrated in Figure 6.8. During both sub tests the subjects had to track a given wrist-joint angle profile. The subject's wrist-joint angle should follow the staircase reference θ_R defined in Figure 6.8. The angle θ_R changed every 7 seconds.

In sub test subjects had to perform the tracking task volitional without FES support while in sub test C support was given be the EMG-proportional control. Thus, in sub test C less volitional muscle activity should be needed compared to sub test V to achieve the same tracking task. Before recording data the subjects had 5 minutes time to exercise the tracking with the EMG-proportional control in order to get used to the test.

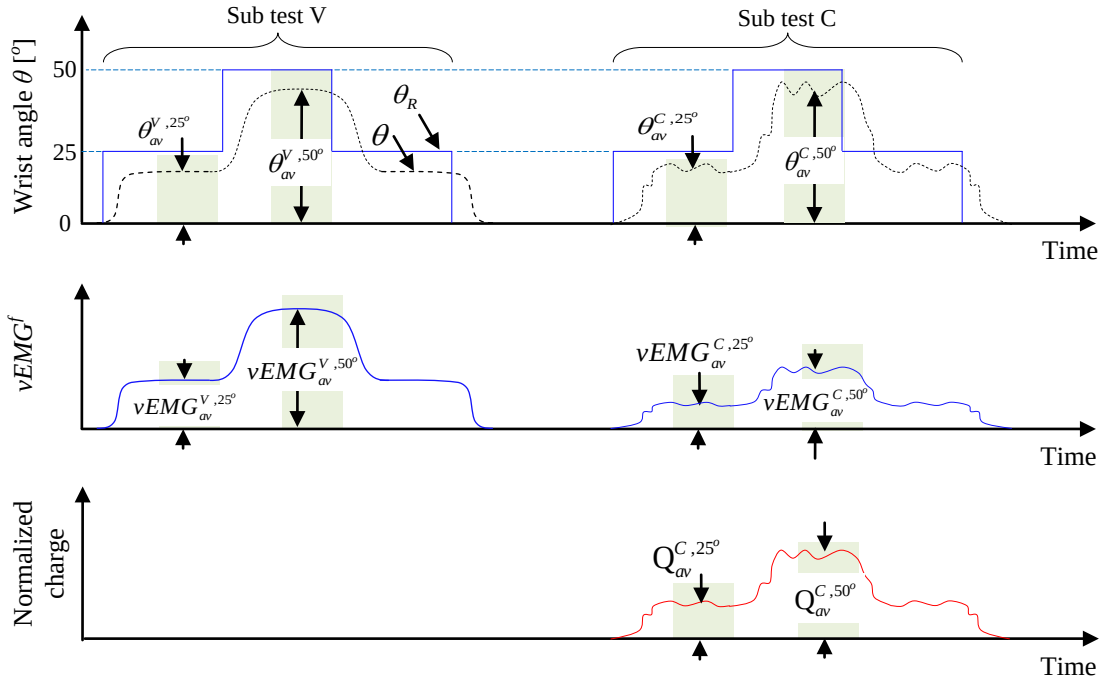

Figure 6. 8: Experimental protocol for evaluation of the EMG-controlled FES. All specific vEMG values, stimulation charges and wrist-joint angles depicted here are average values which are calculated over the shaded steady state areas.

To assess the controller performance, the ratio between the achieved extension angle and the therefore required volitional EMG level was used. This ratio was defined as contraction gain *G*.

From in Figure 6.8 (sub test V), the average contraction gains at 25° and 50° wrist-joint angles are

$$G^{V,25^o} = \frac{\theta_{av}^{V,25^o}}{vEMG_{av}^{V,25^o}} \tag{6. 4}$$

and

$$G^{V,50^o} = \frac{\theta_{av}^{V,50^o}}{vEMG_{av}^{V,50^o}}. \tag{6. 5}$$

And similarly for the EMG-proportional control test C it follows

$$G^{C,25^o} = \frac{\theta_{av}^{C,25^o}}{vEMG_{av}^{C,25^o}} \tag{6. 6}$$

and

$$G^{C,50^o} = \frac{\theta_{av}^{C,50^o}}{vEMG_{av}^{C,50^o}}. \tag{6. 7}$$

The definitions of the specific average wrist-joint angles and volitional EMG values are given in Figure 6.8. Averages were taken for the shaded steady state intervals.

The above calculated gains were utilized to define the following controller performance index

$$C_{PI}^{\theta} = \frac{G^{C,\theta}}{G^{V,\theta}}. \tag{6. 8}$$

This compares the muscle gains obtained with and without FES support. The higher the performance index the lower is the required the volitional effort to achieve the defined tracking task.

6.4.2 Results and Discussion

The controller parameters and tracking test results for all subjects as well as the average values are summarized in Table 6.3. Additional to the values defined before, the variance θ_{var} of the wrist-joint angle and the RMS value θe_{RMS} of the tracking error are given for all sub tests (V and C) and reference angles. Also reported is the base output level EMG_B of the EMG amplifier when the muscle is relaxed and not stimulated. Figure 6.9 shows furthermore the calculated contraction gains in a bar plot.

Table 6. 3: Parameters of the EMG-proportional controller and tracking test results for the 5 subjects (S).

Parameters / Subjects	S 1	S 2	S 3	S 4	S 5	Average
$\theta_{\text{var}}^{V,25^o}$ [°]	0.20	0.22	0.12	0.48	0.17	0.24
$\theta e_{RMS}^{V,25^o}$ [°]	0.93	0.42	5.26	2.02	1.21	1.97
$vEMG_{av}^{V,25^o}$ [mV]	109.27	99.86	27.90	132.89	47.36	83.46
$\theta_{\text{var}}^{V,50^o}$ [°]	0.19	0.17	0.25	0.92	1.20	0.55
$\theta e_{RMS}^{V,50^o}$ [°]	0.46	0.28	11.55	3.60	2.68	3.71
$vEMG_{av}^{V,50^o}$ [mV]	171.63	449.17	76.19	313.00	108.40	223.68
$\theta_{\text{var}}^{C,25^o}$ [°]	2.99	1.13	1.45	8.82	2.49	3.37
$\theta e_{RMS}^{C,25^o}$ [°]	2.98	5.27	7.21	9.00	6.37	6.17
$vEMG_{av}^{C,25^o}$ [mV]	48.10	111.94	20.45	87.07	35.73	60.66
$\theta_{\text{var}}^{C,50^o}$ [°]	1.41	2.52	3.91	0.54	0.64	1.80
$\theta e_{RMS}^{C,50^o}$ [°]	1.52	6.11	8.54	1.12	5.34	4.53
$vEMG_{av}^{C,50^o}$ [mV]	66.66	156.75	38.20	100.44	53.99	83.21
$vEMG_{\max}$ [mV]	97.65	170.89	53.71	146.48	68.35	107.42
$vEMG_{\min}$ [mV]	43.94	107.42	24.41	48.82	34.17	51.75
EMG_B [mV]	13.45	20.29	16.10	10.95	10.43	14.24
$Q_{\min}$	0.20	0.20	0.20	0.10	0.20	0.18
$Q_{\max}$	0.40	0.40	0.45	0.40	0.36	0.40
$G^{V,25^o}$ [degree/mV]	1.15	1.20	3.45	0.84	2.70	1.87
$G^{V,50^o}$ [degree/mV]	1.41	0.54	2.46	0.72	2.14	1.45
$G^{C,25^o}$ [degree/mV]	2.56	1.31	4.27	1.50	4.21	2.77
$G^{C,50^o}$ [degree/mV]	3.70	1.73	5.41	2.47	5.00	3.66
$C_{PI}^{25^o}$	2.21	1.09	1.23	1.78	1.56	1.57
$C_{PI}^{50^o}$	3.20	1.43	1.56	2.92	1.85	2.19

The reported controller performance index is larger than one for all subjects, meaning that the contraction gains increased by applying EMG-proportional control. Less volitional effort was required to achieve the same tracking task.

The natural contraction gain of the volitional tracking task decreases for increasing wrist-joint extension. Opposite to this, the contraction gain under EMG-proportional FES increases for higher wrist-joint angles (cf. Figure 6.9). The impact of this non physiological (inverted) behavior on the use of EMG-proportional control in rehabilitation is not clear at the moment. However, in order to correct this behavior a nonlinear EMG-controlled FES would be required. The observed changes in the contraction gains lead to an increase of the controller performance index for larger wrist-joint angles.

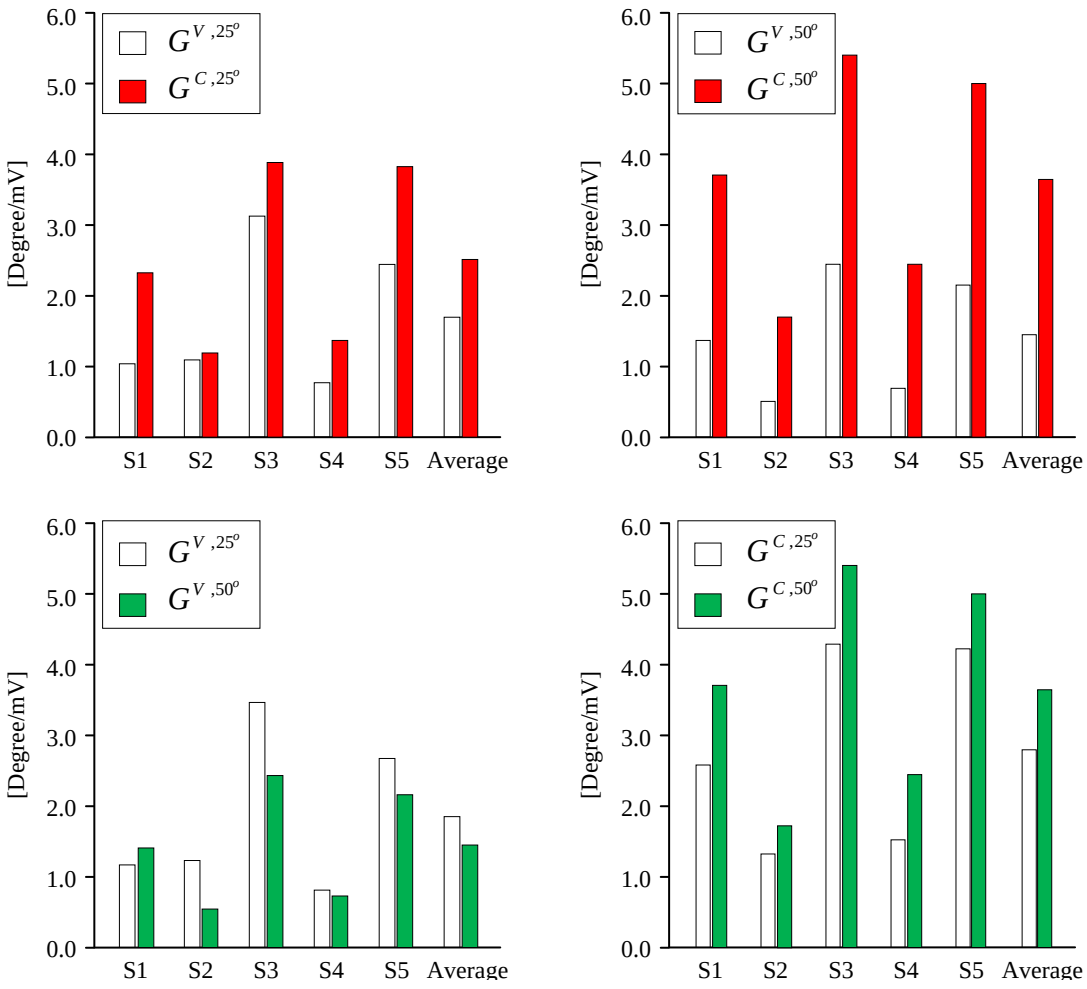

Figure 6. 9: Contraction gains at the different wrist-joint extension with and without FES support.

The preliminary tests also showed that tracking performance in terms of the RMS tracking error and the variance of the wrist-joint angle during steady-state phases clearly suffered from the use of EMG-proportional control compared to pure volitional control.

Figure 6.10 shows the recorded signals during the tracking test for subject S1. For certain references angles and pre-conditions (like previous state of muscle contraction) oscillations could be observed for the EMG-proportional controller. These oscillations may be related to physiological reasons when the contracted muscle moves under the FES electrodes. The movement of the stimulated muscle under electrodes may suddenly change the effectiveness of stimulation positively or negatively. Figure 6.11 presents the result of another tracking test using a more complex stair case reference signal for subject S2. This test was used in the analysis above. However it illustrates more clearly that the above mentioned oscillations do not occur for all reference angles and pre-conditions.

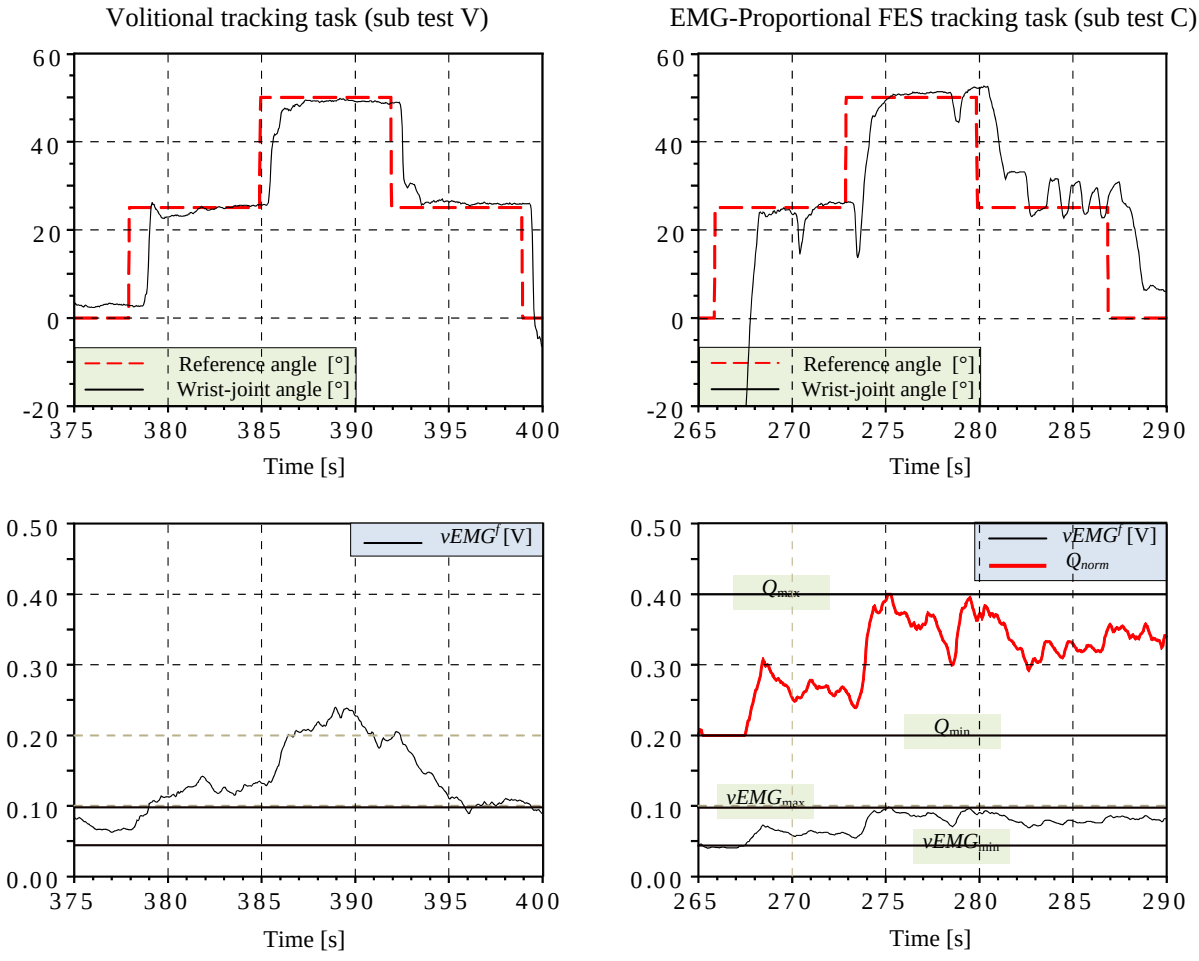

Figure 6. 10: Results of a tracking experiment for subject 1. This test was used in the data analysis.

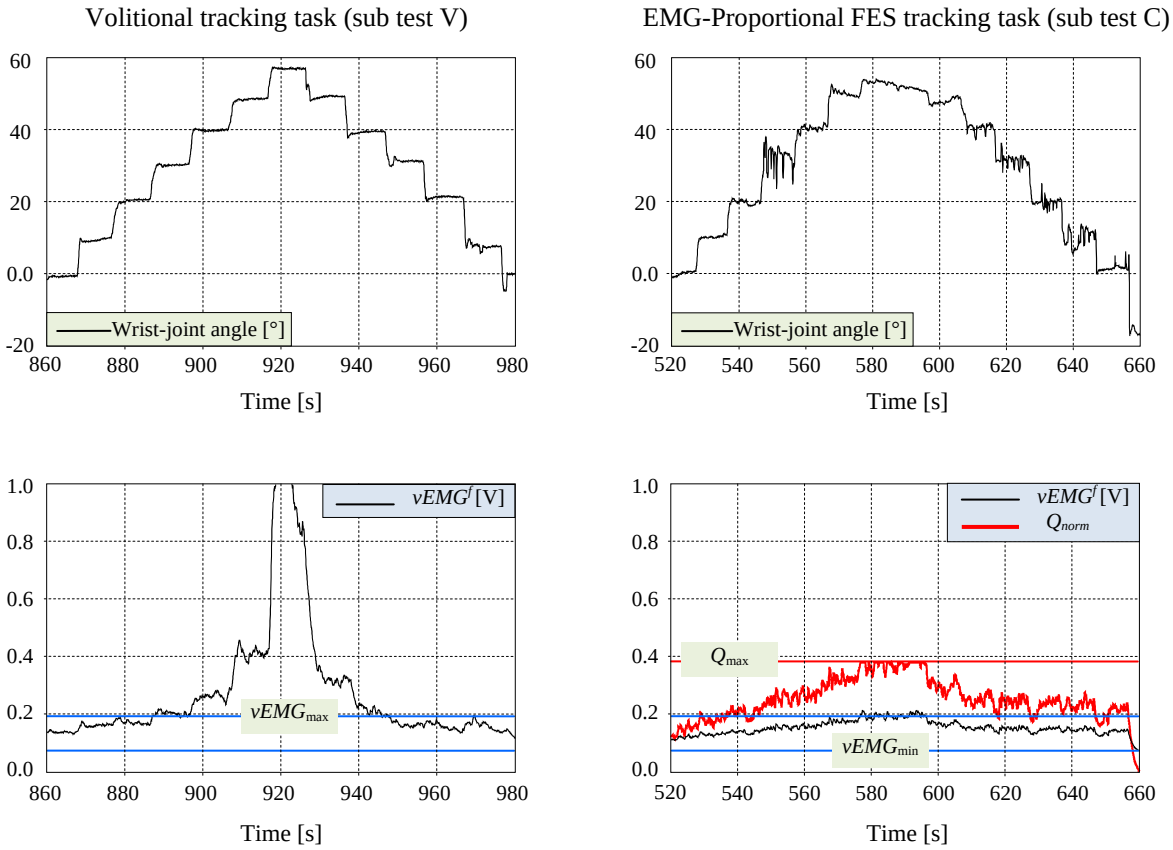

Figure 6. 11: Results of a tracking experiment for subject 2. This test was not used in the data analysis but illustrates the occurrence of oscillations during EMG-proportional FES at certain angles and muscular pre-conditions.

6.5. EMG-Carried FES

When patients are not able to generate smooth volitional EMG profiles, EMG-proportional FES will not be applicable due to risk of oscillating movements. To mitigate this problem, a new control approach has been proposed in this work. This approach can be seen as a compromise between EMG-triggered and EMG-proportional stimulation. The idea of the so-called EMG-carried FES is shown in the Figures 6.12 and 6.13. Activation and de-activation of stimulation is determined by the block with the hysteresis. As soon as the low-pass filtered volitional EMG exceeds the value as $vEMG_{on}$, the stimulation intensity ramps up with slope K until the maximal stimulation and Q_{max} is reached. This stimulation level will be kept until the muscle relaxes and its recorded volitional EMG drops below the level $vEMG_{off}$. At this event, stimulation will reduce with slope $-K$ until Q_{min} is established. The positive feedback loop with the saturation function in Figure 6.13 represents an integrator with integral anti-windup which limits the integrator output between Q_{min} and Q_{max}. In

order to tune the FES-carried stimulation the same pre-experiment was used as for the tuning of the EMG-proportional FES. The angle related to $Q_{\max}$ was set to the value which should be established in a functional task of the hand. Here, an angle of 50° was chosen.

The hysteresis parameters $vEMG_{on}$ and $vEMG_{off}$ were set as follows:

$$vEMG_{ON} = vEMG_{\min} + 0.7\left(vEMG_{\max} - vEMG_{\min}\right) \tag{6. 9}$$

and

$$vEMG_{OFF} = vEMG_{\min} + 0.3\left(vEMG_{\max} - vEMG_{\min}\right). \tag{6. 10}$$

The slope K was chosen in a way that no rapid movements were caused by FES in order to avoid muscular reflexes like the tendon reflex. Figure 6.14 illustrates the operation of the EMG-carried stimulation.

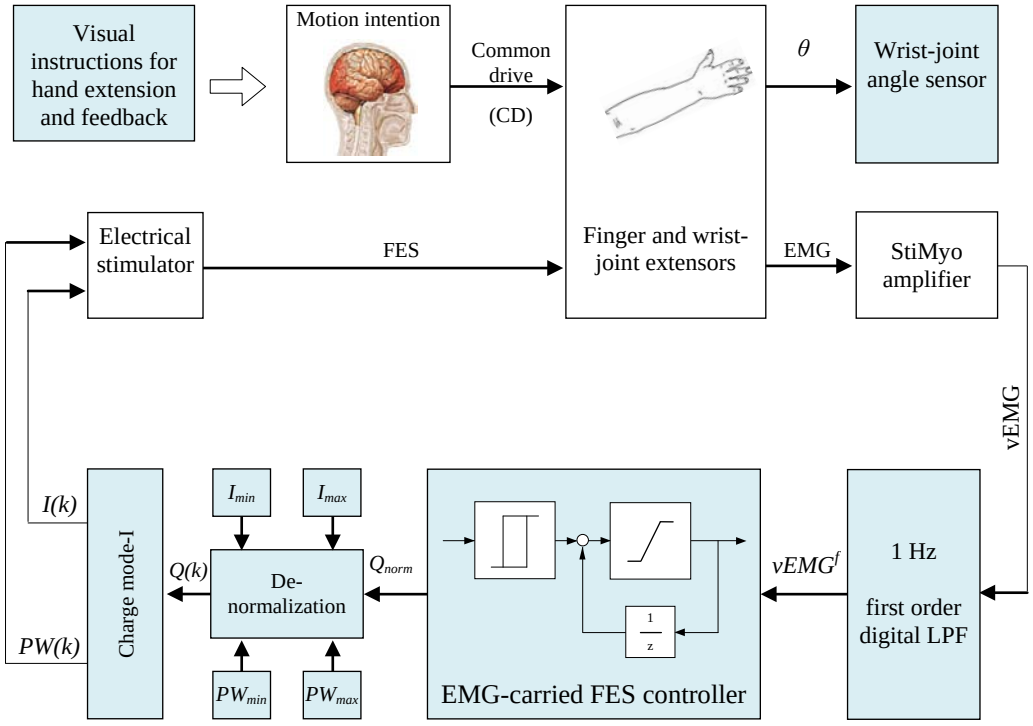

Figure 6. 12: The block diagram of the EMG-carried FES system.

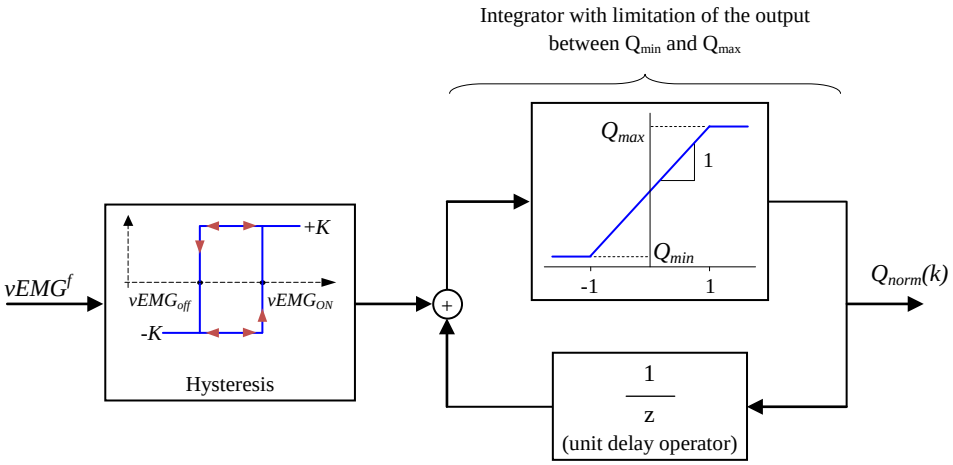

Figure 6. 13: Block diagram of EMG-carried FES controller.

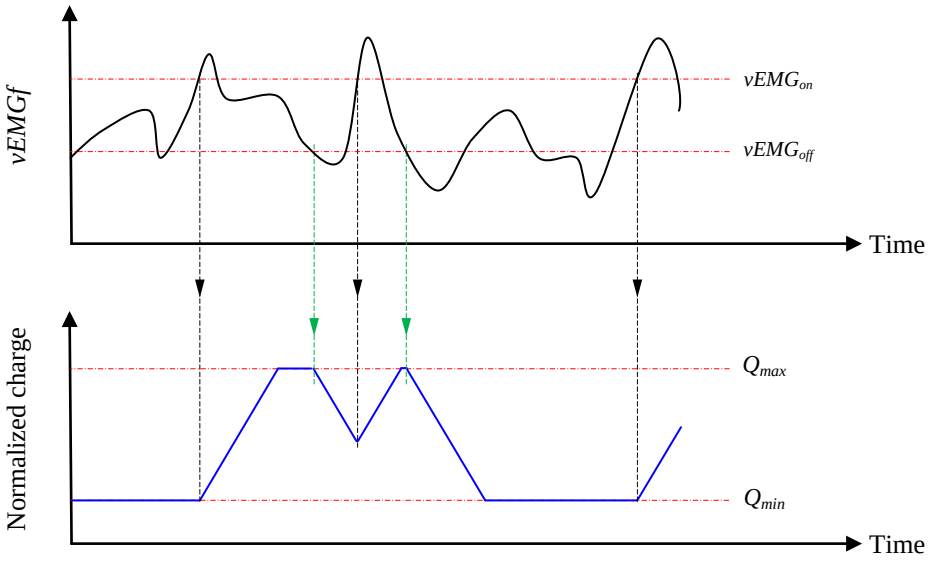

Figure 6. 14: The operation of EMG-carried stimulation.

6.5.1. Experimental Procedure and Data Analysis

As above described, the pre-experiment defined in Section 6.4.1 had to be run in order to find the values of $vEMG_{max}$, $vEMG_{min}$, Q_{max}, and Q_{min}. Based on these values the threshold values $vEMG_{on}$ and $vEMG_{off}$ were calculated using Eqs. (6.9) and (6.10).

To evaluate the feasibility of an EMG-carried stimulation, the experimental protocol described in Figure 6.15 was applied to all 5 subjects who participated already in the amplifier tuning and the testing of the EMG-proportional FES. Each experiment involved two sub tests V (volitional) and C (control). During sub test V the controller was switched off and the subject had to extend his wrist-joint and fingers when instructed. The subject was asked to achieve a wrist-joint angle of about 50°. In sub test C, the subject had to repeat this task while the EMG-carried stimulation was switched on.

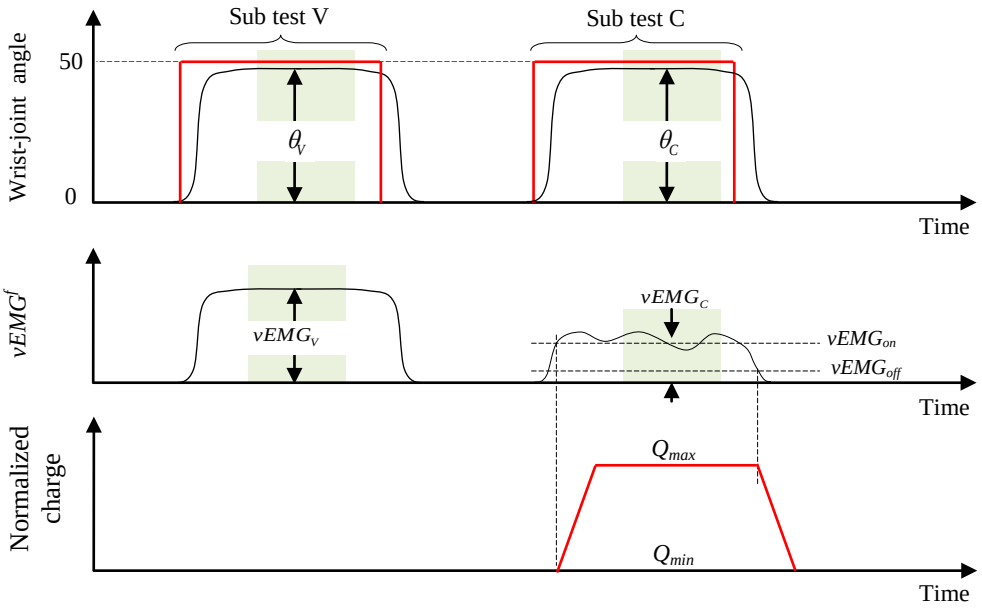

Figure 6. 15: Experimental protocol for investigating the EMG-carried FES controller.

6.5.2. Results and Discussion

All subjects were able to after a short exercise (less than 5 minutes) to use the EMG-carried FES in order to complete the sub test C successfully. As expected less volitional EMG was required in sub test C compared to sub test V for keeping a wrist-joint extension of about 50°. Figure 6.16 shows the result of the experiment for one subject. The subjects reported that they could control the starting and stopping the contraction using the EMG-carried stimulation.

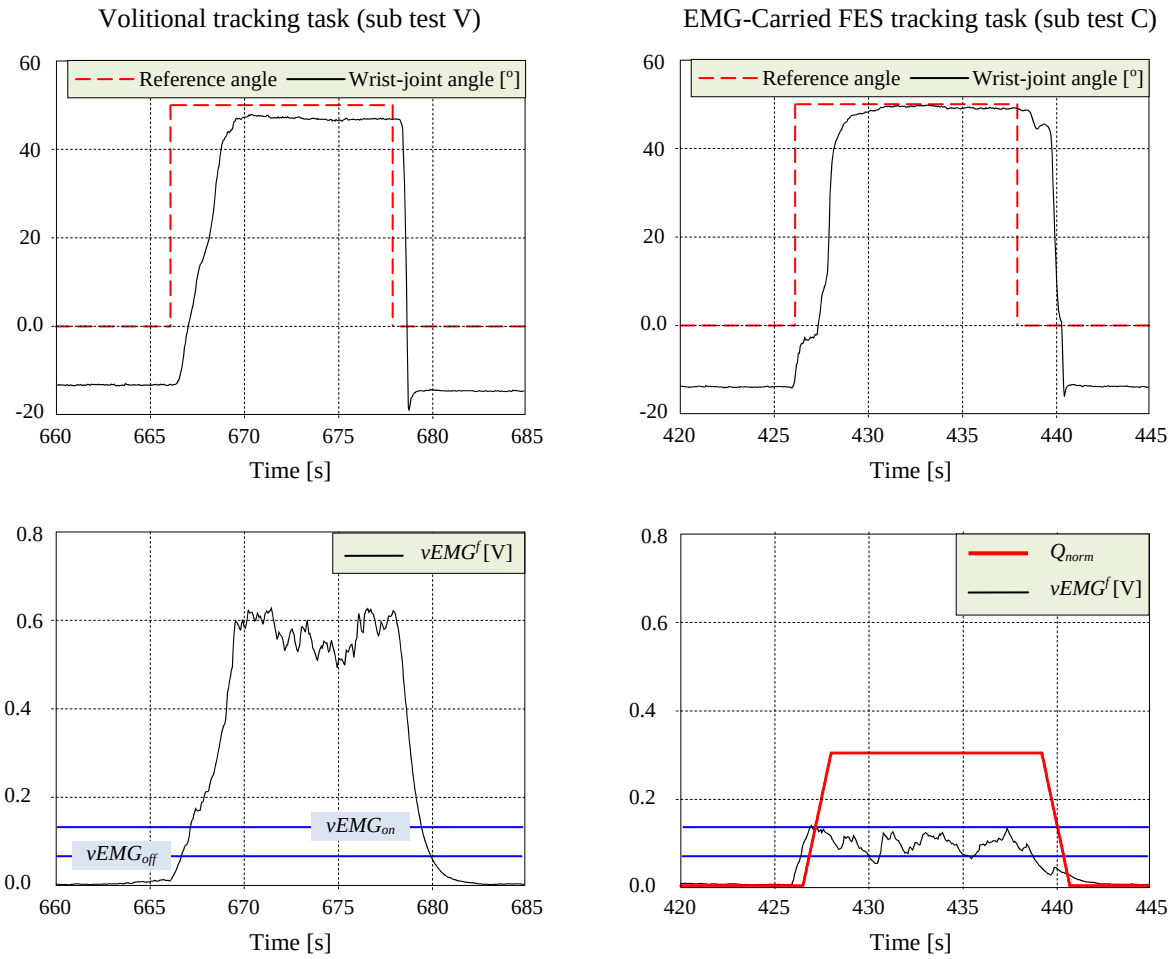

Figure 6. 16: Result of the experimental evaluation of EMG-carried FES for one subject.

6.6. Conclusions and Outlook

An approach for experimental tuning of the StiMyo EMG-amplifier was presented in this chapter. The results showed that the timing of the switches has a strong impact on the quality of assessing volitional muscle contractions during FES. In contrast to this, there was no big difference in the amplifier performance for the different HPF frequencies (150, 170, 200 and 250 Hz) which have been evaluated. The presented tuning of the amplifier was application specific for healthy subjects so that the results cannot be directly transferred to other applications. However it is easy to adapt this tuning procedure to out applications or to repeat it with stroke patients. For healthy subjects the volitional wrist-joint contraction was limited to 20°. In stroke patients one would look for the maximum remaining wrist-joint and finger extension instead. Unfortunately, the EMG measurement period between stimulation pulses could not be extended above 15ms when using patient unspecific settings. Shorter EMG measurement periods result in a more fluctuating amplifier output so that

additional low-pass filtering on the laptop was required before using the detected volitional EMG activity for FES control.

The tuned amplifier was used to investigate two EMG-driven stimulation approaches. Experiments were conducted with healthy subjects in order to analyze the achievable performance when muscle coordination is not impaired. The expected result was, that healthy subjects could perform certain movements using EMG-driven FES with less volitional effort compared pure volitional completion of the same movements. One EMG-driven FES approach consisted in a proportional control of stimulation charge dependent on the detected amount of volitional EMG activity. The wrist-joint angle tracking performance (in terms of tracking error and variance of the wrist-joint angle) was worse in the EMG-proportional FES compared to tracking with pure volitional muscle activity. In some subjects under certain conditions (e.g. reference angle) even oscillations could be observed in the monitored angle. It can be expected that stroke patients may have more problems in performing tracking tasks with EMG-proportional FES due to impaired muscle coordination additional to muscle weakness. To provide an alternative solution also for those patients, a new EMG-driven FES approach was proposed which was named as EMG-carried stimulation. This approach represents a compromise between classical EMG-triggered stimulation and EMG-proportional stimulation. The patients can activate and deactivate the FES-support by their residual muscle activity but cannot modulate the stimulation intensity as freely as in EMG-proportional FES. This feasibility of this approach was again tested with healthy subjects.

The analysis of the EMG-proportional FES showed that the amount of volitional EMG required to achieve a certain angle does not linearly increase for both volitional contraction and EMG-proportional FES; both showed opposed behavior. A nonlinear EMG-controlled FES might be used to correct this behavior. In the simplest case, a piece-wise linear EMG-controlled FES might be applied.

Of course, the results obtained in this Chapter must be confirmed with stroke patients in a next step.

Chapter 7

7. Conclusions and Outlook

In this thesis the detection of the residual volitional/spasticity related muscle activity during functional electrical stimulation was investigated. A 4-channel EMG amplifier named StiMyo was developed which allows the recording of EMG between the stimulation pulses from the stimulation electrodes. A switching circuit driven by a microcontroller was developed to protect the amplifier input from any damage by the stimulation pulses. The circuit also introduces a fast discharging path to repeatedly remove the accumulated charge under the FES/EMG electrodes in order to avoid electrode polarization. An optional permanent electrode/skin discharging resistor was added to prevent any severe effects of electrode polarization such as strong signal suppression which was rarely observed in some tests with subjects. The design process showed that the non FES-induced EMG can be extracted from the recorded signal by using mixed time and frequency domain filter approaches. Big portions of the EMG response related to the direct muscular response on the stimuli, the so-called M-wave, as well as stimulation and switching artifacts are blanked in time domain by means of a mute filter. The required muting period is with up to 35 ms relatively long compared to a stimulation period of 50ms at a stimulation frequency of 20 Hz yielding an EMG measurement period of at least 15 ms between stimuli. For this measurement period, the separation of the non FES-induced EMG from the remaining low-frequent artifacts (tails of discharging curve and M-wave) is achieved in frequency domain by means of a High-Pass Filter (HPF).

During the evaluation of the StiMyo amplifier an action potential related to the discharging process of the electrodes was firstly observed in this work and named as D-wave. The current flow associated with electrode discharging sometimes triggered a second action potential that caused another muscle contraction following the first direct muscle activation caused by the stimulation pulse. It could be shown that the timing of the discharge related action potential wave in the EMG can be influenced by the timing of the switches and the use of the permanent discharging resistor in order to move it out of the EMG-measurement interval.

The designed StiMyo device has been used in two FES applications. One application was FES cycling on an ergo meter were the feasibly to monitor volitional muscle activity during active stimulation was demonstrated. Such an EMG monitoring might be useful to assess the motor coordination of the patient or even for realization of an EMG-biofeedback. Information gained by this EMG measurement may be used to control the cycling program.

Another application under investigation was the EMG-driven FES of wrist-joint and finger extensors. The StiMyo amplifier was tuned for this application to allow the best possible detection of volitional muscle activity during FES. A nearly artifact free assessment of volitional muscle activity could be achieved by the tuning process. Two control methods were investigated. Experimental validation of the proposed methods was carried out in a pilot study with 5 healthy subjects. The first control method aimed at exploiting as much as possible the residual volitional motor control. Therefore, a stimulation intensity which was proportional to the detected volitional EMG was applied. Using this EMG-proportional stimulation, subjects could perform tracking tasks for the wrist-joint angle with less voluntary effort compared to pure volitional movements. However, tracking performance/accuracy suffered from applying EMG-proportional control. When subjects/patients are not able to generate smooth volitional EMG profiles, EMG-proportional FES will not be applicable due to risk of oscillating movements. To mitigate this problem, a second control approach was proposed. This approach can be seen as a compromise between EMG-triggered and EMG-proportional stimulation. The stimulation is initiated as soon as vEMG goes above a defined EMG threshold and stays active until vEMG drops below a second lower EMG threshold. To avoid spastic reactions and tendon reflexes by the stimulation, a rate limitation was implemented for switching on and off the stimulation. This control approach was named EMG-carried stimulation as the subjects/patients must constantly contract a muscle to maintain a supportive, but constant, stimulation. The results related to both control approaches showed the feasibility of using vEMG to obtain an intention-related FES assistance. It is the first time that a quantitative assessment of EMG-driven FES with EMG measurement from stimulation electrodes was presented.

Another important aspect of this work was to use the stimulation charge as control signal. However, this was opening the question on how to realize a given charge by automatically choosing current amplitude and pulse with. Different distributions/relations of pulse widths and current amplitudes were experimentally compared with respect to the minimum charge required for maintaining a desired muscular action and with respect to muscular fatigue. The outcome of this study with healthy subjects was that pulses with high current amplitudes and short pulse widths are preferred. The implemented automatic mapping from a given charge to a pulse width and current amplitude was named charge control in this thesis.

In addition to the two applications outlined in this thesis, the StiMyo device can be employed in a large number of FES applications in which monitoring of muscle activity and even EMG-control of FES are of interest. Examples are FES-assisted walking or FES of the entire upper extremity. It could be also applied during FES-cycling to record and use vEMG as a biofeedback signal.

More research is needed to optimize the location of FES/EMG-recording electrodes. Active electrode/skin discharging could be an interesting option to furthermore shorten the period of stimulation and switching artifacts and to increase the period of EMG detection. Studies with stroke patients need to be carried out to prove the usefulness of the developed device and methods in clinical rehabilitation.

Bibliography

[1] G. Hankey and C. Warlow, “Treatment and secondary prevention of stroke: evidence, costs, and effects on individuals and populations,” *Lancet*, vol. 354, no. 9188, pp. 1457-1463, 1999.

[2] T. Schauer, D. Hossaini, and S. Hesse, “EMG-controlled electrical stimulation of the paretic wrist and finger extensors in stroke patients,” presented at the Proceedings of the TAR 2007 Conference, Berlin, Germany, 2007.

[3] V. Brooks, *The Neural Basis of Motor Control*. Oxford University Press, USA, 1986.

[4] P. Montgomery and B. Connolly, *Clinical Applications for Motor Control*. Slack Inc, 2002.

[5] C. Warlow, *Stroke: a practical guide to management*. Wiley-Blackwell, 2001.

[6] I. Bromley, *Tetraplegia and paraplegia: a guide for physiotherapists*. Elsevier Health Sciences, 2006.

[7] K. Horch and G. Dhillon, *Neuroprosthetics: Theory and Practice*, vol. 2. World Scientific Publishing Company, 2004.

[8] R. Merletti and P. Parker, *Electromyography: physiology, engineering, and noninvasive applications*. Wiley-IEEE, 2004.

[9] J. McGeown, *Master Medicine: Physiology: A core text of human physiology with self-assessment*, 2nd ed. Churchill Livingstone, 2002.

[10] M. Latash, *Neurophysiological Basis of Movement*. Human Kinetics, 2008.

[11] P. Frederick, “The All-Or-None Principle in Graded Response of Seletal Muscle,” *Am J Physiol.*, vol. 44, pp. 517-542, 1917.

[12] M. Latash, *Neurophysiological Basis of Movement*. Human Kinetics, 1998.

[13] E. Henneman, G. Somjen, and D. Carpenter, “Functional significance of cell size in spinal motoneurons,” *Journal of Neurophysiology*, vol. 28, no. 3, pp. 560-580, 1965.

[14] E. Henneman, G. Somjen, and D. Carpenter, “Excitability and inhibitibility of motoneurons of different sizes,” *Journal of Neurophysiology*, vol. 28, no. 3, p. 599, 1965.

[15] E. Henneman, H. Clamann, J. Gillies, and R. Skinner, “Rank order of motoneurons within a pool: law of combination,” *Journal of Neurophysiology*, vol. 37, no. 6, pp. 1338-1349, 1974.

[16] L. Weiss, J. Silver, and J. Weiss, *Easy EMG*, 1st ed. Butterworth-Heinemann, 2004.

[17] L. Sheffler and J. Chae, “Neuromuscular electrical stimulation in neurorehabilitation,” *Muscle & Nerve*, vol. 35, no. 5, pp. 562-590, 2007.

[18] C. Phillips, *Functional Electrical Rehabilitation: Technological Restoration After Spinal Cord Injury*, 1st ed. Springer, 1991.

[19] D. Zhang, T. Guan, F. Widjaja, and W. Ang, “Functional electrical stimulation in rehabilitation engineering: a survey,” 2007, p. 221–226.

[20] I. Cikajlo, Z. Matjačic, T. Bajad, and R. Futami, "Sensory Supported FES Control in Gait Training of Incomplete Spinal Cord Injury Persons," *Artificial Organs*, vol. 29, pp. 459-461, 2005.

[21] S. Robbins, P. Houghton, M. Woodbury, and J. Brown, "The therapeutic effect of functional and transcutaneous electric stimulation on improving gait speed in stroke patients: a meta-analysis," *Archives of physical medicine and rehabilitation*, vol. 87, no. 6, p. 853–859, 2006.

[22] K. Ragnarsson, "Functional electrical stimulation after spinal cord injury: current use, therapeutic effects and future directions," *Spinal Cord*, vol. 46, no. 4, p. 255–274, 2007.

[23] S. Hesse, C. Werner, and A. Bardeleben, "Electromechanical gait training with functional electrical stimulation: case studies in spinal cord injury," *Spinal Cord*, vol. 42, no. 6, p. 346–352, 2004.

[24] T. Johnston, R. Betz, B. Smith, and M. Mulcahey, "Implanted functional electrical stimulation: an alternative for standing and walking in pediatric spinal cord injury," *Spinal Cord*, vol. 41, no. 3, pp. 144-152, 2003.

[25] R. Brissot et al., "Clinical experience with functional electrical stimulation-assisted gait with Parastep in spinal cord-injured patients," *Spine*, vol. 25, no. 4, p. 501, 2000.

[26] G. Yarkony, E. Roth, G. Cybulski, and R. Jaeger, "Neuromuscular stimulation in spinal cord injury: I: Restoration of functional movement of the extremities.," *Archives of physical medicine and rehabilitation*, vol. 73, no. 1, p. 78–86, 1992.

[27] E. Marsolais and R. Kobetic, "Development of a practical electrical stimulation system for restoring gait in the paralyzed patient," *Clinical orthopaedics and related research*, vol. 233, p. 64, 1988.

[28] J. Hausdorff and W. Durfee, "Open loop Position Control of the Knee Joint Using Electrical Stimulation of the Quadriceps and Hamstrings," *Medical and Biological Engineering and Computing*, vol. 29, pp. 269-280, 1991.

[29] G. Yamaguchi and F. Zajac, "Restoring unassisted natural gait to paraplegics via functional neuromuscular stimulation: a computer simulation study," *Biomedical Engineering, IEEE Transactions*, vol. 37, no. 9, pp. 886-902, 1990.

[30] A. Mulder, H. Boom, H. Hermens, and G. Zilvold, "Artificial-reflex stimulation for FES-induced standing with minimum quadriceps force," *Medical & Biological Engineering & Computing*, pp. 483-488, 1990.

[31] R.-P. Jaime, Z. Matjacic, and K. J. Hunt, "Paraplegic standing supported by FES-controlled ankle stiffness," *Neural Systems and Rehabilitation Engineering, IEEE Transactions*, vol. 10, no. 4, pp. 239-248, 2002.

[32] L. Duffell et al., "Long-term intensive electrically stimulated cycling by spinal cord-injured people: effect on muscle properties and their relation to power output," *Muscle & Nerve*, vol. 38, no. 4, pp. 1304-1311, 2008.

[33] D. Newham and N. Donaldson, "FES cycling," in *Operative Neuromodulation*, 2007, pp. 395-402.

[34] K. Seki, M. Sato, and Y. Handa, “Increase of muscle activities in hemiplegic lower extremity during driving a cycling wheelchair,” *The Tohoku Journal of Experimental Medicine*, vol. 219, no. 2, pp. 129-138, 2009.

[35] R. McManus et al., “Seated Bilateral Leg Exercise Effects on Hemiparetic Lower Extremity Function in Chronic Stroke,” *Neurorehabil Neural Repair*, p. 1545968309347679, 2009.

[36] A. Conforto et al., “Effects of Somatosensory Stimulation on Motor Function After Subacute Stroke,” *Neurorehabil Neural Repair*, p. 1545968309349946, 2009.

[37] J. Szecsi, C. Krewer, F. Müller, and A. Straube, “Functional electrical stimulation assisted cycling of patients with subacute stroke: Kinetic and kinematic analysis,” *Clinical Biomechanics*, vol. 23, no. 8, pp. 1086-1094, 2008.

[38] S. Ferrante, A. Pedrocchi, G. Ferrigno, and F. Molteni, “Cycling induced by functional electrical stimulation improves the muscular strength and the motor control of individuals with post-acute stroke. Europa Medicophysica-SIMFER 2007 Award Winner,” *European Journal of Physical and Rehabilitation Medicine*, vol. 44, no. 2, pp. 159-167, 2008.

[39] T. Janssen et al., “Effects of electric stimulation-assisted cycling training in people with chronic stroke,” *Archives of Physical Medicine and Rehabilitation*, vol. 89, no. 3, pp. 463-469, 2008.

[40] P. Gorman and J. Mortimer, “The Effect of Stimulus Parameters on the Recruitment Characteristics of Direct Nerve Stimulation,” *Biomedical Engineering, IEEE Transactions on*, vol. 30, no. 7, pp. 407-414, 1983.

[41] J. Baldi, R. Jackson, R. Moraille, and W. Mysiw, “Muscle atrophy is prevented in patients with acute spinal cord injury using functional electrical stimulation.,” *Spinal cord: the official journal of the International Medical Society of Paraplegia*, vol. 36, no. 7, p. 463, 1998.

[42] J. Gibson, K. Smith, and M. Rennie, “Prevention of disuse muscle atrophy by means of electrical stimulation: maintenance of protein synthesis,” *The Lancet*, vol. 332, no. 8614, p. 767–770, 1988.

[43] T. Martin, R. Stein, P. Hoeppner, and D. Reid, “Influence of electrical stimulation on the morphological and metabolic properties of paralyzed muscle,” *J Appl Physiol*, vol. 72, no. 4, pp. 1401-1406, 1992.

[44] D. Goldspink, J. Easton, S. Winterburn, P. Williams, and G. Goldspink, “The role of passive stretch and repetitive electrical stimulation in preventing skeletal muscle atrophy while reprogramming gene expression to improve fatigue resistance,” *Journal of Cardiac Surgery*, vol. 6, no. 1, pp. 218-224, 1991.

[45] S. Levine, R. Kett, P. Cederna, and S. Brooks, “Electric muscle stimulation for pressure sore prevention: tissue shape variation,” *Arch Phys Med Rehabil*, vol. 71, no. 3, p. 210–15, 1990.

[46] K. Bogie, S. Reger, S. Levine, and V. Sahgal, “Electrical stimulation for pressure sore prevention and wound healing,” *Assistive Technology: The Official Journal of RESNA*, vol. 12, no. 1, pp. 50-66, 2000.

[47] G. Wheeler, "Functional electric stimulation[ndash]assisted rowing: Increasing cardiovascular fitness through functional electric stimulation rowing training in persons with spinal cord injury," *Archives of Physical Medicine and Rehabilitation*, vol. 83, no. 8, pp. 1093-1099, 2002.

[48] B. Kapp, M. Gallagher, M. Underwood, C. McNall, and D. Whitehorn, "Cardiovascular responses elicited by electrical stimulation of the amygdala central nucleus in the rabbit," *Brain Research*, vol. 234, no. 2, pp. 251-262, 1982.

[49] E. Hoff and H. Green, *Cardiovascular Reactions Induced by Electrical Stimulation of the Cerebral Cortex*. Yale J.Biol.Med., 1936, pp. 8-201.

[50] T. Schauer, "Feedback Control of Cycling in Spinal Cord Injury Using Functional Electrical Stimulation," Ph.D. Dissertation, Glasgow, UK: Glasgow University, 2005.

[51] W. Pease, H. Lew, and E. Johnson, *Johnson's Practical Electromyography*, Fourth Edition. Lippincott Williams & Wilkins, 2006.

[52] C. De Luca and M. Knaflitz, *Surface Electromyography, What's New?* CLUT Publishers, Turino, Italy, 1992.

[53] R. Thorsen, I. Carpinella, and M. Ferrarin, "Can the F-Response be Volitionally Repressed during Functional Electrical Stimulation?," *Neuromodulation*, vol. 8, no. 2, p. 141–147, 2005.

[54] F. Biering-Sorensen, J. B. Nielsen, and K. Klinge, "Spasticity-assessment: a review," *Spinal Cord*, vol. 44, no. 12, pp. 708-722, Apr. 2006.

[55] J. Heasman et al., "Detection of fatigue in the isometric electrical activation of paralyzed hand muscles of persons with tetraplegia," *Rehabilitation Engineering, IEEE Transactions on*, vol. 8, no. 3, pp. 286-296, 2000.

[56] L. P. Ince, M. S. Leon, and D. Christidis, "EMG biofeedback for handwriting disabilities: A critical examination of the literature," *Journal of Behavior Therapy and Experimental Psychiatry*, vol. 17, no. 2, pp. 95-100, Jun. 1986.

[57] H. Woodford and C. Price, "EMG biofeedback for the recovery of motor function after stroke," *Cochrane Database of Systematic Reviews*, no. 2, p. CD004585, 2007.

[58] W. Liberson, H. Holmquest, and M. Scott, "Functional electrotherapy: Stimulation of the common peroneal nerve synchronised with the swing phase of gait of hemiplegic subjects," *Arch Phys Med Rehabilitation*, vol. 42, pp. 202-205, 1961.

[59] R. Merletti, M. Knaflitz, and C. DeLuca, "Electrically evoked myoelectric signals," *Critical Reviews in Biomedical Engineering*, vol. 19, no. 4, pp. 293-340, 1992.

[60] T. Schauer, R. Salbert, N.-O. Negård, and J. Raisch, "Detection and Filtering of EMG forAssessing Voluntary Muscle Activity during FES.," 2004.

[61] A. Kamono and Y. Kotaka, "Development of Gait Assist Device for Foot Drop Patients," presented at the Proceedings of 6th Annual Conference of the International FES Society, Cleveland, Ohio, USA, 2001, pp. 178-180.

[62] A. Kamono, Y. Muraoka, Y. Tomita, H. Shimaoka, S. Uchida, and T. Ota, "Development of EMG-controlled electrical stimulation system," in *SICE 2002. Proceedings of the 41st SICE Annual Conference*, 2002, vol. 3, pp. 2022-2027 vol.3.

[63] J. Minzly, J. Mizrahi, N. Hakim, and A. Liberson, "Stimulus artefact suppressor for EMG recording during FES by a constant-current stimulator," *Medical & Biological Engineering & Computing*, vol. 31, no. 1, pp. 72-75, 1993.

[64] Y. Muraoka, "Development of an EMG recording device from stimulation electrodes for functional electrical stimulation," *Frontiers of Medical and Biological Engineering: The International Journal of the Japan Society of Medical Electronics and Biological Engineering*, vol. 11, no. 4, pp. 323-333, 2002.

[65] M. Knaflitz and R. Merletti, "Suppression of stimulation artifacts from myoelectric-evoked potential recordings," *Biomedical Engineering, IEEE Transactions on*, vol. 35, no. 9, pp. 758-763, 1988.

[66] Y. Muraoka, "Development of 2-channel gait assist electrical stimulator for hemiplegia," in *SICE 2002. Proceedings of the 41st SICE Annual Conference*, 2002, vol. 3, pp. 2028-2031 vol.3.

[67] R. Thorsen, "An artefact suppressing fast-recovery myoelectric amplifier," *IEEE Transactions on Biomedical Engineering*, vol. 46, no. 6, pp. 764-766, 1999.

[68] R. Thorsen, R. Spadone, and M. Ferrarin, "A pilot study of myoelectrically controlled FES of upper extremity," *Neural Systems and Rehabilitation Engineering, IEEE Transactions*, vol. 9, no. 2, pp. 161-168, 2001.

[69] C. Frigo, M. Ferrarin, W. Frasson, E. Pavan, and R. Thorsen, "EMG signals detection and processing for on-line control of functional electrical stimulation," *Journal of Electromyography and Kinesiology: Official Journal of the International Society of Electrophysiological Kinesiology*, vol. 10, no. 5, pp. 351-360, 2000.

[70] E. Langzam, E. Isakov, and J. Mizrahi, "Evaluation of methods for extraction of the volitional EMG in dynamic hybrid muscle activation," *Journal of Neuro Engineering and Rehabilitation*, vol. 3, pp. 27-27.

[71] S. Sennels, F. Biering, O. Andersen, and S. Hansen, "Functional neuromuscular stimulation controlled by surface electromyographic signals produced by volitional activation of the same muscle: adaptive removal of the muscle response from the recorded EMG-signal," *IEEE Transactions on Rehabilitation Engineering: A Publication of the IEEE Engineering in Medicine and Biology Society*, vol. 5, no. 2, pp. 195-206, 1997.

[72] H. Yeom, Y. Park, and H. Yoon, "Gram-Schmidt M-Wave Canceller for the EMG Controlled FES," *IEICE - Trans. Inf. Syst.*, vol. E88-D, no. 9, pp. 2213-2217, 2005.

[73] C. B. Tabernig and R. C. Acevedo, "M-wave elimination from surface electromyogram of electrically stimulated muscles using singular value decomposition: Preliminary results," *Medical Engineering & Physics*, vol. 30, no. 6, pp. 800-803, Jul. 2008.

[74] N. Matsushita, Y. Handa, M. Ichie, and N. Hoshimiya, "Electromyogram analysis and electrical stimulation control of paralysed wrist and hand," *Journal of Electromyography and Kinesiology*, vol. 5, no. 2, p. 117–128, 1995.

[75] D. Bolton, “Electromyogram-triggered neuromuscular stimulation and stroke motor recovery of arm/hand functions: a meta-analysis,” *Journal of the Neurological Sciences*, vol. 223, no. 2, pp. 121-127, 2004.

[76] A. Meilink, B. Hemmen, H. Seelen, and G. Kwakkel, “Impact of EMG-triggered neuromuscular stimulation of the wrist and finger extensors of the paretic hand after stroke: a systematic review of the literature,” *Clinical Rehabilitation*, vol. 22, no. 4, pp. 291-305, Apr. 2008.

[77] R. Thorsen, E. Occhi, S. Boccardi, and M. Ferrarin, “Functional electrical stimulation reinforced tenodesis effect controlled by myoelectric activity from wrist extensors,” *Journal of Rehabilitation Research and Development*, vol. 43, no. 2, pp. 247-256, 2006.

[78] S. Saxena, S. Nikolić, and D. Popović, “An EMG-controlled grasping system for tetraplegics,” *Journal of Rehabilitation Research and Development*, vol. 32, no. 1, pp. 17-24, 1995.

[79] Y. Hara, S. Ogawa, K. Tsujiuchi, and Y. Muraoka, “A home-based rehabilitation program for the hemiplegic upper extremity by power-assisted functional electrical stimulation,” *Disability & Rehabilitation*, vol. 30, no. 4, p. 296–304, 2008.

[80] T. Fujiwara et al., “Motor Improvement and Corticospinal Modulation Induced by Hybrid Assistive Neuromuscular Dynamic Stimulation (HANDS) Therapy in Patients With Chronic Stroke,” *Neurorehabil Neural Repair*, vol. 23, no. 2, pp. 125-132, 2009.

[81] J. Giuffrida and P. Crago, “Reciprocal EMG control of elbow extension by FES,” *Neural Systems and Rehabilitation Engineering, IEEE Transactions on*, vol. 9, no. 4, pp. 338-345, 2001.

[82] D. Zhang and W. Ang, “Reciprocal EMG Controlled FES for Pathological Tremor Suppression of Forearm,” in *Engineering in Medicine and Biology Society, 2007. EMBS 2007. 29th Annual International Conference of the IEEE*, 2007, pp. 4810-4813.

[83] C. Chen, Z. He, and Y. Hsueh, “An EMG Feedback Control Functional Electrical Stimulation Cycling System,” *Journal of Signal Processing Systems*, 2009.

[84] D. Graupe, “EMG pattern analysis for patient-responsive control of FES in paraplegics for walker-supported walking,” *Biomedical Engineering, IEEE Transactions*, vol. 36, no. 7, pp. 711-719, 1989.

[85] D. Graupe, K. H. Kohn, A. Kralj, and S. Basseas, “Patient controlled electrical stimulation via EMG signature discrimination for providing certain paraplegics with primitive walking functions,” *Journal of Biomedical Engineering*, vol. 5, no. 3, pp. 220-226, 1983.

[86] A. Dutta, R. Kobetic, and R. Triolo, “Gait Initiation With Electromyographically Triggered Electrical Stimulation in People With Partial Paralysis,” *Journal of Biomechanical Engineering*, vol. 131, no. 8, pp. 081002-9, 2009.

[87] H. Yamaguchi et al., “EMG control switching system for FES,” presented at the Proceedings of the IEEE International Workshop on Robot and Human Interaction, Pisa, Italy, 1999, pp. 7-12.

[88] W. Peasgood, T. Whitlock, A. Bateman, M. Fry, R. Jones, and A. Davis-Smith, "EMG-controlled closed loop electrical stimulation using a digital signal processor," *Electronics Letters*, vol. 36, no. 22, p. 1832, 2000.

[89] J. H. Burridge, P. N. Taylor, S. A. Hagan, D. E. Wood, and I. D. Swain, "The effects of common peroneal stimulation on the effort and speed of walking: a randomized controlled trial with chronic hemiplegic patients," *Clinical Rehabilitation*, vol. 11, no. 3, pp. 201-210, Aug. 1997.

[90] H. Yeom and Y. Chang, "Autogenic EMG-controlled functional electrical stimulation for ankle dorsiflexion control," *Journal of Neuroscience Methods*, vol. 193, no. 1, pp. 118-125, 2010.

[91] R. Futami, K. Seki, and T. Kawanishi, "Application of Local EMG-Driven FES to Incompletely Paralyzed Lower Extremities," presented at the Proceedings of 10th Annual Conference of the International FES Society, Montreal, Canada, 2005.

[92] N. Negard, "Controlled FES-assisted gait training for hemiplegic stroke patients based on inertial sensors," Ph.D. Dissertation, Technischen Universität Berlin, 2009.

[93] R. Mahony, T. Hamel, and J.-M. Pflimlin, "Nonlinear Complementary Filters on the Special Orthogonal Group," *Automatic Control, IEEE Transactions on*, vol. 53, no. 5, pp. 1203-1218, 2008.

[94] P. Crago, P. Peckham, and G. Thrope, "Modulation of Muscle Force by Recruitment During Intramuscular Stimulation," *Biomedical Engineering, IEEE Transactions*, vol. 27, no. 12, pp. 679-684, 1980.

[95] F. Rattay, *Electrical Nerve Stimulation: Theory, Experiments and Applications*, 1st ed. Springer, 2001.

[96] E. Ambrosini, "Cycling Induced by Electrical Stimulation: a sensorized cycle-ergometer to evaluate motor recovery and provide interventions for post-stroke lower limb rehabilitation," Ph.D. Dissertation, Politecnico di Milano, Department of Bioengineering, Milano, Italy, 2011.

[97] J. Bronzino, *The Biomedical Engineering Handbook, Second Edition, Vol. I*, 2nd ed. CRC Press, 2000.

[98] B. Gerdle, S. Karlsson, S. Day, and M. Djupsjöbacka, *Acquisition, Processing and Analysis of the Surface Electromyogram. Modern Techniques in Neuroscience*. Berlin, Germany: Springer-Verlag, 1999.

[99] U. Carraro, C. Schenk, and E. Gamm, *Electronic Circuits: Handbook for Design and Application*, 2nd ed. Springer, Berlin, 2008.

[100] D. Marioli, E. Sardini, and A. Taroni, "High-accuracy measurement techniques for capacitance transducers," *Measurement Science and Technology*, vol. 4, no. 3, pp. 337-343, 1993.

[101] S. Huang, A. Stott, R. Green, and M. Beck, "Electronic transducers for industrial measurement of low value capacitances," *Journal of Physics E: Scientific Instruments*, vol. 21, no. 3, pp. 242-250, 1988.

[102] F. Reverter, X. Li, and G. C. M. Meijer, "Stability and accuracy of active shielding for grounded capacitive sensors," *Measurement Science and Technology*, vol. 17, no. 11, pp. 2884-2890, 2006.

[103] M. van-Rijn, A. Peper, and C. Grimbergen, "High-quality recording of bioelectric events. Part 1: Interference reduction, theory and practice'," *Med. Biol. Eng. Comput*, vol. 28, p. 389–397, 1990.

[104] J. G. Webster, *Medical Instrumentation Application and Design*, 4th ed. Wiley, 2009.

[105] A. Boxtel, "Skin resistance during square-wave electrical pulses of 1 to 10 mA," *Medical & Biological Engineering & Computing*, vol. 15, no. 6, pp. 679-687, 1977.

[106] S. J. Dorgan and R. B. Reilly, "A model for human skin impedance during surface functional neuromuscular stimulation," *Rehabilitation Engineering, IEEE Transactions on*, vol. 7, no. 3, pp. 341-348, 1999.

[107] Y. Hara, S. Ogawa, and Y. Muraoka, "Hybrid power-assisted functional electrical stimulation to improve hemiparetic upper-extremity function," *American Journal of Physical Medicine & Rehabilitation*, vol. 85, no. 12, p. 977, 2006.

[108] R. Shalaby, T. Schauer, W. Liedecke, and J. Raisch, "Amplifier design for EMG recording from stimulation electrodes during functional electrical stimulation leg cycling ergometry," *Biomedizinische Technik/Biomedical Engineering*, vol. 56, no. 1, pp. 23-33, 2011.

[109] S. Kautz, P. Duncan, S. Perera, R. Neptune, and S. Studenski, "Coordination of hemiparetic locomotion after stroke rehabilitation," *Neurorehabilitation and Neural Repair*, vol. 19, no. 3, p. 250, 2005.

[110] D. Brown, S. Nagpal, and S. Chi, "Limb-loaded cycling program for locomotor intervention following stroke," *Physical Therapy*, vol. 85, no. 2, pp. 159-168, 2005.

[111] M.-J. Lee et al., "Comparison of effect of aerobic cycle training and progressive resistance training on walking ability after stroke: a randomized sham exercise-controlled study," *Journal of the American Geriatrics Society*, vol. 56, no. 6, pp. 976-985, 2008.

[112] M. Katz-Leurer, I. Sender, O. Keren, and Z. Dvir, "The influence of early cycling training on balance in stroke patients at the subacute stage. Results of a preliminary trial," *Clinical Rehabilitation*, vol. 20, no. 5, pp. 398 -405, May. 2006.

[113] D. Brown and G. DeBacher, "Bicycle Ergometer and Electromyographic Feedback for Treatment of Muscle Imbalance in Patients with Spastic Hemiparesis: Suggestion from the Field," *Phys Ther*, vol. 67, no. 11, pp. 1715-1719, 1987.

[114] F. Eigler, *Funktionelle Elektrostimulation am Beinergometer in der Rehabilitation nach Schlaganfall: Der Einsatz funktioneller Elektrostimulation während des Trainings am zyklischen Beinbewegungstrainer (FES-LCE) in der stationären Rehabilitation nach zerebralem ischämischem Infarkt*. Germany: , 2009.

[115] E. Ambrosini, S. Ferrante, A. Pedrocchi, G. Ferrigno, and F. Molteni, "Cycling Induced by Electrical Stimulation Improves Motor Recovery in Postacute Hemiparetic Patients: A Randomized Controlled Trial," *Stroke*, vol. 42, no. 4, pp. 1068-1073, Apr. 2011.

[116] E. Ambrosini, S. Ferrante, T. Schauer, G. Ferrigno, F. Molteni, and A. Pedrocchi, “Design of a symmetry controller for cycling induced by electrical stimulation: preliminary results on post-acute stroke patients,” *Artificial Organs*, vol. 34, no. 8, pp. 663-667, 2010.

[117] B. Stapelfeldt, G. Mornieux, R. Oberheim, A. Belli, and A. Gollhofer, “Development and evaluation of a new bicycle instrument for measurements of pedal forces and power output in cycling,” *International Journal of Sports Medicine*, vol. 28, no. 4, pp. 326-332, Apr. 2007.

[118] A. Sander and S. Schwarz, *Anatomie fast. Der Crashkurs*, 1st ed. Börm Bruckmeier, 2003.